Improved accuracy for fluid flow problems via enhanced physics

---

A Thesis
Presented to
the Graduate School of
Clemson University

In Partial Fulfillment
of the Requirements for the Degree
Doctor of Philosophy
Mathematical Sciences

---

by
Michael A. Case
May 2010

Accepted by:
Dr. Leo Rebholz, Committee Chair
Dr. Eleanor Jenkins, Co-Chair
Dr. Chris Cox
Dr. Nigel Kaye

This thesis is an investigation of numerical methods for approximating solutions to fluid flow problems, specifically the Navier-Stokes equations (NSE) and magnetohydrodynamic equations (MHD), with an overriding theme of enforcing more physical behavior in discrete solutions. It is well documented that numerical methods with more physical accuracy exhibit better long-time behavior than comparable methods that enforce less physics in their solutions. This work develops, analyzes and tests finite element methods that better enforce mass conservation in discrete velocity solutions to the NSE and MHD, helicity conservation for NSE, cross-helicity conservation in MHD, and magnetic field incompressibility in MHD.

Table of Contents

List of Tables

List of Figures

Chapter 1

Introduction

The incompressible Navier-Stokes equations (NSE) are the standard model for simulating free flows in computational fluid dynamics. Although they are one of the most investigated mathematical equations [53, 54, 30, 23, 26, 21, 24, 5, 22, 49, 14], obtaining accurate and reliable numerical solutions for them remains a significant challenge, making new methods and strategies for their solution the subject of frequent study. The difficulty in obtaining accurate numerical approximations for a flow is often due to the high number of degrees of freedom (dof) required to resolve velocity fields asociated with high Reynolds numbers (Re) [30]. The situation becomes even more complex for flows with electric charge, which are governed by the nonlinearly coupled NSE and Maxwell equations, which is known as magnetohydrodynamic (MHD) flow. This thesis is a study of new numerical methods and improvements to existing methods for improving the accuracy for computed solutions of the NSE and MHD.

A widely held belief in computational fluid dynamics (CFD) is that with greater fidelity to a physical model comes greater numerical accuracy, especially over longer time intervals. Conservation of physical quantities is an integral component to the physical fidelity of the NSE, and also MHD. Despite the relationship between physical fidelity and numerical accuracy, most schemes ensure only the conservation of energy because typically it is not easy to devise such a scheme. In this thesis we look to further the development of dual-conserving schemes which conserve at least a second integral quantity along with energy. Arakawa's energy and enstrophy conserving scheme

[1] and related extensions for the 2D NSE [19], the energy and potential enstrophy conserving schemes developed by Arakawa and Lamb as well as those of Navon [2, 41, 42] for the shallow water equations provide support for conserving a second physical quantity in addition to energy is worthwhile. The recent work of J.-G. Liu and W.Wang for the axisymmetric 3D NSE [36] and most recently L. Rebholz for the 3D NSE [47] suggests that physical fidelity can be improved thru the conservation of both energy and helicity. Dual conservation of physical quantities usually comes with an additional computational cost forcing those who implement enhanced physical schemes to weigh the trade-offs between fidelity and computational cost.

Scott-Vogelius (SV) elements create such a dilemma in that SV elements guarantee pointwise mass conservation but at the cost of mild-mesh restrictions, a more costly linear solve, and the required use of higher order elements in 3D. In Chapter 2, we provide a review of SV elements and compare them to the popular Taylor-Hood (TH) elements. Additionally we will propose methods which have the promise of improving mass conservation for TH elements at a lower computational cost as well as approaches for reducing the additional cost of SV elements.

Chapter 3 introduces an extension of the 3D NSE energy and helicity scheme [47] for use outside of the periodic setting. It exhibits properties that can reduce the effect that Bernoulli Pressure, $P = \frac{1}{2}|\mathbf{u}|^2 + p$, has on the error in the velocity approximation, $\mathbf{u}_h$. For common element choices the a priori error estimate for the velocity error contains the term $\psi = C\nu^{-1}\inf_{q_h \in Q_h} \|p - q_h\|$, however when p is replaced with P, ψ can become poorly scaled when the kinematic viscosity, $\nu = \mathrm{Re}^{-1}$, is very small and the velocity contains boundary layers [21, 34], diminishing the quality of $\mathbf{u}_h$. To improve the scaling of ψ, we introduce $\gamma\nabla(\nabla\cdot\mathbf{u})$ into the momentum equation. Known to many as grad-div stabilization [10, 31, 37], we compare two grad-div stabilizing terms and analyze how they effect the error estimate as well as the dual conservation of energy and helicity. Numerical experiments conducted using the Ethier-Steinman problem suggest that the proposed alternative grad-div stabilizing term is a slight improvement over the usual term with respect to velocity and helicity error, but either is a dramatic improvement over a direct, energy-conserving-only scheme.

While the incompressibility condition is important to the NSE it is doubly important to the field of magnetohydrodynamics (MHD), where there is not only the familiar continuity equation

for velocity, $\nabla \cdot \mathbf{u} = 0$, but also a solenoidal condition on the magnetic field, $\nabla \cdot \mathbf{B} = 0$. The study of MHD pertains to the interaction of fluid flow and magnetic fields which are often used to heat, pump, stir and levitate liquid metals in the metallurigical industries [11]. In order for the interaction of the fluid and magnetic field to be substantial the fluids in question must be conductors and non-magnetic, which includes liquid metals, plasmas and strong electrolytes. At one time MHD was perhaps best known for its association with colossal failures in power generation [11], however in the last 30 years MHD has been found to be pertinent to the flow of liquid sodium coolants in fast-breeder reactors, and the confinement of hot plasma thru magnetic forces during controlled thermonuclear fusion. Via the extension of the philosophy of *enhanced physics*, we were able to develop a numerical scheme for MHD flows which possesses both dual-conservation, energy and cross-helicity, and enforces pointwise incompressibility $\|\nabla \cdot \mathbf{u}_h\| = \|\nabla \cdot \mathbf{B}_h\| = 0$.

This thesis is arranged as follows. Chapter 2 provides an introduction to the Scott-Vogelius elements and some preliminary comparisons of results against Taylor-Hood elements. Chapter 3 presents the extension of the energy-helicity conserving scheme to the case of wall-bounded flows. In chapter 4, we study the SV elements for approximating solutions to the NSE, and establish an important connection between these solutions and those found using Taylor-Hood elements and grad-div stabilization. Chapter 5 derives and analyzes a new scheme for MHD flows that conserves energy and cross-helicity globally, and enforces incompressibility of the magnetic and velocity fields pointwise. A rigorous stability and convergence analysis of the scheme is presented.

Chapter 2

Scott-Vogelius Elements

Our interest in the Scott-Vogelius elements stems from the property, for $(\mathbf{X}_h, Q_h) = (\mathbf{P}_k, P_{k-1}^{disc})$ with $k \geq dim$, and if the mesh is constructed as a barycenter refinement of a quasi-uniform mesh, this element pair is LBB stable and satisfies

$$\nabla \cdot \mathbf{X}_h \subset Q_h^{SV}. \tag{2.1}$$

As a result of (2.1) when we consider the weak formulation of the incompressibility condition

$$(q_h, \nabla \cdot \mathbf{u}_h) = 0,$$

we can select our test function, q_h, such that

$$q_h = \nabla \cdot \mathbf{u}_h \Rightarrow \|\nabla \cdot \mathbf{u}_h\|^2 = 0.$$

In general, a naive selection for the discrete pressure space can introduce numerical instability into the approximation. More specifically if Q_h is chosen too large in relation to the discrete velocity space, such that if $\Pi_{L^2}^{Q_h}$ denotes the L^2 projection operator into Q_h, the discrete divergence operator $\text{div}_h : \mathbf{X}_h \to Q_h$ with $\text{div}_h \mathbf{v}_h := \Pi_{L^2}^{Q_h}$ is not surjective and equivalently LBB is not satisfied. The absence of LBB removes the usual stability condition on the pressure permitting erroneous oscillations to appear which ultimately diminishes the quality of $\mathbf{u}_h$. The idea of using $(\mathbf{P}_k, P_{k-1}^{\text{disc}})$

as an element pair is first attributed to [52], recent extensions of SV elements in [58, 34, 6] to Stokes flow, Steady NSE equations and Oseen equations support our investigation into the merits of SV element approximations for the time dependent incompressible NSE equations.

We note that Scott-Vogelius elements are implemented using a Clough-Tocher macro-element to tessellate all of Ω. This is usually done by taking an existing quasi-uniform conforming mesh and creating a Clough-Tocher macro-element out of each element in the tessellation. In practice we have not found this to be a considerable hurdle, while there does not appear to be any commercial software which explicitly offers a barycentric refinement we feel that the majority of scientists will be able to implement the mesh restriction fairly easily. The barycentric refinement is necessary to ensure LBB holds [34, 58], in fact any refinement in which a 4-way split is achieved will have the property of LBB stability, refining about the barycenter helps to ensure a balanced mesh while also simplifying the proof given in [58].

Pointwise mass-conservation for the NSE has also been achieved with Discontinuous Galerkin (DG) schemes such as those in [8, 9]. We note that these proposed DG schemes make the assumption that $\mathbf{u} \in \mathbf{H}(\mathrm{div})$ as opposed to $\mathbf{H}^1(\Omega)$ and often utilize a post processing routine to achieve pointwise mass-conservation. Furthermore DG methods are often difficult to extend to existing legacy codes for the NSE where as SV elements have the promise of obtaining pointwise mass conservation without the headaches of extending existing routines to DG. Results for similar element pairs that satisfy LBB and $\nabla \cdot \mathbf{X}_h \subseteq Q_h$ are presented in [59, 60]. We feel SV elements are advantageous to the element pairs proposed in [59, 60] as "serious" computing is going to be done with triangles and tetrahedra opposed to quadrilaterals and parallelepipeds, while the Powell-Sabin splits proposed in [60] enforce a stricter mesh restriction and have yet to be extended to three dimensions.

In the sequel, we will compare SV elements to TH elements. These elements differ in structure only in that the pressure space for TH elements is continuous, although the TH element has less restrictions in order to be LBB stable. Hence, on the same mesh, the $\mathbf{X}_h$ space is the same for both elements, but Q_h is not, and so will be labeled with superscripts to distinguish. Moreover, the subspace of discretely divergence free functions in $\mathbf{X}_h$, called $\mathbf{V}_h$ and defined by

$$\mathbf{V}_h := \{\mathbf{v}_h \in \mathbf{X}_h \ : \ (\nabla \cdot \mathbf{v}_h, q_h) = 0 \ \forall q_h \in Q_h\},$$

will also differ and be similarly labeled.

An unanticipated advantage to utilizing Q_h^{SV} is competitive assembly despite the increase in $\dim(Q_h)$, which can be attributed to the lack of dependence SV elements have on neighboring elements when the **B** block is assembled. Assembly can also be improved in the **A** block as we can handle the nonlinearity more efficiently due to pointwise mass conservation. For high-level computing assembly is usually deemed negligible with respect to computational cost when compared with the cost of the linear solve. With the $\dim(Q_h^{SV}) > \dim(Q_h^{TH})$ SV elements require a significant bump in computational cost on equivalent meshes. The extent of the additional cost in the linear solve is being actively studied, however we do not think it is unreasonable for preconditioners similar to those presented in [3, 39, 4, 13, 15] to reduce the additional cost as the **A** block is identical for both SV and TH elements. In addition to computational cost there is also a concern for the resulting velocity error as

$$\dim(\mathbf{V}_h) = \dim(\mathbf{X}_h) - \dim(Q_h).$$

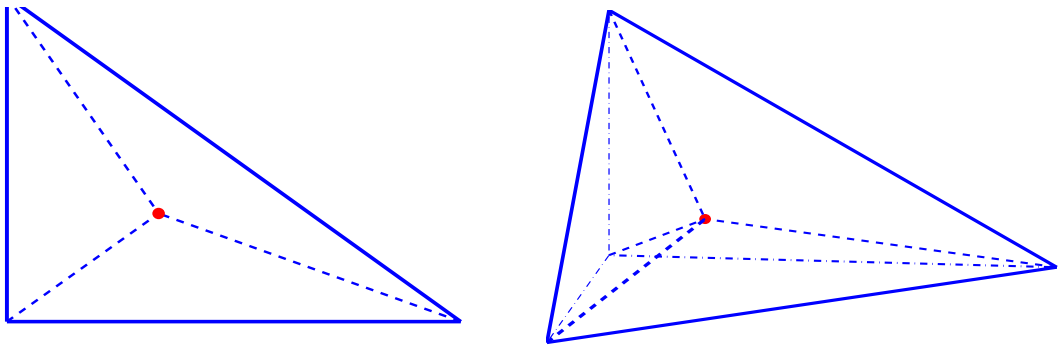

Figure 2.1: (LEFT) 2D and (RIGHT) 3D Clough-Tocher macro-element, shown with dashed lines representing barycenter refinements

2.0.1 Preliminary numerical experiments

In the forthcoming numerical experiments for Stokes Flow and the time dependent incompressible NSE we attempt to compare $(\mathbf{P}_k, P_{k-1})$ elements with $(\mathbf{P}_k, P_{k-1}^{\text{disc}})$. When constructing these experiments we wanted to highlight the advantages of SV elements and the low quality of

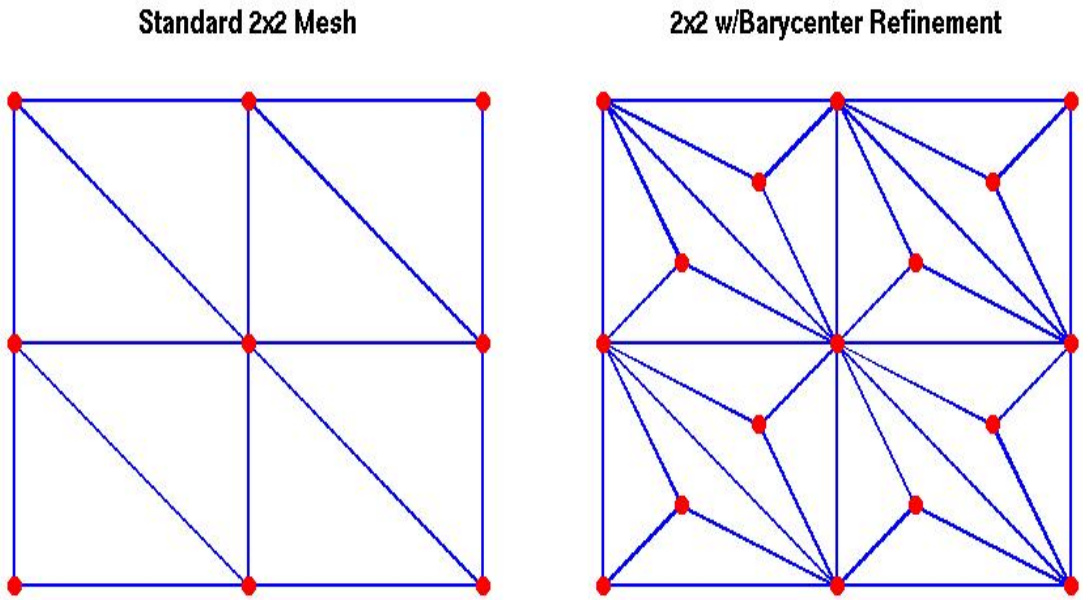

Figure 2.2: (LEFT) 2D conforming mesh and (RIGHT) mesh resulting from barycentric refinement.

the enforcement of mass conservation seen in TH element approximations. For the Stokes Flow experiment we attempted to compare SV elements with TH elements when similar total dof are used. The time-dependent examples for both two and three dimensional flow compare results for the same mesh. Despite the advantage in the total dof since $\mathbf{V}_h^{SV} \subset \mathbf{V}_h^{TH}$, SV elements are already at a competitive disadvantage with respect to L^2 error on the same mesh. With that said, one should not come away from the forthcoming comparisons with the impression TH elements are incapable of resolving the velocity field for a comparable total dof.

2.0.1.1 Stokes Flow

We first consider the Stokes Equations on $\Omega = (-1,1)^3$:

$$-\nu\Delta\mathbf{u} + \nabla p = \mathbf{f}, \tag{2.2}$$

$$\nabla \cdot \mathbf{u} = 0. \tag{2.3}$$

We can form a finite element scheme for the solution of the Stokes problem:

$$\text{find } (\mathbf{u}_h, p_h) \in (\mathbf{X}_h, Q_h) \text{ s.t.} \tag{2.4}$$

$$\nu(\nabla \mathbf{u}_h, \nabla \mathbf{v}_h) - (\nabla \cdot \mathbf{v}_h, p_h) = \mathbf{f}, \ \forall \mathbf{v}_h \in \mathbf{X}_h, \tag{2.5}$$

$$(\nabla \cdot \mathbf{u}_h, q_h) = 0, \ \forall q_h \in Q_h. \tag{2.6}$$

Choosing $\mathbf{u} = [\cos(N\pi z), \sin(N\pi z), \sin(N\pi x)]$ and $p = \cos(N\pi(x+y))$ gives us a nontrivial Stokes problem and helps us illustrate how poor mass conservation can be when using Taylor-Hood elements.

Table 2.1: Sample Problem Velocity Error, $\nu = 1.0$..

Elem.	N	$\dim(\mathbf{V}_h)$	L^2 Error	$\mathbf{H}^1$ Error	$\|\text{div } \mathbf{u}_h\|$
TH32	2	31620	0.0058	0.1914	0.1549
SV32	2	8511	3.89e-4	0.0071	5.151e-14
TH32	8	31620	0.0678	1.4555	0.4165
SV32	8	8511	0.1021	2.029	4.795e-14

The results from Table 2.1 suggest that Taylor-Hood elements can have respectable velocity error for a simple flow while doing a poor job of conserving mass. For the $N = 2$ case, the Scott-Vogelius solution has better L^2 and H^1 velocity errors. However, for $N = 8$, Taylor-Hood solutions have slightly better errors. Although not shown, from the table the $H(div)$ norm can be calculated, and the Scott-Vogelius solution would be better in this norm for $N = 8$.

We now consider the Stokes problem with pressure stabilization

$$\nabla p_\epsilon - \nu \Delta \mathbf{u}_\epsilon = \mathbf{f}, \ \text{ on } \ \Omega, \tag{2.7}$$

$$\text{div } \mathbf{u}_\epsilon + \epsilon p_\epsilon = 0 \ \text{ on } \ \Omega. \tag{2.8}$$

$$\tag{2.9}$$

which has the following weak formulation,

$$\begin{aligned} &\text{find } (\mathbf{u}_h, p_h) \in (\mathbf{X}_h, Q_h) \text{ s.t.} \\ -(p_\epsilon, \nabla \cdot q_h) + \nu(\nabla \mathbf{u}_\epsilon, \mathbf{v}_h) &= \mathbf{f},\ \forall \mathbf{v}_h \in \mathbf{X}_h, \qquad (2.10) \\ \text{div } \mathbf{u}_\epsilon + \epsilon p_\epsilon &= 0, \forall q_h \in Q_h. \qquad (2.11) \end{aligned}$$

Table 2.2: Sample Problem Velocity Error, $\nu = 1.0$. w/Pres. Stab., $\epsilon =$ 1.0e-6.

Elem.	N	$\dim(\mathbf{V}_h)$	L^2 Error	$\mathbf{H}^1$ Error	$\|\text{div } \mathbf{u}_h\|$
TH32	2	31620	0.0058	0.1914	0.1549
SV32	2	8511	3.890e-4	0.0071	2.1391e-6
TH32	8	31620	0.0678	1.4539	0.4165
SV32	8	8511	0.1022	2.0298	1.971e-6

The Stokes results in Tables 2.1 & 2.2 were computed for $(\mathbf{P}_3, P_2^{\text{disc}})$ elements on a $4 \times 4 \times 4$ mesh with barycenter refinement resulting in 39,231 total dof, 23,871 velocity dof and 15,360 pressure dof. $(\mathbf{P}_3, P_2)$ results were generated on a $6 \times 4 \times 4$ mesh with barycenter refinement giving us 39,486 total dof, 23,871 vel. dof and only 3,933 pres. dof. These results suggest that Scott-Vogelius elements drastically improve mass-conservation for similar computational cost, while also improving the conditioning of the linear system in the presence of pressure stabilization. Pressure stabilization does require additional assembly and storage of another matrix block but relative to the assembly of the $\mathbf{A}$ block the extra work is not significant. Additionally pressure stabilization allows us to drop the condition on the pressure nodes (i.e. Dirichlet, $\int p\ dx = 0$). The results for Stokes Flow further support the concept that we cannot expect Scott-Vogelius elements to provide an improvement in error in the L^2 or H^1 norms, even when the total dof are comparable as $\dim(\mathbf{V_h}^{SV}) < \dim(\mathbf{V_h}^{TH})$. However, we can expect improvement in error in the $H(div)$ norm.

2.0.2 Time Dependent NSE results

For time dependent flow we use the following Crank-Nicholson Galerkin temporal-spatial discretization,

$$\text{find } (\mathbf{u}_h, p_h) \in (\mathbf{X}_h, Q_h),$$

$$(\mathbf{u}_h^0, \mathbf{v}_h) + (\lambda, \nabla \cdot \mathbf{v}_h) + (\nabla \cdot \mathbf{u}_h^0, q_h) = (\mathbf{u}_0, \mathbf{v}_h),\ \forall \mathbf{v}_h \in \mathbf{V}_h, \tag{2.12}$$

$$\frac{1}{\Delta t}(\mathbf{u}_h^{n+1} - \mathbf{u}_h^n, \mathbf{v}_h) - (p_h^{n+\frac{1}{2}}, \nabla \cdot \mathbf{v}_h) + \nu(\nabla \mathbf{u}_h^{n+\frac{1}{2}}, \nabla \mathbf{v}_h)$$
$$+(\mathbf{u}_h^{n+\frac{1}{2}} \cdot \nabla \mathbf{u}_h^{n+\frac{1}{2}}, \mathbf{v}_h) + \frac{1}{2}((\nabla \cdot \mathbf{u}_h^{n+\frac{1}{2}})\mathbf{u}_h^{n+\frac{1}{2}}, \mathbf{v}_h) = (\mathbf{f}^{n+\frac{1}{2}}, \mathbf{v}_h),\ \forall \mathbf{v}_h \in \mathbf{X}_h, \tag{2.13}$$

$$(q_h, \nabla \mathbf{u}_h^{n+\frac{1}{2}}) = 0,\ \forall q_h \in Q_h, \tag{2.14}$$

where $n = 1, 2, \ldots, M = T/\Delta t$.

2.0.2.1 Time Dependent Flow around a cylinder

2D flow around a cylinder is a well studied benchmark problem [29, 31, 27, 50]. In this experiment Ω is defined by $(0, 2.2) \times (0, 0.41)$ representing a thin channel with flow in the positive x direction with a circle of radius 0.05 centered at $(0.2, 0.2)$. No-slip boundary conditions are applied on the top and bottom of the channel along with the boundary of the cylinder.

The time dependent inflow and outflow profiles are enforced on the left and right boundaries:

$$\mathbf{u}(0, y, t) = \mathbf{u}(2, 2, y, t) = \frac{6}{0.41^2}[\sin(\pi t/8) y(0.41 - y), 0], \quad 0 \le y \le 0.41. \tag{2.15}$$

The forcing is set to zero, $\mathbf{f} = \mathbf{0}$ and the viscosity, $\nu = 0.001$ proving a time dependent Reynolds number, $0 \le \mathrm{Re}(t) \le 100$. The initial condition is $\mathbf{u}^0 = \mathbf{0}$, while we approximate up to $T = 8$ with a time step of $\Delta t = 0.01$.

An accurate prediction of the velocity field will predict a vortex street forming behind the cylinder at $t = 4$ and a fully formed vortex street by $t = 7$. We note that in addition to the velocity field we will be measuring the quality of div $\mathbf{u}_h$. We compared Scott-Vogelius and Taylor-Hood elements using the mesh depicted in Figure 2.3 resulting in 6,578 velocity dof for each element type

with 4,797 pres. dof for SV elements and only 845 pressure dof for TH elements. A plot of the velocity results for each element choice at $t = 7$ is presented in Figure 4.2, where we see the vortex street start to breakdown when TH elements are used. Figure 4.3 illustrates that even with the a proper velocity field, TH elements are doing a poor job of conserving mass as time increases. The performance discrepancy displayed in this experiment is indicative of the lack of dof used for the TH elements but also the lack of fidelity to incompressibility. We point out that for similar dof on more refined meshes we were able to ascertain the proper velocity profile using TH elements however the quality of the mass conservation remained poor.

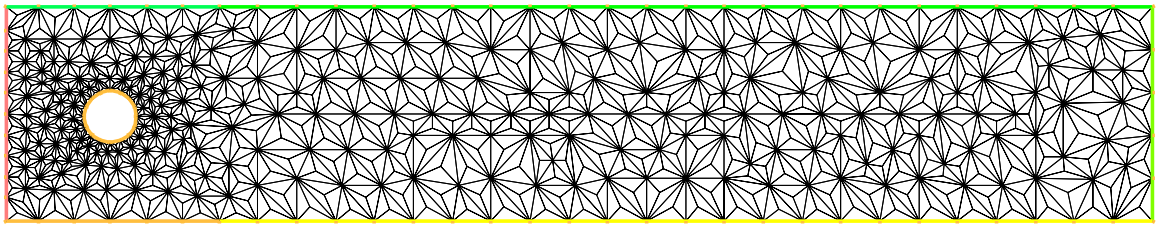

Figure 2.3: Shown above is the mesh used for the flow around a cylinder computations in this experiment.

2.0.2.2 Time Dependent Flow over a Step

Channel flow over a 2D backward and forward facing step has been studied extensively in [10, 23, 28, 31, 33]. $\Omega = (0, 40) \times (0, 10)$ with a 1×1 step removed at the $x = 5$ coordinate. No-slip boundary conditions are applied to the step as well as the top and bottom walls of the channel. On the inflow and outflow faces of the channel a parabolic condition is enforced

$$\mathbf{u} = \frac{1}{25} \left[y(10 - y), 0 \right].$$

We employ a viscosity of $\nu = 1/600$ and simulate the flow by initializing without the step and then inserting the step into a smooth flow and run until $T = 40$ with a time-step of $\Delta t = 0.01$. The mesh used to compute the solution is shown in Figure 2.6 and provides 7,414 velocity dof with $5,418$ and 951 pressure dof for SV and TH elements respectively.

Velocity field streamlines with speed contours are shown at $T = 10,\ 20,\ 30$ and 40 for the SV element solution in Figure 2.7 and for TH elements in Figure 2.8. The SV element solution forms and sheds eddies, has a smooth velocity profile, and in general agrees with the "true" solution found in [32], which utilizes 27,228 total dof. The TH element solution is observed to be slightly underresolved. Although it forms and sheds eddies, by $T = 40$, the eddies behind the step appear to be stretching instead of detaching. Moreover, the velocity field is developing oscillations evident in the speed contours. Figure 2.9 displays a poor quality of mass conservation for TH elements comparable to what we have observed in the previous experiments.

2.0.2.3 3D Lid -Driven Cavity

The Lid-driven cavity problem is a popular benchmark problem described in greater detail within [57, 44]. $\Omega = (-1, 1)^3$ with no-slip boundary conditions applied to all of the walls except on the boundary where $z = 1$, the lid. The lid has a profile of $[1, 0, 0]$ which is imposed on $\mathbf{u}$ at the boundary. Viscosity at $\nu = 1/50$, yields a Reynolds number, $\mathrm{Re} = 2 \cdot 50 = 100$ while we impose that $\mathbf{u}^0 = \mathbf{0}$. The mesh for this experiment is displayed in Figure 2.10 and has 57,804 velocity dof with 6,360 pressure dof for TH elements and 37,840 pressure dof for SV type. The problem is solved directly for the steady solution with a Newton iteration taking 7 iterations to converge to a tolerance of 10^{-10} for each element type. Figures 2.11 and 2.12 display vector fields which closely resemble those in [57, 44] while Figure 2.13 supports a near-accurate flow for both elements. However, as we have seen in the previous experiments the mass conservation for TH elements, depicted in Figure 2.12, is poor especially in the corners for each midplane.

2.0.3 Discussion of Results

The numerical results appear to support the use of SV elements because of their ability to provide pointwise mass conservation. However, TH elements were underresolved in some of the experiments and not incapable of resolving the velocity field on fine meshes for comparable computational cost, still the concern with implementing TH elements comes from the low quality in mass conservation even when the velocity field appears to be correct as we saw in the driven cavity

experiment, thus how can any $\mathbf{u}_h$ approximation be expected to have any physical meaning when the quality of mass conservation is so poor. Furthermore, we feel these experiments support the philosophy of *enhanced physics* as early on TH elements perform at a reasonable level with respect to the velocity profiles for both the 2D cylinder and 2D step problem but ultimately breakdown as time increases despite the fact that $\dim(\mathbf{V}_h^{TH}) > \dim(\mathbf{V}_h^{SV})$.

We feel there is promise in extending the preliminary convective SV results given in this section to not only rotational NSE schemes but any FEM scheme which enforces incompressibility.

Additionally we are interested in comparing the mass conservation results obtained thru SV elements with those obtained for TH elements with grad-div stabilization in the momentum equation on a barycenter-refined mesh. If a relationship between these basis functions can be established it could aid greatly in reducing the computational cost of improved mass conservation for NSE computations.

Finally we mention that we are interested in expanding on the physical problems presented in this section (i.e. channel flow and two faced step problems). The current computer codes being used to generate the results given in this report will be extended to parallel routines that will allow for us to test our analytical results in a more efficient fashion and comment on existing preconditioners for the NSE and their ability to offset the computational costs associated with SV elements.

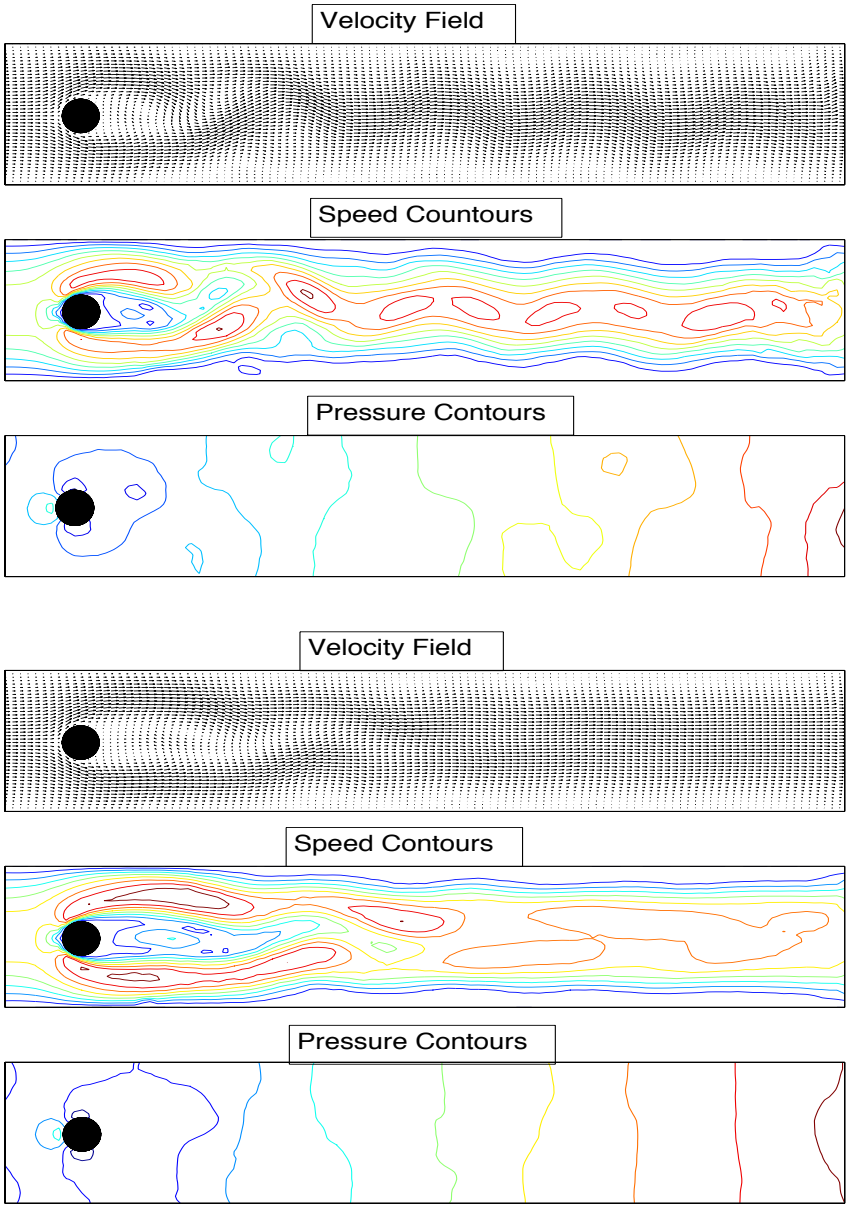

Figure 2.4: Shown above are the t=7 velocity fields, speed contours, and pressure contours plots for solution obtained using Scott-Vogelius elements (top) Taylor-Hood elements (bottom).

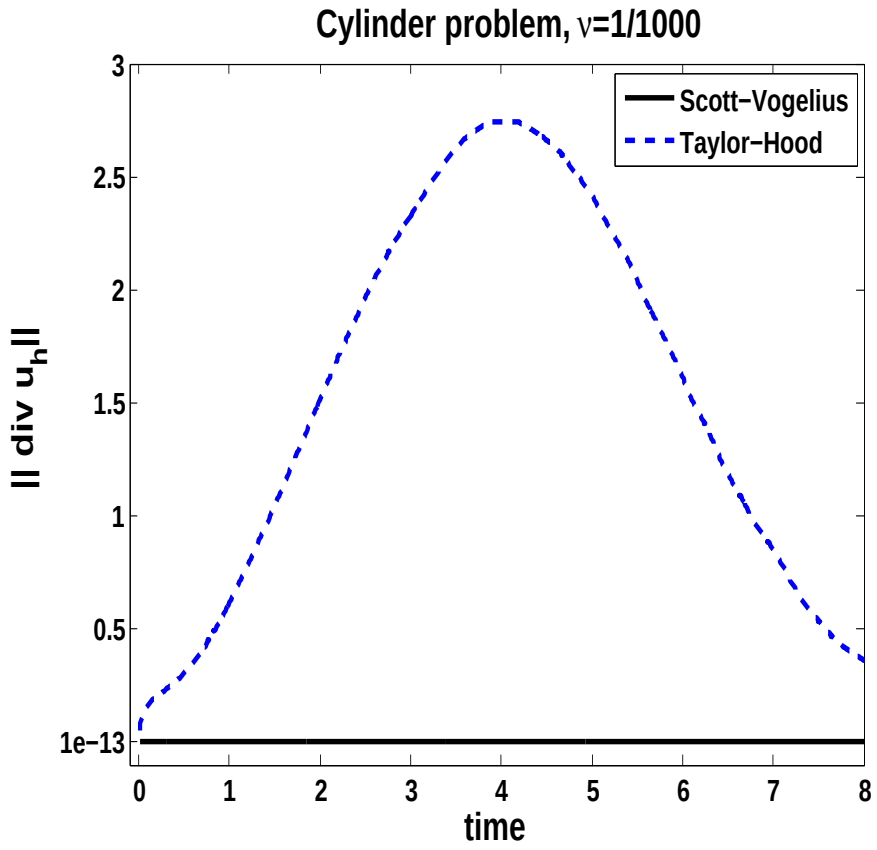

Figure 2.5: Shown above are the plots of $\|\nabla \cdot \mathbf{u}_h^n\|$ vs. time for the SV and TH solutions for the 2D cylinder problem.

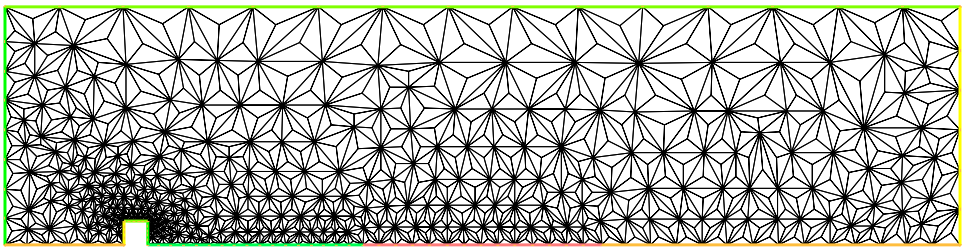

Figure 2.6: The barycenter-refined mesh used for the 2D step computations

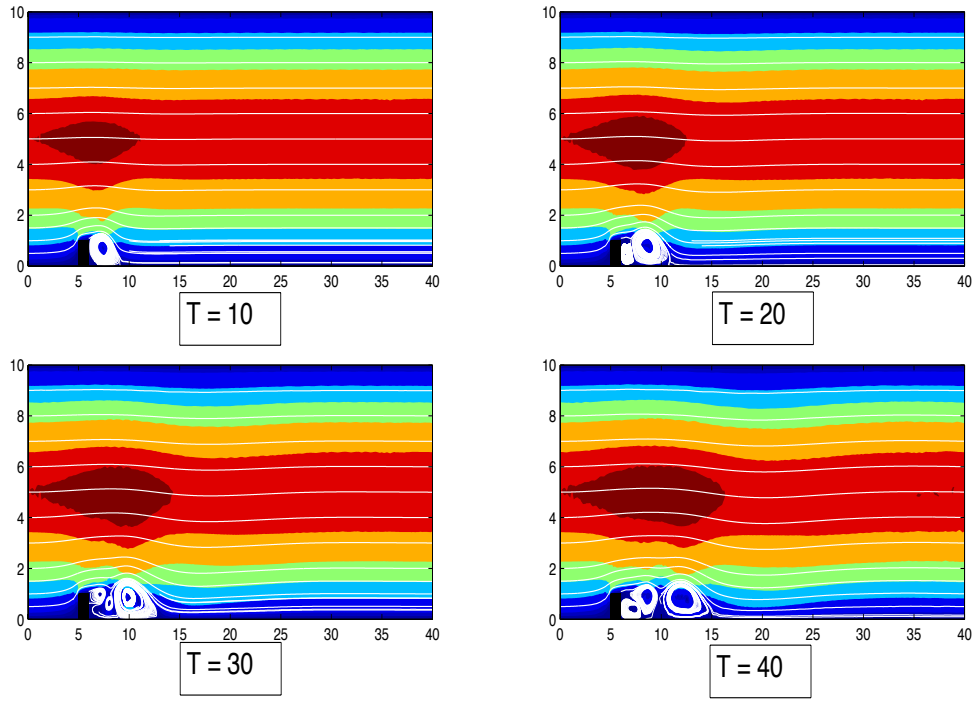

Figure 2.7: For SV elements the flow profile appears to agree with the "true" solution[32].

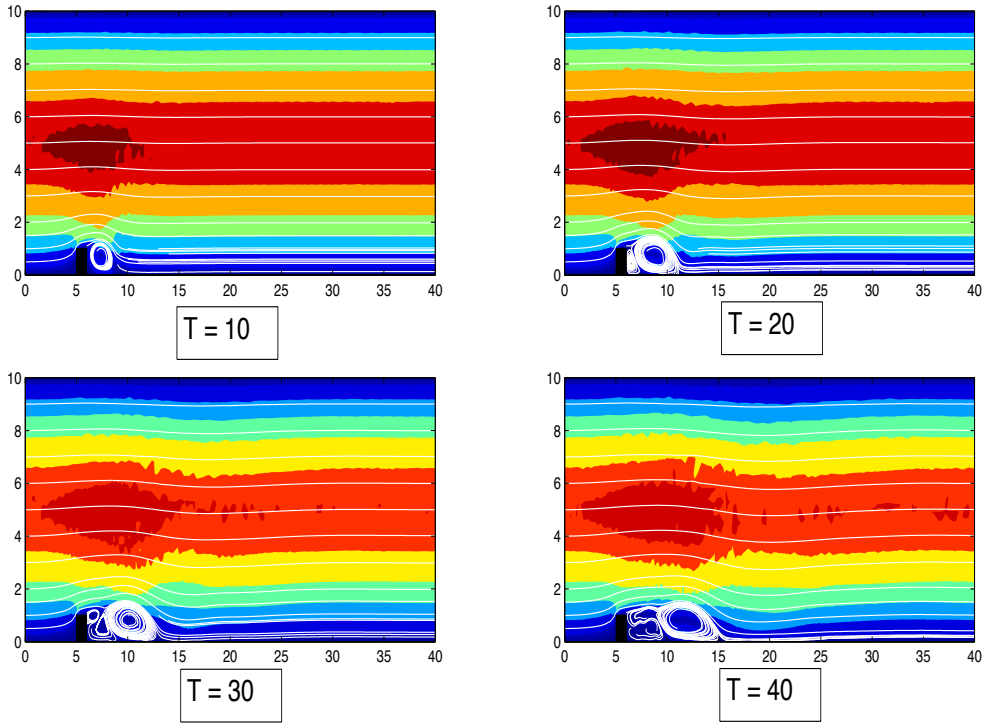

Figure 2.8: For TH elements the velocity field is underresolved and fails to shed eddies at $T = 40$.

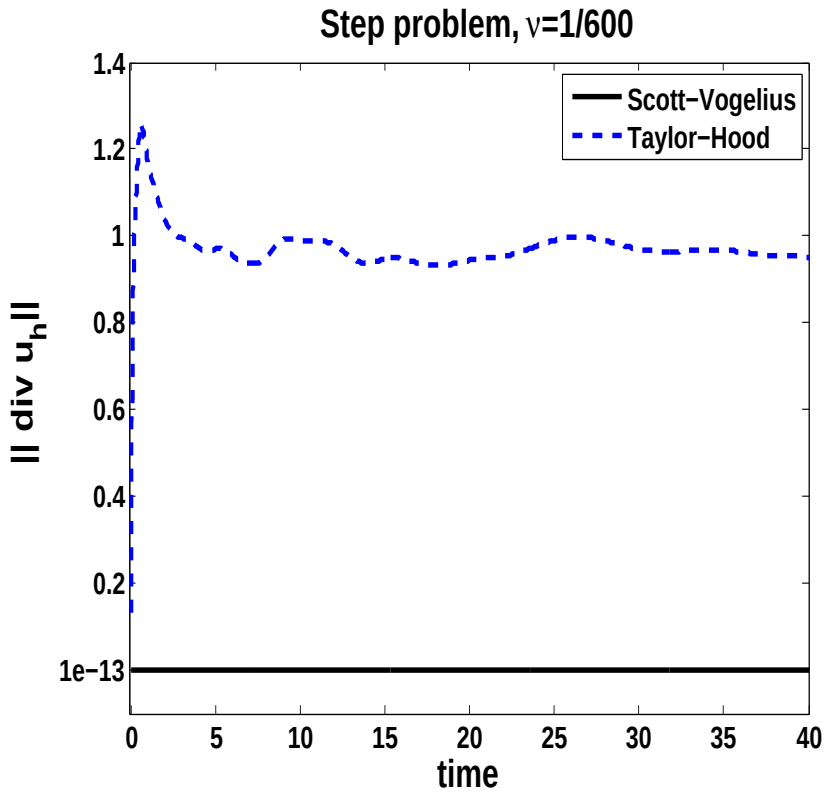

Figure 2.9: Shown above are the plots of $\|\nabla \cdot \mathbf{u}_h^n\|$ vs. time for the SV and TH solutions for the 2D step problem.

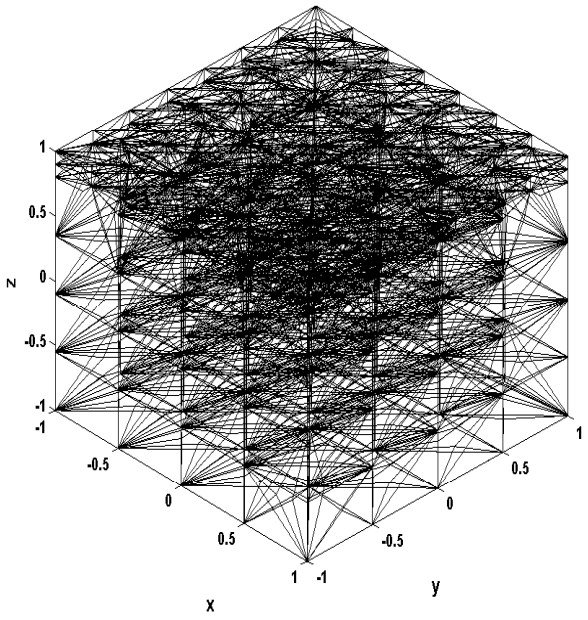

Figure 2.10: The barycenter-refined mesh used for the 3D lid-driven cavity problem.

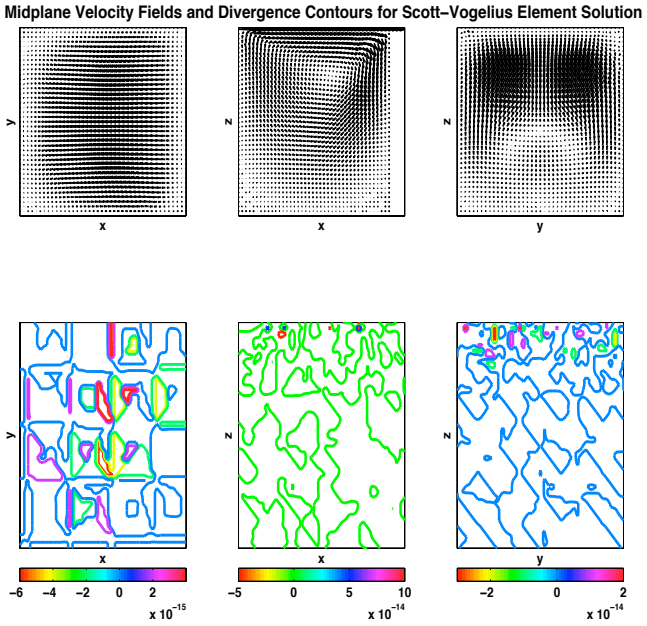

Figure 2.11: 3D lid-driven cavity results with SV elements. Note the small scale next to the color bar.

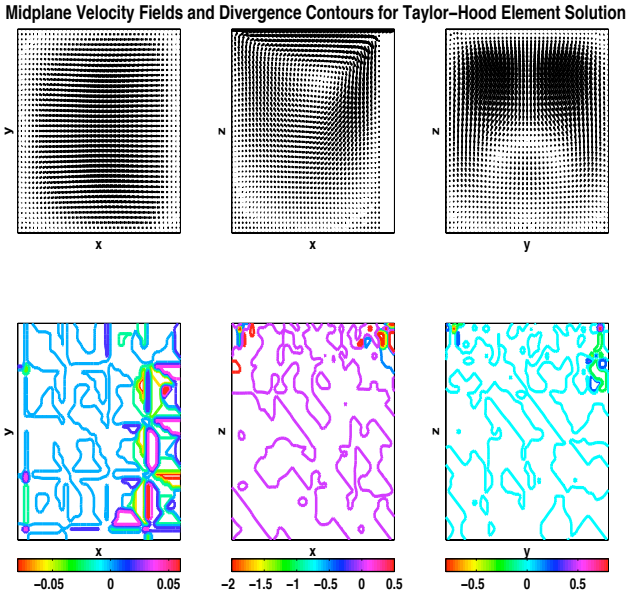

Figure 2.12: 3D lid-driven cavity results with TH elements. Note the scale next to the color bar and the contours in the corners of each midplane.

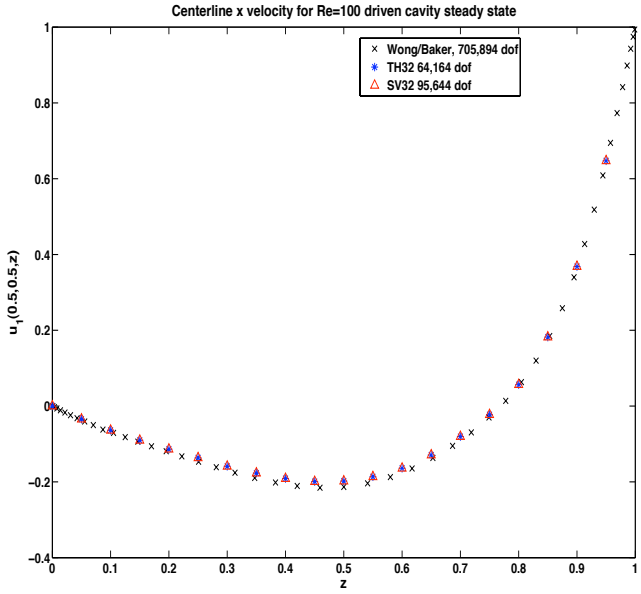

Figure 2.13: 3D lid-driven cavity results compared to "true" solution on centerline.

Chapter 3

Stable computing with an enhanced physics based scheme for the 3d Navier-Stokes equations

3.1 Introduction

This chapter extends the methodology of the enhanced-physics based scheme for the 3D Navier-Stokes equations (NSE) proposed in [47] (defined in Section 2) from its original derivation for space-periodic problems to a more general class of problems. This scheme is referred to as *enhanced-physics* because it is the only scheme that conserves *both* discrete energy and discrete helicity for the full 3D NSE. The key ingredient for the dual conservation scheme is using the rotational form of the nonlinearity with a projected vorticity, which allows the discrete nonlinearity to preserve both of the quantities. Since the (continuous) NSE nonlinearity conserves both energy and helicity, and jointly cascades them from the large scales through the inertial range to small viscosity dominated scales [7, 12], if the discrete nonlinearity does not also conserve energy and helicity it will introduce numerical error into the cascade, and bring into question the physical relevance of computed approximations.

It is a widely held belief in computational fluid dynamics (CFD) that the more *physically*

correct a numerical scheme is, the more accurate its predictions will be, especially over long time intervals. In systems of conservation laws for fluids there is typically a second integral invariant in addition to energy, and its accurate treatment in a numerical scheme generally produces more accurate simulations than do schemes that do not specifically conserve this quantity. Beginning with Arakawa's energy and enstrophy conserving scheme for the 2D NSE [1] and related extensions [19], to energy and potential enstrophy schemes pioneered by Arakawa and Lamb, and Navon, [2, 41, 42], and most recently to an energy and helicity conserving scheme for 3D axisymmetric flow by J.-G. Liu and W. Wang [36], enhanced physics based schemes have provided more accurate simulations, especially over longer time intervals.

The fundamental challenge in extending the scheme of [47] to non-periodic problems is to avoid the large errors often present when the rotational form of the nonlinearity and the Bernoulli pressure is used. In the usual a priori error analysis for the velocity approximation for the NSE, a consequence that the discrete divergence free velocity is not exactly divergence free, is a pressure error contribution

$$\frac{C}{\nu} \inf_{q_h \in Q_h} \|p - q_h\| \ , \tag{3.1}$$

where ν = 1/Reynolds number denotes the kinematic viscosity [21, 34]. For problems whose pressure gradients are small this term is often negligible. However, using the rotational form of the NSE, and introducing the Bernoulli pressure $p + \frac{1}{2}|u|^2$ can bring prominence to this term, since the gradient of the Bernoulli pressure may be large due to boundary layers in the velocity field.

Following recent work in [31, 37, 10], a natural way to mitigate the pressure's error influence on the velocity approximation is to introduce grad-div stabilization. As we show, this reduces the effect of the Bernoulli pressure error. In the interest of physical fidelity, we also introduce a modified grad-div stabilization having the same effect on the error, but with less impact on the energy balance. Computational results show a slight improvement when this alternate stabilization is used instead of usual grad-div stabilization.

This chapter is arranged as follows. Section 2 presents mathematical preliminaries and notation, and defines the scheme studied in the remainder of the chapter. Section 3 is a study of stability and conservation laws for the scheme, and Section 4 presents a rigorous convergence

analysis. Section 5 shows a numerical example which clearly illustrates the advantage of the scheme. Concluding remarks are given in Section 6.

3.2 Mathematical Preliminaries

We assume that Ω denotes a polyhedral domain in $\mathbb{R}^3$. The $L^2(\Omega)$ norm and inner product are denoted by $\|\cdot\|$ and $(\cdot,\cdot)$. Likewise, the $L^p(\Omega)$ norms and the Sobolev $W_p^k(\Omega)$ norms are denoted $\|\cdot\|_{L^p}$ and $\|\cdot\|_{W_p^k}$, respectively. For the semi-norm in $W_p^k(\Omega)$ we use $|\cdot|_{W_p^k}$. H^k is used to represent the Sobolev space $W_2^k(\Omega)$, and $\|\cdot\|_k$ denotes the norm in H^k. For functions $v(x,t)$ defined on the entire time interval $[0,T]$, we define $(1 \le m < \infty)$

$$\|v\|_{\infty,k} := \operatorname*{ess\,sup}_{[0,T]} \|v(t,\cdot)\|_k\,, \text{ and } \|v\|_{m,k} := \left(\int_0^T \|v(t,\cdot)\|_k^m\, dt\right)^{1/m}.$$

For the analysis, we assume no slip (i.e. homogeneous Dirichlet) boundary conditions for velocity and therefore use as our velocity and pressure spaces

$$X := (H_0^1(\Omega))^d,\ Q := L_0^2(\Omega)\,,$$

where Q is denoting the *mean zero* subspace of $L^2(\Omega)$.

We use as the norm on X the H^1 seminorm which, because of the boundary condition, is a norm, i.e. for $v \in X$, $\|v\|_X := \|\nabla v\|$. We denote the dual space of X by $X^\star$, with the norm $\|\cdot\|_\star$. The space of divergence free functions is defined by

$$V := \{v \in X :\ (\nabla\cdot v, q) = 0\ \ \forall q \in Q\}\,.$$

We denote conforming velocity, pressure finite element spaces based on a regular tetrahedralization, $\mathcal{T}_h$, of Ω (with maximum tetrahedron diameter h) by

$$X_h \subset X,\ Q_h \subset Q.$$

We assume that $X_h,\ Q_h$ satisfy the usual inf-sup condition necessary for the stability of the pressure, i.e.

$$\inf_{q_h \in Q_h} \sup_{v_h \in X_h} \frac{(q_h, \nabla \cdot v_h)}{\|q_h\| \, \|v_h\|_X} \,. \tag{3.2}$$

Specifically, we assume that (X_h, Q_h) is made of $(P_k, P_{k-1}),\ k \geq 2$ velocity pressure elements. Thus we have, for a given regular tetrahedralization $\mathcal{T}_h$,

$$\begin{aligned} X_h &:= \left\{ v_h : v_h|_e \in P_k(e),\, \forall_{e \in \mathcal{T}_h},\, v_h \in [C^0(\overline{\Omega})]^3, v_h|_{\partial\Omega} = 0 \right\}, \\ Q_h &:= \left\{ q_h : q_h|_e \in P_{k-1}(e),\, \forall_{e \in \mathcal{T}_h},\, q_h \in C^0(\overline{\Omega}),\, q_h \in L^2_0(\Omega) \right\} . \end{aligned}$$

The discretely divergence free subspace of X_h is

$$V_h = \{ v_h \in X_h : (\nabla \cdot v_h, q_h) = 0 \ \ \forall q_h \in Q_h \} \,.$$

We also use a more general space for the discrete vorticity space. Even though the velocity satisfies homogeneous Dirichlet boundary conditions, it is believed to be inappropriate to enforce homogeneous Dirichlet boundary conditions for the vorticity. A more physically consistent boundary condition is instead a no-slip boundary condition *along* the boundary, and hence we define the space

$$W_h := \left\{ v_h : v_h \in [C^0(\Omega)]^3, \forall_{e \in \mathcal{T}_h} (v_h)_{|e} \in P_k(e), v_h \times n|_{\partial\Omega} = 0 \right\} \supset X_h \,.$$

We use $t^n := n\Delta t$, and for both continuous and discrete functions of time

$$v^{n+\frac{1}{2}} := \frac{v((n+1)\Delta t) \, + \, v(n\Delta t)}{2} \,.$$

3.2.1 Enhanced-physics based numerical schemes

We study three variations of the enhanced-physics based scheme of [47] extended to homogeneous Dirichlet boundary conditions for velocity. The first is a direct extension of the scheme to homogeneous boundary conditions. The second scheme adds usual grad-div stabilization (see [46]), that is, it adds the term $\gamma(\nabla \cdot (u_h^{n+1} + u_h^n)/2, \nabla \cdot v_h)$ to a Crank-Nicolson scheme. This term

is derived from adding the (identically zero) term $-\gamma\nabla(\nabla\cdot u)$ at the continuous level. Discretely, this term penalizes for lack of mass conservation, and is known to reduce the effect of the pressure error on the velocity error for large Reynolds number problems [31, 37, 46]. In finite element computations of rotational form models the (Bernoulli) pressure error tends to be the dominant error source because it is as complex as the velocity but is approximated with lower degree polynomials, and its effect on the velocity error is amplified by the Reynolds number. The potential downside from using this stabilization is a change in the energy balance. However, in practice this tradeoff is worthwhile.

In the interest of physical fidelity to the energy balance, in the third scheme we introduce an alternative stabilization that provides the same effect on reducing the effect of the pressure error on the velocity error, but with minimal impact on the physical energy balance (Section 3). The added stabilization term arises by adding the (also identically zero) term $-\gamma\nabla(\nabla\cdot u_t)$ at the continuous level, leading to the term $\gamma\frac{1}{\Delta t}(\nabla\cdot(u_h^{n+1}-u_h^n),\nabla\cdot v_h)$ in the FEM formulation. The computational results (Section 5) from using this stabilization show an improvement in accuracy over the usual grad-div stabilization for our test problem. However, we note that for steady problems this term will not have a stabilizing effect since it will be trivially zero.

There has been recent work done to optimally choose the constant γ that scales the stabilization term. Herein, we simply choose $\gamma = 1$ in the computations, which the analysis suggests is an appropriate choice. However, one could also choose this parameter element-wise, which would lead to better results [43]. We leave optimal parameter choice for these schemes as an interesting topic of future study.

Algorithm 3.2.1 (Enhanced-physics based schemes for homogeneous Dirichlet boundary conditions)**.** *Given a time step $\Delta t > 0$, finite end time $T := M\Delta t$, and initial velocity $u_h^0 \in V_h$, find $w_h^0 \in W_h$ and $\lambda_h^0 \in Q_h$ satisfying $\forall(\chi_h, r_h) \in (W_h, Q_h)$*

$$(w_h^0,\chi_h)+(\lambda_h^0,\nabla\cdot\chi_h) = (\nabla\times u_h^0,\chi_h), \tag{3.3}$$

$$(\nabla\cdot w_h^0, r_h) = 0. \tag{3.4}$$

Then for $n = 0, 2, ..., M-1$, *find* $(u_h^{n+1}, w_h^{n+1}, p_h^{n+1}, \lambda_h^{n+1}) \in (X_h, W_h, Q_h, Q_h)$ *satisfying* $\forall (v_h, \chi_h, q_h, r_h) \in (X_h, W_h, Q_h, Q_h)$

$$
\begin{aligned}
&(\frac{u_h^{n+1} - u_h^n}{\Delta t}, v_h) + STAB - (p_h^{n+1}, \nabla \cdot v_h) \\
&\quad + (w_h^{n+\frac{1}{2}} \times u_h^{n+\frac{1}{2}}, v_h) + \nu(\nabla u_h^{n+\frac{1}{2}}, \nabla v_h) &&= (f(t^{n+\frac{1}{2}}), v_h) && (3.5)\\
&(\nabla \cdot u_h^{n+1}, q_h) &&= 0 && (3.6)\\
&(w_h^{n+\frac{1}{2}}, \chi_h) + (\lambda_h^{n+1}, \nabla \cdot \chi_h) &&= (\nabla \times u_h^{n+\frac{1}{2}}, \chi_h) && (3.7)\\
&(\nabla \cdot w_h^{n+\frac{1}{2}}, r_h) &&= 0. && (3.8)
\end{aligned}
$$

where

$$
STAB = \begin{cases} 0 & \textit{Scheme 1} \\ \gamma(\nabla \cdot u_h^{n+\frac{1}{2}}, \nabla \cdot v_h) & \textit{Scheme 2} \\ \frac{\gamma}{\Delta t}(\nabla \cdot (u_h^{n+1} - u_h^n), \nabla \cdot v_h) & \textit{Scheme 3} \end{cases}
$$

Remark 1. *We have found it computationally advantageous to decouple the 4 equation system (3.5)-(3.8) into a velocity-pressure system (3.5)-(3.6) and a projection system (3.7)-(3.8), then solve (3.5)-(3.8) by iterating between the two sub-systems. This typically requires more iterations and linear solves to converge than solving the fully-coupled system using a Newton method. However the linear solves are much easier in the decoupled system. Note also that for the decoupled system the work required is only slightly more than a usual implicit Crank-Nicolson method (i.e. without vorticity projection) since the extra work is (relatively inexpensive) projection solves. Moreover, for nonhomogeneous boundary conditions, this decoupling leads to a simplified boundary condition for the vorticity:* $w_h = I_h(\nabla \times u_h)$ *on the boundary, where* I_h *is an appropriate interpolation operator.*

3.3 Stability, conservation laws, and existence of solutions

In this section we prove fundamental mathematical and physical properties of the 3 schemes: unconditional stability, solution existence and conservation laws. We begin with stability.

Lemma 3.3.1. *Solutions to Algorithm 3.2.1 are nonlinearly stable. That is, they satisfy:*

Scheme 1:

$$\left\|u_h^M\right\|^2 + \nu\Delta t \sum_{n=0}^{M-1} \left\|\nabla u_h^{n+\frac{1}{2}}\right\|^2 \leq \frac{\Delta t}{\nu} \sum_{n=0}^{M-1} \|f\|_*^2 + \left\|u_h^0\right\|^2 = C(data)\,. \tag{3.9}$$

Scheme 2:

$$\left\|u_h^M\right\|^2 + \Delta t \sum_{n=0}^{M-1} \left(2\gamma \left\|\nabla \cdot u_h^{n+\frac{1}{2}}\right\|^2 + \nu \left\|\nabla u_h^{n+\frac{1}{2}}\right\|^2\right) \leq \frac{\Delta t}{\nu} \sum_{n=0}^{M-1} \|f\|_*^2 + \left\|u_h^0\right\|^2 = C(data)\,. \tag{3.10}$$

Scheme 3:

$$\begin{aligned}\left\|u_h^M\right\|^2 + \gamma \left\|\nabla \cdot u_h^M\right\|^2 + \nu\Delta t \sum_{n=0}^{M-1} \left\|\nabla u_h^{n+\frac{1}{2}}\right\|^2 \\ \leq \frac{\Delta t}{\nu} \sum_{n=0}^{M-1} \|f\|_*^2 + \left\|u_h^0\right\|^2 + \gamma \left\|\nabla \cdot u_h^0\right\| = C(data)\,.\end{aligned} \tag{3.11}$$

Schemes 1,2,3:

$$\Delta t \sum_{n=0}^{M-1} \left\|w_h^{n+\frac{1}{2}}\right\|^2 \leq \Delta t \sum_{n=0}^{M-1} \left\|\nabla u_h^{n+\frac{1}{2}}\right\|^2 = C(data)\,. \tag{3.12}$$

Schemes 1,2,3:

$$\Delta t \sum_{n=1}^{M} \left(\|p_h^n\|^2 + \|\lambda_h^n\|^2\right) \leq C(data)\,. \tag{3.13}$$

$C(data)$ is a constant dependent on T, ν, γ, f, u_h^0 and Ω.

Proof. To prove the bounds on velocity for each of the schemes, choose $v_h = u_h^{n+\frac{1}{2}}$ in (3.5). The nonlinear and pressure terms are then zero. The triangle inequality, and summing over time steps then completes the proofs of (3.9),(3.10),(3.11).

To prove (3.12) choose $\chi_h = w_h^{n+\frac{1}{2}}$ in (3.7) and $r_h = \lambda_h^{n+1}$ in (3.8). After combining the equations we obtain

$$\begin{aligned}\left\|w_h^{n+\frac{1}{2}}\right\|^2 = (\nabla \times u_h^{n+\frac{1}{2}}, w_h^{n+\frac{1}{2}}) &\leq \left\|\nabla \times u_h^{n+\frac{1}{2}}\right\| \left\|w_h^{n+\frac{1}{2}}\right\| \\ &\leq \frac{1}{2}\left\|\nabla \times u_h^{n+\frac{1}{2}}\right\|^2 + \frac{1}{2}\left\|w_h^{n+\frac{1}{2}}\right\|^2 \leq \left\|\nabla u_h^{n+\frac{1}{2}}\right\|^2 + \frac{1}{2}\left\|w_h^{n+\frac{1}{2}}\right\|^2.\end{aligned}$$

Rearranging, and summing over time steps we obtain (3.12).

To obtain the stated bound for λ_h^n, we begin with the inf-sup condition satisfied by X_h ($\subset W_h$) and Q_h and use (3.7) to obtain

$$\begin{aligned}\|\lambda_h^n\| &\leq \frac{1}{\beta}\sup_{\chi_h\in X_h}\frac{(\lambda_h^n,\nabla\cdot\chi_h)}{\|\chi_h\|_X} \leq \frac{1}{\beta}\sup_{\chi_h\in X_h}\frac{(\nabla\times u_h^{n-\frac{1}{2}},\chi_h)-(w_h^{n-\frac{1}{2}},\chi_h)}{\|\chi_h\|_X}\\ &\leq \frac{1}{\beta}\left(\|\nabla\times u_h^{n-\frac{1}{2}}\|+\|w_h^{n-\frac{1}{2}}\|\right) \leq \frac{2}{\beta}\left(\|\nabla u_h^{n-\frac{1}{2}}\|+\|w_h^{n-\frac{1}{2}}\|\right).\end{aligned}$$

Using the bounds for $\nabla u_h^{n+\frac{1}{2}}$ (see (3.9)-(3.11)) and $w_h^{n+\frac{1}{2}}$ (see (3.12)) we obtain the bound for λ_h^n. The bound for the pressure is established in an analogous manner. □

Lemma 3.3.2. *Solutions exist to each of the three schemes presented in Algorithm 3.2.1.*

Proof. For each of the schemes, this is a straight-forward extension of the existence proof given for the periodic case in [47]. The result is a consequence of the Leray-Schauder fixed point theorem, and the stability bounds of Lemma 3.3.1. □

We now study the conservation laws for energy and helicity in the schemes. It is shown in [47] that, when restricted to the periodic case, the non-stabilized scheme of Algorithm 3.2.1 (Scheme 1) conserves energy and helicity. In the case of homogeneous boundary conditions for velocity, this physically important feature for energy is still preserved. However, as one might expect, the stabilization terms in Schemes 2 and 3 alter the energy balance. Lemma 3.3.3 shows these energy balances.

The energy balance of Scheme 1, the unstabilized scheme, is analogous to that for the continuous NSE. However, for Scheme 2, we see the effect of the stabilization on the energy balance in the term $\gamma\Delta t\sum_{n=0}^{M-1}\left\|\nabla\cdot u_h^{n+\frac{1}{2}}\right\|^2$ on the left hand side of (3.15). For most choices of elements, one may have that each term in this sum is small, but over a long time interval this sum can grow to significantly (and non-physically) alter the balance. The energy balance for Scheme 3 differs from Scheme 1's energy balance in the addition of only two small terms, instead of a sum. Hence this indicates that the modified grad-div stabilization, for problems over a long time interval, offers a more physically relevant energy balance than the usual grad-div stabilization (Scheme 2).

Lemma 3.3.3. *The schemes of Algorithm 3.2.1 admit the following energy conservation laws.*

Scheme 1:

$$\frac{1}{2}\left\|u_h^M\right\|^2 + \nu\Delta t \sum_{n=0}^{M-1}\left\|\nabla u_h^{n+\frac{1}{2}}\right\|^2 = \Delta t \sum_{n=0}^{M-1}(f(t^{n+\frac{1}{2}}), u_h^{n+\frac{1}{2}}) + \frac{1}{2}\left\|u_h^0\right\|^2 . \quad (3.14)$$

Scheme 2:

$$\frac{1}{2}\left\|u_h^M\right\|^2 + \nu\Delta t \sum_{n=0}^{M-1}\left\|\nabla u_h^{n+\frac{1}{2}}\right\|^2 + \gamma\Delta t \sum_{n=0}^{M-1}\left\|\nabla\cdot u_h^{n+\frac{1}{2}}\right\|^2 = \Delta t \sum_{n=0}^{M-1}(f(t^{n+\frac{1}{2}}), u_h^{n+\frac{1}{2}}) + \frac{1}{2}\left\|u_h^0\right\|^2 . \quad (3.15)$$

Scheme 3:

$$\frac{1}{2}(\left\|u_h^M\right\|^2 + \gamma\left\|\nabla\cdot u_h^M\right\|^2) + \nu\Delta t \sum_{n=0}^{M-1}\left\|\nabla u_h^{n+\frac{1}{2}}\right\|^2 = \Delta t \sum_{n=0}^{M-1}(f(t^{n+\frac{1}{2}}), u_h^{n+\frac{1}{2}}) + \frac{1}{2}(\left\|u_h^0\right\|^2 + \gamma\left\|\nabla\cdot u_h^0\right\|^2) . \quad (3.16)$$

Proof. The proofs of these results follow from choosing $v_h = u_h^{n+\frac{1}{2}}$ in Algorithm 3.2.1 for each of the schemes. The key point is that the nonlinear term vanishes with this choice of test function, and thus does not contribute to the energy balance equations. □

We now consider the discrete helicity conservation in Algorithm 3.2.1. We begin with the case of imposing Dirichlet boundary conditions on the projected vorticity, i.e. $W_h = X_h$. Although this case is nonphysical, analysis of it is the first step in understanding more complex boundary conditions.

In this case, the schemes' discrete nonlinearity preserves helicity, however the stabilization terms do not. We state the precise results in the next lemma. Denote the discrete helicity at time level n by $H_h^n := (u_h^n, \nabla\times u_h^n)$. Note that from (3.6),(3.7), $H_h^n := (u_h^n, w_h^n)$.

Lemma 3.3.4. *If $W_h := X_h$, the schemes of Algorithm 3.2.1 admit the following helicity conser-*

vation laws.

Scheme 1:

$$H_h^M + 2\nu\Delta t \sum_{n=0}^{M-1} (\nabla u_h^{n+\frac{1}{2}}, \nabla w_h^{n+\frac{1}{2}}) = 2\nu\Delta t \sum_{n=0}^{M-1} (f(t^{n+\frac{1}{2}}), \nabla w_h^{n+\frac{1}{2}}) + H_h^0 \,. \quad (3.17)$$

Scheme 2:

$$H_h^M + 2\nu\Delta t \sum_{n=0}^{M-1} (\nabla u_h^{n+\frac{1}{2}}, \nabla w_h^{n+\frac{1}{2}}) + 2\gamma\Delta t \sum_{n=0}^{M-1} (\nabla \cdot u_h^{n+\frac{1}{2}}, \nabla \cdot w_h^{n+\frac{1}{2}})$$
$$= 2\Delta t \sum_{n=0}^{M-1} (f(t^{n+\frac{1}{2}}), \nabla w_h^{n+\frac{1}{2}}) + H_h^0 \,. \quad (3.18)$$

Scheme 3:

$$H_h^M + 2\nu\Delta t \sum_{n=0}^{M-1} (\nabla u_h^{n+\frac{1}{2}}, \nabla w_h^{n+\frac{1}{2}}) + 2\gamma \sum_{n=0}^{M-1} (\nabla \cdot (u_h^{n+1} - u_h^n), \nabla \cdot w_h^{n+\frac{1}{2}})$$
$$= 2\Delta t \sum_{n=0}^{M-1} (f(t^{n+\frac{1}{2}}), \nabla w_h^{n+\frac{1}{2}}) + H_h^0 \,. \quad (3.19)$$

Proof. Choosing $v_h = w_h^{n+\frac{1}{2}}$ elimates the nonlinear term and the pressure term from (3.5) for each of the 3 schemes, and reduces the time difference term to

$$\begin{aligned} \frac{1}{\Delta t}(u_h^{n+1} - u_h^n, w_h^{n+\frac{1}{2}}) &= \frac{1}{\Delta t}(u_h^{n+1} - u_h^n, \nabla \times u_h^{n+\frac{1}{2}}) \\ = \frac{1}{2\Delta t}\left((u_h^{n+1}, \nabla \times u_h^{n+1}) \right. &+ \left. (u_h^{n+1}, \nabla \times u_h^n) - (u_h^n, \nabla \times u_h^{n+1}) - (u_h^n, \nabla \times u_h^n)\right) \\ &= \frac{1}{2\Delta t}\left(H_h^{n+1} - H_h^n\right) , \end{aligned} \quad (3.20)$$

as, for $v,\, w \in H_0^1(\Omega),\ (v, \nabla \times w) = (w, \nabla \times v)$.

Using (3.20) Scheme 1 becomes,

$$\frac{1}{2\Delta t}\left(H_h^{n+1} - H_h^n\right) + \nu(\nabla u_h^{n+\frac{1}{2}}, \nabla w_h^{n+\frac{1}{2}}) = (f(t^{n+\frac{1}{2}}), w_h^{n+\frac{1}{2}}) \tag{3.21}$$

Multiplying by $2\Delta t$ and summing over time steps completes the proof of (3.17).

The proofs of (3.18) and (3.19) follow the same way, except they will contain their respective stabilization terms. □

Lemma 3.3.4 shows that if we impose Dirichlet boundary conditions on the vorticity, then the nonlinearity is able to preserve helicity. Hence for Scheme 1, we see a helicity balance analogous to that of the true physics. However, the stabilization terms do not preserve helicity, and thus appear in the helicity balances for Schemes 2 and 3.

Interestingly, if the term $\gamma(\nabla \cdot w_h^{n+1}, \nabla \cdot \chi_h)$ is added to the left hand side of the vorticity projection equation (3.7), one can show that Scheme 3 conserves both helicity and energy. This results from the cancellation of the stabilization term in Scheme 3's momentum equation when v_h is chosen to be $w_h^{n+\frac{1}{2}}$ and χ_h is chosen as u_h^{n+1} and u_h^n respectively. However, computations using this additional term with Scheme 3 were inferior to those of Scheme 3 defined above.

Similar conservation laws for helicity, even for Scheme 1, do not appear to hold for the nonhomogeneous boundary condition for vorticity, i.e. $X_h \neq W_h$. Due to the definitions of these spaces, extra terms arise in the balance that correspond to the difference between the projection of the curl into discretely divergence-free subspaces of W_h and X_h. These extra terms will be small except at strips along the boundary, but nonetheless global helicity conservation will fail to hold. However, more typical schemes, e.g. usual trapezoidal convective form or rotational form [30], introduce nonphysical helicity over the entire domain and thus the schemes of Algorithm 2.1 still provide a better treatment of helicity than such schemes.

3.4 Convergence

Three numerical schemes are described in Algorithm 2.1. We prove in detail convergence of solutions of Scheme 3 to an NSE solution. Convergence results for Schemes 1 and 2 can be

established in an analogous manner.

We define the following additional norms:

$$
\begin{aligned}
|||v|||_{\infty,k} &:= \max_{0\le n\le M} \|v^n\|_k\,, & |||v_{1/2}|||_{\infty,k} &:= \max_{1\le n\le M} \|v^{n-1/2}\|_k\,,\\
|||v|||_{m,k} &:= \left(\sum_{n=0}^{M} \|v^n\|_k^m \Delta t\right)^{1/m}, & |||v_{1/2}|||_{m,k} &:= \left(\sum_{n=1}^{M} \|v^{n-1/2}\|_k^m \Delta t\right)^{1/m}.
\end{aligned}
$$

We also let $P_{V_h} : L^2 \to V_h$ denote the projection of L^2 onto V_h, i.e. $P_{V_h}(w) := s_h$ where

$$(s_h, v_h) \;=\; (w, v_h)\,, \forall v_h \in V_h\,.$$

For simplicity in stating the a priori theorem we summarize here the regularity assumptions for the solution $u(x,t)$ to the NSE.

$$u \in L^2(0,T;H^{k+1}(\Omega)) \cap L^\infty(0,T;H^1(\Omega)), \tag{3.22}$$

$$u(\cdot,t) \in H_0^1(\Omega), \quad \nabla \times u \in L^2(0,T;H^{k+1}(\Omega))\,, \tag{3.23}$$

$$u_t \in L^2(0,T;H^{k+1}(\Omega)) \cap L^\infty(0,T;H^{k+1}(\Omega)), \tag{3.24}$$

$$u_{tt} \in L^2(0,T;H^{k+1}(\Omega))\,, \tag{3.25}$$

$$u_{ttt} \in L^2(0,T;L^2(\Omega)) \tag{3.26}$$

$$(u \times (\nabla \times u))_{tt} \in L^2(0,T;L^2(\Omega))\,. \tag{3.27}$$

Theorem 3.4.1. *For u, p solutions of the NSE with $p \in L^2(0,T;H^k(\Omega))$, u satisfying (3.22)-(3.27), $f \in L^2(0,T;X^*(\Omega))$, and $u_0 \in V_h$, (u_h^n, w_h^n) given by Scheme 3 of Algorithm 2.1 for $n = 1, ..., M$ and Δt sufficiently small, we have that*

$$\left\|u(T)-u_h^M\right\| + \left\|\nabla\cdot(u(T)-u_h^M)\right\| + \left(\nu\Delta t\sum_{n=0}^{M-1}\left\|\nabla(u^{n+\frac12}-u_h^{n+\frac12})\right\|^2\right)^{1/2} \leq$$

$$C(\gamma,T,\nu^{-3},u)\left(h^k\|u(T)\|_{k+1} + h^k|||u|||_{2,k+1} + h^k|||p|||_{2,k} + h^k|||u_t|||_{2,k+1}\right.$$

$$+ h^k|||u_t|||_{\infty,k+1} + h^k|||u_t|||_{\infty,1}\ |||u|||_{2,k+1} + (\Delta t)^{1/2}\,h^k\|u_{tt}\|_{2,k+1} + (\Delta t)^2\,\|u_{ttt}\|_{2,0}$$

$$\left. + (\Delta t)^2\,\|u_{tt}\|_{2,1} + (\Delta t)^2\,\|(u\times(\nabla\times u))_{tt}\|_{2,0} + h^{k+1}|||u|||_{\infty,1}\,|||\nabla\times u|||_{2,k+1}\,.\right) \quad (3.28)$$

Proof of Theorem. Since (u,p) solves the NSE, we have $\forall v_h\in X_h$ that

$$(u_t(t^{n+\frac12}),v_h) - (u(t^{n+\frac12})\times(\nabla\times u(t^{n+\frac12})),v_h) - (p(t^{n+\frac12}),\nabla\cdot v_h)$$

$$+\nu(\nabla u(t^{n+\frac12}),\nabla v_h) = (f(t^{n+\frac12}),v_h). \quad (3.29)$$

Adding $(\frac{u^{n+1}-u^n}{\Delta t},v_h)$ and $\nu(\nabla u^{n+\frac12},\nabla v_h)$ to both sides of (3.29) we obtain

$$\frac{1}{\Delta t}(u^{n+1}-u^n,v_h) + \left((\nabla\times u(t^{n+\frac12})\times u(t^{n+\frac12})),v_h\right) - (p(t^{n+\frac12}),\nabla\cdot v_h) + \nu(\nabla u^{n+\frac12},\nabla v_h)$$

$$= (f(t^{n+\frac12}),v_h) + \left(\frac{u^{n+1}-u^n}{\Delta t} - u_t(t^{n+\frac12}),v_h\right) + \nu(\nabla u^{n+\frac12}-\nabla u(t^{n+\frac12}),\nabla v_h). \quad (3.30)$$

Next, subtracting (3.5) from (3.30), label $e^n := u^n - u_h^n$, and adding the identically zero term $\gamma(\nabla\cdot(\frac{u^{n+1}-u^n}{\Delta t}),\nabla\cdot v_h)$ to the LHS gives

$$\frac{1}{\Delta t}(e^{n+1}-e^n,v_h) + \nu(\nabla e^{n+\frac12},\nabla v_h) + \frac{\gamma}{\Delta t}(\nabla\cdot(e^{n+1}-e^n,\nabla\cdot v_h))$$

$$= -\left(\nabla\times u(t^{n+\frac12})\times u(t^{n+\frac12}),v_h\right) + \left(w_h^{n+\frac12}\times u_h^{n+\frac12},v_h\right) + \left(p(t^{n+\frac12}) - p_h^{n+1},\nabla\cdot v_h\right)$$

$$+\left(\frac{u^{n+1}-u^n}{\Delta t} - u_t(t^{n+\frac12}),v_h\right) + \nu\left(\nabla u^{n+\frac12}-\nabla u(t^{n+\frac12}),\nabla v_h\right). \quad (3.31)$$

We split the error into two pieces Φ_h and η: $e^n = u^n - u_h^n = (u^n - U^n) + (U^n - u_h^n) := \eta^n + \Phi_h^n$,

where $U^n \in V_h$, yielding

$$\begin{aligned}\frac{1}{\Delta t}(\Phi_h^{n+1}-\Phi_h^n, v_h) + \nu(\nabla\Phi_h^{n+\frac{1}{2}}, \nabla v_h) + \frac{\gamma}{\Delta t}(\nabla\cdot(\Phi_h^{n+1}-\Phi_h^n), \nabla\cdot v_h) = -\frac{1}{\Delta t}(\eta^{n+1}-\eta^n, v_h) \\ - \nu(\nabla\eta^{n+\frac{1}{2}}, \nabla v_h) - \frac{\gamma}{\Delta t}(\nabla\cdot(\eta^{n+1}-\eta^n), \nabla\cdot v_h) - \left((\nabla\times u(t^{n+\frac{1}{2}}))\times u(t^{n+\frac{1}{2}}), v_h\right) \\ + (w_h^{n+\frac{1}{2}}\times u_h^{n+\frac{1}{2}}, v_h) + (p(t^{n+\frac{1}{2}}) - p_h^{n+1}, \nabla\cdot v_h) + \left(\frac{u^{n+1}-u^n}{\Delta t} - u_t(t^{n+\frac{1}{2}}), v_h\right) \\ + \nu(\nabla u^{n+\frac{1}{2}} - \nabla u(t^{n+\frac{1}{2}}), \nabla v_h). \quad (3.32)\end{aligned}$$

Choosing $v_h = \Phi_h^{n+\frac{1}{2}}$ yields

$$\begin{aligned}\frac{1}{2\Delta t}\left(\left\|\Phi_h^{n+1}\right\|^2 - \|\Phi_h^n\|^2\right) + \nu\left\|\nabla\Phi_h^{n+\frac{1}{2}}\right\|^2 + \frac{\gamma}{2\Delta t}\left(\left\|\nabla\cdot\Phi_h^{n+1}\right\|^2 - \|\nabla\cdot\Phi_h^n\|^2\right) \\ = -\frac{1}{\Delta t}(\eta^{n+1}-\eta^n, \Phi_h^{n+\frac{1}{2}}) - \nu(\nabla\eta^{n+\frac{1}{2}}, \nabla\Phi_h^{n+\frac{1}{2}}) - \frac{\gamma}{\Delta t}\left(\nabla\cdot(\eta^{n+1}-\eta^n), \nabla\cdot\Phi_h^{n+\frac{1}{2}}\right) \\ - \left(\nabla\times u(t^{n+\frac{1}{2}})\times u(t^{n+\frac{1}{2}}), \Phi_h^{n+\frac{1}{2}}\right) + (w_h^{n+\frac{1}{2}}\times u_h^{n+\frac{1}{2}}, \Phi_h^{n+\frac{1}{2}}) + (p(t^{n+\frac{1}{2}}) - p_h^{n+1}, \nabla\cdot\Phi_h^{n+\frac{1}{2}}) \\ + \left(\frac{u^{n+1}-u^n}{\Delta t} - u_t(t^{n+\frac{1}{2}}), \Phi_h^{n+\frac{1}{2}}\right) + \nu(\nabla u^{n+\frac{1}{2}} - \nabla u(t^{n+\frac{1}{2}}), \nabla\Phi_h^{n+\frac{1}{2}}). \quad (3.33)\end{aligned}$$

We have the following bounds for the terms on the RHS (see [16]).

$$-\nu(\nabla\eta^{n+\frac{1}{2}}, \nabla\Phi_h^{n+\frac{1}{2}}) \;\le\; \frac{\nu}{12}\left\|\nabla\Phi_h^{n+\frac{1}{2}}\right\|^2 + 3\nu\left\|\nabla\eta^{n+\frac{1}{2}}\right\|^2 \quad (3.34)$$

$$\begin{aligned}\frac{1}{\Delta t}(\eta^{n+1}-\eta^n, \Phi_h^{n+\frac{1}{2}}) &\le \frac{1}{2}\left\|\frac{\eta^{n+1}-\eta^n}{\Delta t}\right\|^2 + \frac{1}{2}\left\|\Phi_h^{n+\frac{1}{2}}\right\|^2 \\ &= \frac{1}{2}\int_\Omega\left(\frac{1}{\Delta t}\int_{t^n}^{t^{n+1}}\eta_t\,dt\right)^2 d\Omega + \frac{1}{2}\left\|\Phi_h^{n+\frac{1}{2}}\right\|^2 \\ &\le \frac{1}{2}\int_\Omega\left(\frac{1}{\Delta t}\int_{t^n}^{t^{n+1}}|\eta_t|^2\,dt\right)d\Omega + \frac{1}{2}\left\|\Phi_h^{n+\frac{1}{2}}\right\|^2 \\ &= \frac{1}{2}\frac{1}{\Delta t}\int_{t^n}^{t^{n+1}}\|\eta_t\|^2\,dt + \frac{1}{2}\left\|\Phi_h^{n+\frac{1}{2}}\right\|^2. \quad (3.35)\end{aligned}$$

Similarly,

$$\frac{\gamma}{\Delta t}\left(\nabla\cdot(\eta^{n+1}-\eta^n),\nabla\cdot\Phi_h^{n+\frac{1}{2}}\right) \;\le\; \gamma\left\|\nabla\cdot\eta_t(t^{n+1})\right\|^2 \;+\; \gamma\int_{t^n}^{t^{n+1}}\|\nabla\cdot\eta_{tt}\|^2\,dt \;+\frac{\gamma}{2}\left\|\nabla\cdot\Phi_h^{n+\frac{1}{2}}\right\|^2. \tag{3.36}$$

$$\begin{aligned}\left(\frac{u^{n+1}-u^n}{\Delta t}-u_t(t^{n+\frac{1}{2}}),\Phi_h^{n+\frac{1}{2}}\right) &\le \frac{1}{2}\left\|\frac{u^{n+1}-u^n}{\Delta t}-u_t(t^{n+\frac{1}{2}})\right\|^2+\frac{1}{2}\left\|\Phi_h^{n+\frac{1}{2}}\right\|^2\\ &= \frac{(\Delta t)^3}{2560}\int_{t^n}^{t^{n+1}}\|u_{ttt}\|^2\,dt \;+\; \frac{1}{2}\left\|\Phi_h^{n+\frac{1}{2}}\right\|^2 \qquad (3.37)\\ \nu(\nabla u^{n+\frac{1}{2}}-\nabla u(t^{n+\frac{1}{2}}),\nabla\Phi_h^{n+\frac{1}{2}}) &\le 3\nu\left\|\nabla u^{n+\frac{\nu}{12}}-\nabla u(t^{n+\frac{1}{2}})\right\|^2+\frac{\nu^2}{2}\left\|\Phi_h^{n+\frac{1}{2}}\right\|^2 \qquad (3.38)\\ &= \frac{\nu(\Delta t)^3}{16}\int_{t^n}^{t^{n+1}}\|\nabla u_{tt}\|^2\,dt \;+\; \frac{\nu}{12}\left\|\Phi_h^{n+\frac{1}{2}}\right\|^2 \qquad (3.39)\end{aligned}$$

For the pressure term, since $\Phi_h^{n+\frac{1}{2}}\in V_h$, for any $q_h\in Q_h$,

$$(p(t^{n+\frac{1}{2}})-p_h^{n+1},\nabla\cdot\Phi_h^{n+\frac{1}{2}})=(p(t^{n+\frac{1}{2}})-q_h,\nabla\cdot\Phi_h^{n+\frac{1}{2}}), \tag{3.40}$$

which implies

$$(p(t^{n+\frac{1}{2}})-p_h^{n+1},\nabla\cdot\Phi_h^{n+\frac{1}{2}})\le\frac{1}{2\gamma}\inf_{q_h\in Q_h}\left\|p(t^{n+\frac{1}{2}})-q_h\right\|^2+\frac{\gamma}{2}\left\|\nabla\cdot\Phi_h^{n+\frac{1}{2}}\right\|^2. \tag{3.41}$$

Utilizing (3.34)-(3.41) we now have

$$\begin{aligned}&\frac{1}{2\Delta t}\left(\left\|\Phi_h^{n+1}\right\|^2-\|\Phi_h^n\|^2\right)+\frac{\gamma}{2\Delta t}\left(\left\|\nabla\cdot\Phi_h^{n+1}\right\|^2-\|\nabla\cdot\Phi_h^n\|^2\right)+\frac{5\nu}{6}\left\|\nabla\Phi_h^{n+\frac{1}{2}}\right\|^2\\ &\le 3\nu\left\|\nabla\eta^{n+\frac{1}{2}}\right\|^2+\frac{\gamma}{\Delta t}\left\|\nabla\cdot\eta_t(t^{n+1})\right\|^2+\frac{\gamma}{\Delta t}\int_{t^n}^{t^{n+1}}\|\nabla\cdot\eta_{tt}\|^2\,dt+\frac{1}{2\gamma}\inf_{q_h\in Q_h}\left\|p(t^{n+\frac{1}{2}})-q_h\right\|^2\\ &+C(1+\nu)\Delta t^3\left(\int_{t^n}^{t^{n+1}}\|u_{ttt}\|^2\,dt+\int_{t^n}^{t^{n+1}}\|\nabla u_{tt}\|^2\,dt\right)+\frac{\nu^2+1}{2}\left\|\Phi_h^{n+\frac{1}{2}}\right\|^2+\gamma\left\|\nabla\cdot\Phi_h^{n+\frac{1}{2}}\right\|^2\\ &+(w_h^{n+\frac{1}{2}}\times u_h^{n+\frac{1}{2}},\Phi_h^{n+\frac{1}{2}})-\left((\nabla\times u(t^{n+\frac{1}{2}}))\times u(t^{n+\frac{1}{2}}),\Phi_h^{n+\frac{1}{2}}\right)+\frac{1}{2}\frac{1}{\Delta t}\int_{t^n}^{t^{n+1}}\|\eta_t\|^2\,dt\,. \qquad (3.42)\end{aligned}$$

For the nonlinear terms we have

$$\begin{aligned}(w_h^{n+\frac{1}{2}} \times u_h^{n+\frac{1}{2}}, \Phi_h^{n+\frac{1}{2}}) - \left((\nabla \times u(t^{n+\frac{1}{2}})) \times u(t^{n+\frac{1}{2}}), \Phi_h^{n+\frac{1}{2}}\right) + \left((\nabla \times u^{n+\frac{1}{2}}) \times u^{n+\frac{1}{2}}, \Phi_h^{n+\frac{1}{2}}\right) \\ - \left((\nabla \times u^{n+\frac{1}{2}}) \times u^{n+\frac{1}{2}}, \Phi_h^{n+\frac{1}{2}}\right) \\ = \left((w_h^{n+\frac{1}{2}} - \nabla \times u^{n+\frac{1}{2}}) \times u^{n+\frac{1}{2}}, \Phi_h^{n+\frac{1}{2}}\right) + \left(w_h^{n+\frac{1}{2}} \times (u_h^{n+\frac{1}{2}} - u^{n+\frac{1}{2}}), \Phi_h^{n+\frac{1}{2}}\right) \\ + \left((\nabla \times u^{n+\frac{1}{2}}) \times u^{n+\frac{1}{2}} - (\nabla \times u(t^{n+\frac{1}{2}})) \times u(t^{n+\frac{1}{2}}), \Phi_h^{n+\frac{1}{2}}\right) \\ = \left((w_h^{n+\frac{1}{2}} - \nabla \times u^{n+\frac{1}{2}}) \times u^{n+\frac{1}{2}}, \Phi_h^{n+\frac{1}{2}}\right) - \left(w_h^{n+\frac{1}{2}} \times \eta^{n+\frac{1}{2}}, \Phi_h^{n+\frac{1}{2}}\right) \\ + \left((\nabla \times u^{n+\frac{1}{2}}) \times u^{n+\frac{1}{2}} - (\nabla \times u(t^{n+\frac{1}{2}})) \times u(t^{n+\frac{1}{2}}), \Phi_h^{n+\frac{1}{2}}\right) \quad (3.43)\end{aligned}$$

We bound the second to last and last terms in (3.43) by

$$\begin{aligned}(w_h^{n+\frac{1}{2}} \times \eta^{n+\frac{1}{2}}, \Phi_h^{n+\frac{1}{2}}) &\leq C \left\|w_h^{n+\frac{1}{2}}\right\| \left\|\nabla \eta^{n+\frac{1}{2}}\right\| \left\|\nabla \Phi_h^{n+\frac{1}{2}}\right\| \\ &\leq \frac{\nu}{12} \left\|\nabla \Phi_h^{n+\frac{1}{2}}\right\|^2 + 3\nu^{-1} \left\|w_h^{n+\frac{1}{2}}\right\|^2 \left\|\nabla \eta^{n+\frac{1}{2}}\right\|^2 \quad (3.44)\end{aligned}$$

$$\begin{aligned}&(u(t^{n+\frac{1}{2}}) \times (\nabla \times u(t^{n+\frac{1}{2}})) - u^{n+\frac{1}{2}} \times (\nabla \times u^{n+\frac{1}{2}}), \Phi_h^{n+\frac{1}{2}}) \\ &\quad \leq \frac{\nu}{12} \left\|\nabla \Phi_h^{n+\frac{1}{2}}\right\|^2 + 3\nu^{-1} \left\|u(t^{n+\frac{1}{2}}) \times (\nabla \times u(t^{n+\frac{1}{2}})) - u^{n+\frac{1}{2}} \times (\nabla \times u^{n+\frac{1}{2}})\right\|^2 \\ &\quad\quad \leq \frac{\nu}{12} \left\|\nabla \Phi_h^{n+\frac{1}{2}}\right\|^2 + \frac{3}{48} \nu^{-1} (\Delta t)^3 \int_{t^n}^{t^{n+1}} \|(u \times (\nabla \times u))_{tt}\|^2 \, dt. \quad (3.45)\end{aligned}$$

For the first term in (3.43), we first need a bound on $\left\|\nabla \times u^{n+\frac{1}{2}} - w_h^{n+\frac{1}{2}}\right\|$. This is obtained by restricting χ_h to V_h in (3.7) and then subtracting $(\nabla \times u^{n+\frac{1}{2}}, \chi_h)$ from both sides of (3.7), which gives us

$$\begin{aligned}(\nabla \times u^{n+\frac{1}{2}} - w_h^{n+\frac{1}{2}}, \chi_h) &= (\nabla \times (u^{n+\frac{1}{2}} - u_h^{n+\frac{1}{2}}), \chi_h) \\ &= (\nabla \times \eta^{n+\frac{1}{2}}, \chi_h) + (\nabla \times \Phi_h^{n+\frac{1}{2}}, \chi_h) \,.\end{aligned}$$

By the definition of P_{V_h},

$$\begin{aligned}(P_{V_h}(\nabla\times u^{n+\frac{1}{2}})-w_h^{n+\frac{1}{2}},\chi_h) &= (\nabla\times u^{n+\frac{1}{2}}-w_h^{n+\frac{1}{2}},\chi_h)\\ &= (\nabla\times(u^{n+\frac{1}{2}}-u_h^{n+\frac{1}{2}}),\chi_h)\\ &= (\nabla\times\eta^{n+\frac{1}{2}},\chi_h)+(\nabla\times\Phi_h^{n+\frac{1}{2}},\chi_h)\end{aligned}$$

Choose $\chi_h = P_{V_h}(\nabla\times u^{n+\frac{1}{2}})-w_h^{n+\frac{1}{2}}$ we obtain

$$\left\|P_{V_h}(\nabla\times u^{n+\frac{1}{2}})-w_h^{n+\frac{1}{2}}\right\|^2 \le 2\left(\left\|\nabla\eta^{n+\frac{1}{2}}\right\|^2+\left\|\nabla\Phi_h^{n+\frac{1}{2}}\right\|^2\right). \tag{3.46}$$

Now using (3.46) and, from Poincare's inequality, $\left\|\Phi_h^{n+\frac{1}{2}}\right\| \le C\left\|\nabla\Phi_h^{n+\frac{1}{2}}\right\|$ we obtain

$$\begin{aligned}&\left((P_{V_h}(\nabla\times u^{n+\frac{1}{2}})-w_h^{n+\frac{1}{2}})\times u^{n+\frac{1}{2}},\Phi_h^{n+\frac{1}{2}}\right)\\ &\qquad\le C\left\|\nabla u^{n+\frac{1}{2}}\right\|\left\|P_{V_h}(\nabla\times u^{n+\frac{1}{2}})-w_h^{n+\frac{1}{2}}\right\|\left\|\Phi_h^{n+\frac{1}{2}}\right\|^{\frac{1}{2}}\left\|\nabla\Phi_h^{n+\frac{1}{2}}\right\|^{\frac{1}{2}}\\ &\qquad\le C\left\|\nabla u^{n+\frac{1}{2}}\right\|\left(\left\|\nabla\eta^{n+\frac{1}{2}}\right\|\left\|\nabla\Phi_h^{n+\frac{1}{2}}\right\|+\left\|\Phi_h^{n+\frac{1}{2}}\right\|^{\frac{1}{2}}\left\|\nabla\Phi_h^{n+\frac{1}{2}}\right\|^{\frac{3}{2}}\right)\\ &\le \frac{\nu}{12}\left\|\nabla\Phi_h^{n+\frac{1}{2}}\right\|^2+C\nu^{-1}\left\|\nabla u^{n+\frac{1}{2}}\right\|^2\left\|\nabla\eta^{n+\frac{1}{2}}\right\|^2+\frac{\nu}{12}\left\|\nabla\Phi_h^{n+\frac{1}{2}}\right\|^2+C\nu^{-3}\left\|\nabla u^{n+\frac{1}{2}}\right\|^4\left\|\Phi_h^{n+\frac{1}{2}}\right\|^2.\end{aligned} \tag{3.47}$$

Also, we have that

$$\begin{aligned}&\left((\nabla\times u^{n+\frac{1}{2}}-P_{V_h}(\nabla\times u^{n+\frac{1}{2}}))\times u^{n+\frac{1}{2}},\Phi_h^{n+\frac{1}{2}}\right)\\ &\qquad\le C\left\|\nabla\times u^{n+\frac{1}{2}}-P_{V_h}(\nabla\times u^{n+\frac{1}{2}})\right\|\left\|\nabla u^{n+\frac{1}{2}}\right\|\left\|\nabla\Phi_h^{n+\frac{1}{2}}\right\|\\ &\qquad\le \frac{\nu}{12}\left\|\nabla\Phi_h^{n+\frac{1}{2}}\right\|^2+C\left\|\nabla u^{n+\frac{1}{2}}\right\|^2\left\|\nabla\times u^{n+\frac{1}{2}}-P_{V_h}(\nabla\times u^{n+\frac{1}{2}})\right\|^2\end{aligned} \tag{3.48}$$

Combining (3.48) and (3.47) we obtain the required bound for $\left((w_h^{n+\frac{1}{2}}-\nabla\times u^{n+\frac{1}{2}})\times u^{n+\frac{1}{2}},\Phi_h^{n+\frac{1}{2}}\right)$.

Noting that $\left\|\nabla\cdot\Phi_h^{n+\frac{1}{2}}\right\|^2 \le 1/2\left(\left\|\nabla\cdot\Phi_h^{n+1}\right\|^2+\|\nabla\cdot\Phi_h^n\|^2\right)$, substituting the bounds derived in (3.44), (3.45), (3.47), and (3.48) into (3.42) yields

$$\begin{aligned}
&\frac{1}{2\Delta t}\left(\left\|\Phi_h^{n+1}\right\|^2-\|\Phi_h^n\|^2\right)+\frac{\gamma}{2\Delta t}\left(\left\|\nabla\cdot\Phi_h^{n+1}\right\|^2-\|\nabla\cdot\Phi_h^n\|^2\right)+\frac{\nu}{2}\left\|\nabla\Phi_h^{n+\frac{1}{2}}\right\|^2\\
&\qquad\le\left(\frac{\nu^2+4}{2}+C\nu^{-3}\left\|\nabla u^{n+\frac{1}{2}}\right\|^4\right)\left\|\Phi_h^{n+\frac{1}{2}}\right\|^2+\frac{\gamma}{2}\left(\left\|\nabla\cdot\Phi_h^{n+1}\right\|^2+\|\nabla\cdot\Phi_h^n\|^2\right)\\
&\qquad\quad+\frac{1}{2\gamma}\inf_{q_h\in Q_h}\left\|p(t^{n+1})-q_h\right\|^2+C\nu\left\|\nabla\eta^{n+\frac{1}{2}}\right\|^2+\gamma\left\|\nabla\cdot\eta_t(t^{n+1})\right\|^2\\
&\quad+C\nu^{-1}\left\|w_h^{n+\frac{1}{2}}\right\|^2\left\|\nabla\eta^{n+\frac{1}{2}}\right\|^2+\nu^{-1}\left\|\nabla u^{n+\frac{1}{2}}\right\|^2\left\|\nabla\eta^{n+\frac{1}{2}}\right\|^2+\frac{1}{2}\frac{1}{\Delta t}\int_{t^n}^{t^{n+1}}\|\eta_t\|^2\,dt\\
&\qquad+\gamma\int_{t^n}^{t^{n+1}}\|\nabla\cdot\eta_{tt}\|^2\,dt+C\Delta t^3\left(\int_{t^n}^{t^{n+1}}\|u_{ttt}\|^2\,dt+\int_{t^n}^{t^{n+1}}\|\nabla u_{tt}\|^2\,dt\right)\\
&+C\nu^{-1}(\Delta t)^3\int_{t^n}^{t^{n+1}}\|(u\times(\nabla\times u))_{tt}\|^2\,dt+C\left\|\nabla u^{n+\frac{1}{2}}\right\|^2\left\|\nabla\times u^{n+\frac{1}{2}}-P_{V_h}(\nabla\times u^{n+\frac{1}{2}})\right\|^2 \qquad (3.49)
\end{aligned}$$

Next multiply by $2\Delta t$, sum over time steps, and using the Gronwall inequality (from [25]) yields

$$\begin{aligned}
&\left\|\Phi_h^M\right\|^2+\gamma\left\|\nabla\cdot\Phi_h^M\right\|^2+\nu\Delta t\sum_{n=0}^{M-1}\left\|\nabla\Phi_h^{n+\frac{1}{2}}\right\|^2\\
&\quad\le Cexp\left(2\Delta t\sum_{n=0}^{M-1}\gamma+\frac{\nu^2+4}{2}+C\nu^{-3}\left\|\nabla u^{n+\frac{1}{2}}\right\|^4\right)\left(\Delta t\sum_{n=1}^{M}\frac{1}{2\gamma}\inf_{q_h\in Q_h}\|p(t^n)-q_h\|^2\right.\\
&\qquad+\Delta t\sum_{n=0}^{M}\nu\|\nabla\eta^n\|^2+\Delta t\sum_{n=1}^{M}\gamma\|\nabla\eta_t(t^n)\|^2+\Delta t\sum_{n=0}^{M-1}\nu^{-1}\left\|w_h^{n+\frac{1}{2}}\right\|^2\left\|\nabla\eta^{n+\frac{1}{2}}\right\|^2\\
&\quad+\Delta t\sum_{n=0}^{M-1}\nu^{-1}\left\|\nabla u^{n+\frac{1}{2}}\right\|^2\left\|\nabla\eta^{n+\frac{1}{2}}\right\|^2+\sum_{n=0}^{M-1}\int_{t^n}^{t^{n+1}}\|\eta_t\|^2\,dt+\Delta t\sum_{n=0}^{M-1}\gamma\int_{t^n}^{t^{n+1}}\|\nabla\cdot\eta_{tt}\|^2\,dt\\
&\qquad+(\Delta t)^4\|u_{ttt}\|_{2,0}^2+(\Delta t)^4\|\nabla u_{tt}\|_{2,0}^2+(\Delta t)^4\|(u\times(\nabla\times u))_{tt}\|_{2,0}^2\\
&\qquad\left.+\Delta t\sum_{n=0}^{M-1}\left\|\nabla u^{n+\frac{1}{2}}\right\|^2\left\|\nabla\times u^{n+\frac{1}{2}}-P_{V_h}(\nabla\times u^{n+\frac{1}{2}})\right\|^2\right) \qquad (3.50)
\end{aligned}$$

Recall the approximation properties of $U^n \in V_h$, $q_h \in Q_h$, and P_{V_h} [30]

$$\begin{aligned}
\inf_{U^n \in V_h} \|\eta(t^n)\|_s &\leq Ch^{k+1-s} \|u(t^n)\|_{k+1}, \ s = 0, 1, \quad \text{and} \\
\inf_{q_h \in Q_h} \|p(t^n) - q_h\| &\leq Ch^k \|p(t^n)\|_k \\
\|w^n - P_{V_h}(w^n)\| &\leq Ch^{k+1} \|w^n\|_{k+1} .
\end{aligned}$$

Estimate (3.50) then becomes

$$\begin{aligned}
&\left\|\Phi_h^M\right\|^2 + \gamma \left\|\nabla \cdot \Phi_h^M\right\|^2 + \nu\Delta t \sum_{n=0}^{M-1} \left\|\nabla \Phi_h^{n+\frac{1}{2}}\right\|^2 \\
&\qquad \leq Cexp\left(2\Delta t \sum_{n=0}^{M-1} \gamma + \frac{\nu^2+4}{2} + C\nu^{-3} \left\|\nabla u^{n+\frac{1}{2}}\right\|^4\right) \left(\frac{1}{2\gamma} h^{2k} |||p|||^2_{2,k}\right. \\
&\qquad + \nu\, h^{2k} |||u|||^2_{2,k+1} + \gamma\, h^{2k} |||u_t|||^2_{2,k+1} + \nu^{-1} h^{2k} |||u_t|||^2_{\infty,1} |||u|||^2_{2,k+1} \\
&\qquad + \Delta t\, \gamma\, h^{2k} \|u_{tt}\|^2_{2,k+1} + h^{2k+2} \|u_t\|^2_{2,k+1} + (\Delta t)^4 \|u_{ttt}\|^2_{2,0} + (\Delta t)^4 \|\nabla u_{tt}\|^2_{2,0} \\
&\qquad + (\Delta t)^4 \|(u \times (\nabla \times u))_{tt}\|^2_{2,0} + \left(\nu\Delta t \sum_{n=0}^{M-1} \left\|w_h^{n+\frac{1}{2}}\right\|^2\right) \nu^{-2} h^{2k} |||u_t|||^2_{\infty,k+1} \\
&\qquad\qquad \left. + h^{2k+2} |||u|||^2_{\infty,1} |||\nabla \times u|||^2_{2,k+1}\right) . \quad (3.51)
\end{aligned}$$

Finally, from the boundness estimate for $\nu\Delta t \sum_{n=0}^{M-1} \left\|w_h^{n+\frac{1}{2}}\right\|^2$ from (3.12), and an application of the triangle inequality we obtain (3.28).

□

Remark 2. *As expected, if (X_h, Q_h) is chosen to be the inf-sup stable pair (P_k, P_{k-1}), $k \geq 2$, then with the smoothness assumptions (3.22)-(3.27) and $p \in L^2(0, T; H^k(\Omega))$ the H^1 convergence for the velocity is*

$$|||u - u_h|||_{2,1} \leq C(\Delta t^2 + h^k) \quad (3.52)$$

Remark 3. *The significant computational improvement of Schemes 2 and 3 over Scheme 1 is somewhat masked in the statement of the a priori error bound for the velocity (for Scheme 3) given in (3.28). For Scheme 1 the pressure contribution to the bound is $C/\nu \|p - q_h\|$, whereas for*

Schemes 2 and 3 the pressure contribution is given by $C\|p - q_h\|$, see (3.41). The presence of ν in the denominator for Scheme 1 suggests a superior numerical performance of Schemes 2 and 3 if a large pressure error is present.

3.5 Numerical Experiments

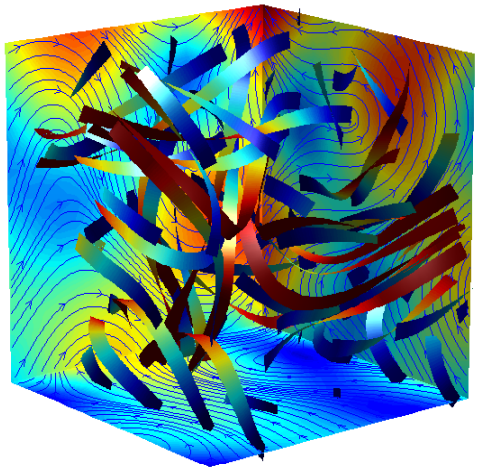

Figure 3.1: The velocity solution to the Ethier-Steinman problem with $a = 1.25$, $d = 1$ at $t = 0$ on the $(-1, 1)^3$ domain. The complex flow structure is seen in the streamribbons in the box and the velocity streamlines and speed contours on the sides.

This section presents two numerical experiments, the first to confirm convergence rates, and the second, over a longer time interval, to compare the schemes' accuracies against each other and a commonly used scheme. For both experiments, we compute approximations to the Ethier-Steinman exact NSE solution on $[-1, 1]^3$ [17], although we choose different parameters and viscosities for the two tests. We find in the first numerical experiment that the computed convergence rates from successive mesh and timestep refinements indeed match the predicted rates from Section 4. For the second experiment, the advantage of using the stabilized enhanced physics based scheme is demonstrated.

For chosen parameters a, d and viscosity ν, the exact Ethier-Steinman NSE solution is given

by

$$
\begin{aligned}
u_1 &= -a\left(e^{ax}\sin(ay+dz)+e^{az}\cos(ax+dy)\right)e^{-\nu d^2 t} && (3.53)\\
u_2 &= -a\left(e^{ay}\sin(az+dx)+e^{ax}\cos(ay+dz)\right)e^{-\nu d^2 t} && (3.54)\\
u_3 &= -a\left(e^{az}\sin(ax+dy)+e^{ay}\cos(az+dx)\right)e^{-\nu d^2 t} && (3.55)\\
p &= -\frac{a^2}{2}(e^{2ax}+e^{2ay}+e^{2az}+2\sin(ax+dy)\cos(az+dx)e^{a(y+z)} \\
&\quad +2\sin(ay+dz)\cos(ax+dy)e^{a(z+x)} \\
&\quad +2\sin(az+dx)\cos(ay+dz)e^{a(x+y)})e^{-2\nu d^2 t} && (3.56)
\end{aligned}
$$

We give the pressure in its usual form, although our scheme approximates instead the Bernoulli pressure $P = p + \frac{1}{2}|u|^2$. This problem was developed as a 3d analogue to the Taylor vortex problem, for the purpose of benchmarking. Although unlikely to be physically realized, it is a good test problem because it is not only an exact NSE solution, but also it has non-trivial helicity which implies the existence of complex structure [40] in the velocity field. The $t = 0$ solution for $a = 1.25$ and $d = 1$ is illustrated in Figure 3.1. For both experiments below, we use $u^0 = (u_1(0), u_2(0), u_3(0))^T$ as the initial condition and enforce Dirichlet boundary conditions for velocity to be the interpolant of $u(t)$ on the boundary, while a do-nothing boundary condition is used for the vorticity projection. All computations with schemes 2 and 3 use stabilization parameter $\gamma = 1$.

3.5.1 Numerical Test 1: Convergence rate verification

h	Δt	$\|\|\|u-u_{S1}\|\|\|_{2,1}$	rate	$\|\|\|u-u_{S2}\|\|\|_{2,1}$	rate	$\|\|\|u-u_{S3}\|\|\|_{2,1}$	rate
1	0.001	0.01560	-	0.01556	-	0.01579	-
0.5	0.0005	0.00390	2.00	0.00391	1.99	0.00395	2.00
0.25	0.00025	0.000979	1.99	0.000979	2.00	0.000984	2.01
0.125	0.000125	0.000245	2.00	0.000245	2.00	0.000246	2.00

Table 3.1: The $|||u_{NSE} - u_h|||_{2,1}$ errors and experimental convergence rates for each of the three scheme of Algorithm 3.2.1.

To verify convergence rates predicted in Section 4, we compute approximations to (3.53)-(3.56) with parameters $a = d = \pi/4$, viscosity $\nu = 1$, and end time $T = 0.001$. Since (P_2, P_1)

elements are being used, we expect $O(h^2 + \Delta t^2)$ convergence of $|||u_{NSE} - u_h|||_{2,1}$ for each of the three schemes of Algorithm 3.2.1. Errors and experimental convergence rates in this norm are shown in Table 3.1, which match those predicted by the theory.

3.5.2 Numerical Test 2: Comparison of the schemes

For our second test, we compute approximations to (3.53)-(3.56) with $a = 1.25$, $d = 1$, kinematic viscosity $\nu = 0.002$, end time $T = 0.5$, using all 3 schemes from Algorithm 3.2.1. We use 3,072 tetrahedral elements, which provides 41,472 velocity degrees of freedom, and 46,875 degrees of freedom for the projected vorticity since here there are degrees of freedom on the boundary. It is important to note that due to the splitting of the projection equations from the NSE system in the solver, as the projection equations are well-conditioned, the time spent for assembling and solving the projection equations is negligible.

In addition to the 3 schemes of Algorithm 3.2.1, for comparison, we also compute approximations using the well-known convective form Crank-Nicolson (CCN) FEM for the Navier-Stokes equations [30, 23, 26]. We run the simulations with timestep $\Delta t = 0.005$. Results of the simulations are shown in Figures 3.2 and 3.3, where $L^2(\Omega)$ error and helicity error are plotted against time. Is clear from the pictures that the enhanced physics based scheme is more accurate than the CCN scheme, and its advantage becomes more pronounced over longer time intervals. Also it is seen how the stabilizations of the enhanced-physics scheme improve the accuracy of the approximations.

3.6 Conclusions and future directions

We have extended the methodology of the enhanced-physics based scheme of [47] to a more general set of problems. This extension required the use of grad-div type stabilizations since the scheme uses a Bernoulli pressure which can be a dominant source of error in finite element computations. Additionally we proposed an alternate grad-div stabilization to the usual grad-div stabilziation, but provides a more physical solution by not altering the energy balance. We also provided numerical computations that illustrated the advantage of the enhanced physics based scheme as well as the modified grad-div stabilization that we introduced.

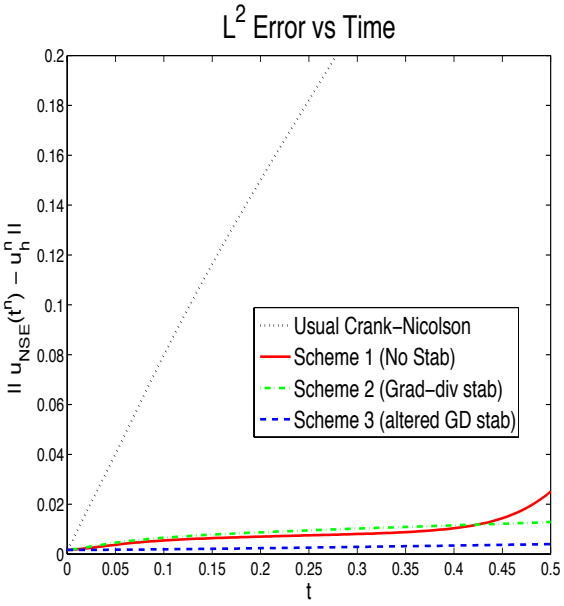

Figure 3.2: The plot above shows L_2 error of the velocity vs time for the four schemes of Test 2. We see in the plot that the stabilizations add accuracy to the enhanced-physics scheme, and that the alternate grad-div stabilization gives slightly better results than the usual grad-div stabilization. It can also be seen that the enhanced-physics scheme is far more accurate in this metric than the usual CCN scheme.

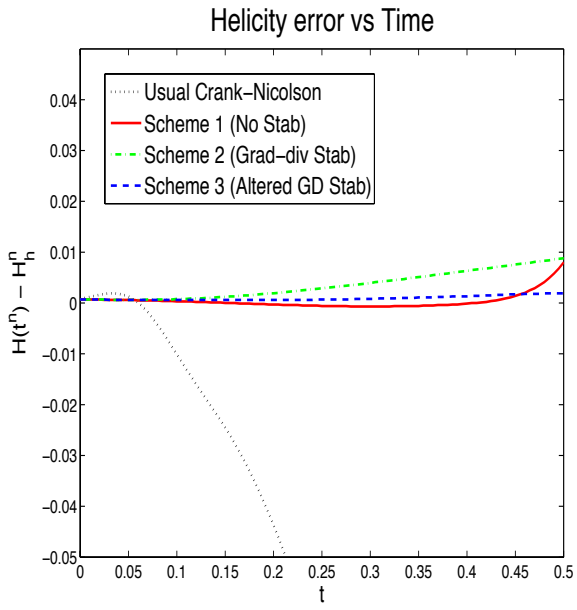

Figure 3.3: The plot above shows helicity error vs time for the four schemes of Test 2. We see in the plot that helicity is far more accurate in the enhanced-physics scheme, and even better with stabilizations, than the usual CCN scheme.

As discussed in the Introduction, with the rotational form of the NSE and introduction of the Bernoulli pressure, the pressure term in the a priori error estimate for the velocity approximation can have a significant impact. An alternative to a grad-div stabilization method may be to choose the approximation spaces (X_h, Q_h) so that the pressure term does not appear in the a priori error estimate for the velocity approximation. Recently stable approximation spaces (X_h, Q_h), Scott-Vogelius elements [58] (see [56, 55, 51, 52] for $\Omega \subset \mathbb{R}^2$), have been introduced for which $[\nabla \cdot X_h] \subset Q_h$, which guarantees that discretly divergence free approximations for the velocity are also L^2 divergence free. These elements require a special mesh, and are higher order (at least) $P_3(e) - (\text{discontinuous})P_2(e)$ compared to the commonly used Taylor-Hood elements $P_2(e) - P_1(e)$. Future work will include a comparison of the stabilized methods investigated above with approximations using Scott-Vogelius elements.

Chapter 4

Improving mass conservation in FE approximations of the Navier Stokes equations using C^0 velocity fields: A connection between grad-div stabilization and Scott-Vogelius elements

4.1 Introduction

This chapter studies two finite element methods for approximating solutions to the Navier-Stokes equations (NSE), that use continuous velocity fields and provide accurate approximations as well as excellent mass conservation. Under the restriction that the mesh be created as a barycenter refinement of a triangular/tetrahedral mesh and that the degree k of approximating polynomial for velocity be chosen at least as large as the dimension of the problem, $k \geq d$, the $((P_k)^d, P_{k-1}^{disc})$

pair (called the Scott-Vogelius (SV) pair), has recently been shown to be inf-sup stable and admit optimal approximation properties [60, 58]. Moreover, it has the fundamental physical property that since $\nabla \cdot (P_k)^d \subset P_{k-1}^{disc}$, the weak enforcement of mass conservation imposed by the usual Galerkin finite element method for Stokes or the NSE actually enforces strong (pointwise) conservation of mass. A minor result of this chapter is the presentation of the first numerical tests of the Galerkin method with SV elements for the time dependent NSE; the results were excellent.

The second method studied herein is the Galerkin method for the NSE with Taylor-Hood (TH) elements and grad-div stabilization (with parameter γ), but restricted to the case where SV elements are inf-sup stable and have optimal approximation properties. This method is well studied in the general case [45, 46, 20, 46, 31, 20], and it is well known that the stabilization improves mass conservation and relaxes the effect of the pressure error on the velocity error. However when restricted to this setting, other special properties can be found. Specifically, we show the solutions corresponding to a sequence of parameters $\gamma_n \to \infty$ converge to the SV solution. This provides theoretical justification that one can choose γ significantly larger than $O(1)$, which is often a good choice in the general setting [20], and still obtain an accurate solution with excellent mass conservation. Roughly speaking, in this special (although not very restrictive) setting, one has mathematical justification that raising γ past $O(1)$ by several orders of magnitude will not "destroy" the momentum equation, although care for numerical roundoff error still must be taken.

Although the incompressible NSE are one of the most investigated mathematical equations [53, 54, 30, 23, 26, 21, 24, 5, 22, 49, 14], their numerical solution remains a difficult challenge, and new methods and strategies for their solution are regularly proposed. Nevertheless, even in the case of laminar, single phase Newtonian fluids, some aspects of their numerical approximation were sometimes underestimated, such as the importance of mass conservation [46, 18, 38, 20, 43, 34, 35]. It is well-known that mixed finite element discretizations of the incompressible NSE are prone to different kinds of numerical instabilities, when one combines a certain discrete velocity space X_h in a naive way with a discrete pressure space Q_h. The violation of discrete inf-sup stability [5, 21, 49] is the classical example for when the discrete pressure space is too large in relation to the discrete velocity space. The opposite extreme is when the discrete pressure space is too small. In this case

the approximation does not adequately satisfy the conservation of mass equation, thereby giving a poor approximation to the physical solution. It is this second problem that is the motivation of this work.

There are a number of strategies for avoiding poor mass conservation: several element choices are known provide pointwise mass conservation [60, 58], discontinuous Galerkin methods admit local mass conservation [48], penalization techniques such as grad-div stabilization discussed herein reduce global mass conservation error, and a posteriori methods can be used to enforce the conservation of mass on already computed solutions [41]. For each technique, there are naturally both good features and drawbacks, and therefore a determination of which method is "best" is certainly problem dependent.

Still, in most cases, the use of TH elements with grad-div stabilization is one of the easiest to implement. For many years TH elements have been a popular choice of approximating element in fluid flow simulations, with most downloadable finite element packages have some TH elements implemented. Hence getting a TH code and adding grad-div stabilization is typically convenient and simple. However, until now, it was believed that the improvement in mass conservation using grad-div stabilization, although sometimes significant over usual TH solutions, was limited to an $O(1)$ choice of the stabilization parameter. With this limitation, one had to decide whether the provided mass conservation was good enough, or instead if a different element choice or DG should be used instead. Hence this work provides a simple solution to correct for poor mass conservation in existing codes, and therefore may lead to TH elements being a good choice on a much wider set of problems.

This chapter is arranged as follows. In Section 2, we give notation and preliminaries, including a brief discussion of the SV element. Section 3 proves that on barycenter refined meshes and $k \geq d$, grad-div stabilized TH solutions of the NSE converge to SV solutions as the grad-div parameter tends to ∞. Section 4 presents numerical experiments that illustrate the theory.

4.2 Preliminaries

We will represent the L^2 norm and inner product by $\|\cdot\|$ and $(\cdot,\cdot)$, respectively. All other norms used will be clearly denoted with subscripts.

Recall the time dependent incompressible NSE on a polygonal (2d), or polyhedral (3d), domain Ω, and for simplicity with homogeneous Dirichlet boundary conditions:

$$\begin{aligned} \mathbf{u}_t - \nu\nabla\mathbf{u} + \mathbf{u}\cdot\nabla\mathbf{u} + \nabla p &= \mathbf{f}, \quad \text{in } \Omega\times(0,T], && (4.1)\\ \nabla\cdot\mathbf{u} &= 0, \quad \text{in } \Omega\times(0,T], && (4.2)\\ \mathbf{u}(\mathbf{x},0) &= \mathbf{u}_0, \quad \text{in } \Omega && (4.3)\\ \mathbf{u} &= \mathbf{0} \ \text{ on } \ \partial\Omega\times(0,T]. && (4.4) \end{aligned}$$

Here, $\mathbf{u}$ represents velocity, p the (zero-mean) pressure, $\mathbf{f}$ an external force, and ν the kinematic viscosity.

Throughout the report, $(X_h, Q_h) \subset (H_0^1(\Omega), L_0^2(\Omega))$ will denote either the Taylor-Hood or Scott-Vogelius element pair. Due to the assumptions that the approximating polynomial degree $k \geq d$ and the mesh be constructed by a barycenter refinement of a quasi-uniform mesh (details in the following section), (X_h, Q_h) will be inf-sup stable.

The following lemma will be used in the analysis that follows.

Lemma 4.2.1. *There exists a constant $C^*(\Omega)$, dependent only on the size of Ω, that satisfies $\forall u, v, w \in H_0^1(\Omega)$,*

$$\begin{aligned} |(u\cdot\nabla v, w)| + |((\nabla\cdot u)v, w)| &\leq C^* \|\nabla u\| \|\nabla v\| \|\nabla w\|^{1/2} \|w\|^{1/2} && (4.5)\\ |(u\cdot\nabla v, w)| + |((\nabla\cdot u)v, w)| &\leq C^* \|\nabla u\| \|\nabla v\| \|\nabla w\| && (4.6) \end{aligned}$$

Proof. The first inequality follows from Holder's inequality, Ladyzhenskaya inequalities and the Sobolev imbedding theorem. The second follows directly from the first with the Poincare inequality in $H_0^1(\Omega)$. □

4.2.1 Scott-Vogelius and Taylor-Hood elements

The SV element pair is not yet very well known, and so we now give a brief description of it. In essence, the SV pair is the same as the TH pair except that

(i) $k \geq d$, where d is the space dimension,

(ii) the pressure space is discontinuous, and

(iii) the mesh is required to be a barycenter refinement of a regular mesh.

That is, polynomials of degree k and $k-1$ are used to approximate the velocity and pressure spaces respectively, with $k \geq d$ (which is only a restriction in 3d compared to TH), and the mesh $\mathcal{T}_h$ that is used must be derived from a regular triangularization (tetrahedralization) of Ω, where each element is refined by connecting its barycenter to the vertices. An illustration of such a refinement is given in Figure 4.1. With such a mesh construction and $k \geq d$, it was proved by Zhang in [58] that the SV elements are LBB stable under these restrictions. It is well known that the TH pair is LBB stable for this case [21].

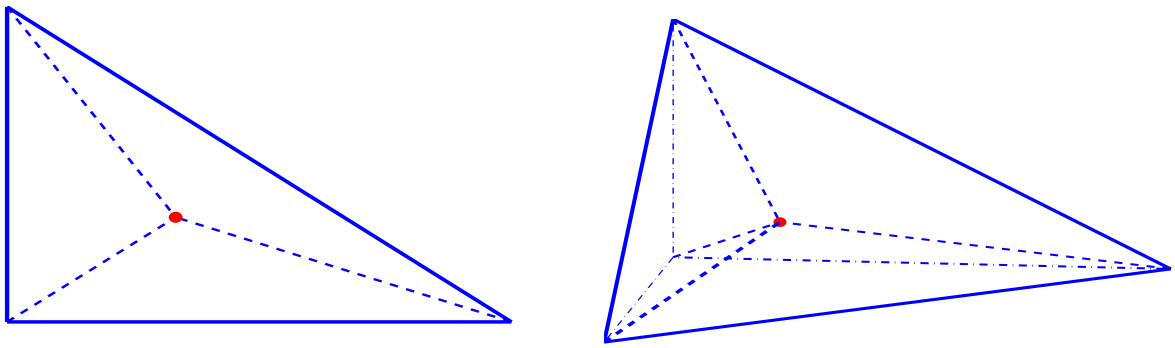

Figure 4.1: (LEFT) 2d and (RIGHT) 3d macro-element, shown with dashed lines representing barycenter refinements

We now formally define the element pairs. In space dimension d, for both Taylor-Hood and Scott-Vogelius elements we define X_h to be the space of continuous element-wise vector functions of polynomial order $k \geq d$ on $\mathcal{T}_h$

$$X_h := \left\{ \mathbf{v}_h \in [C(\Omega)]^d \colon \mathbf{v}_{h|T} \in [P_k(T)]^d, \text{for all } T \in \mathcal{T}_h \ , \ \mathbf{v}_h = \mathbf{0} \text{ on } \partial\Omega \right\}.$$

For Taylor-Hood, we define

$$Q_h^{\mathrm{TH}} := \left\{ q_h \in L^2(\Omega) \cap C(\Omega) \colon q_{h|T} \in P_{k-1}, \text{for all } T \in \mathcal{T}_h \right\},$$

while the pressure space of the Scott-Vogelius element is only different from Taylor-Hood's in that its pressures are discontinuous:

$$Q_h^{\mathrm{SV}} := \left\{ q_h \in L^2(\Omega) \colon q_{h|T} \in P_{k-1}, \text{for all } T \in \mathcal{T}_h \right\}.$$

Note that the dimension of the pressure space for SV elements is significantly larger than that for TH elements. This creates a greater total number of degrees of freedom needed for linear solves using SV elements, however it is not immediately clear whether this will lead to a significant increase in computational time if preconditioners such as Augmented Lagrangian type are used [4]. The authors plan to consider this questions in future studies.

Although the velocity spaces of the TH and SV elements are the same, the spaces of discretely divergence free subspaces are different, and will be denoted by

$$\begin{aligned} V_h^{SV} &:= \{ \mathbf{v}_h \in X_h \ : (\nabla \cdot \mathbf{v}_h, q_h) = 0 \ \forall q_h \in Q_h^{SV} \} \\ V_h^{TH} &:= \{ \mathbf{v}_h \in X_h \ : (\nabla \cdot \mathbf{v}_h, q_h) = 0 \ \forall q_h \in Q_h^{TH} \}. \end{aligned}$$

The SV element is very interesting from the mass conservation point of view since its discrete velocity space and its discrete pressure space fulfill an important property, namely

$$\nabla \cdot X_h \subset Q_h^{\mathrm{SV}}. \tag{4.7}$$

Thus, using SV elements, weak mass conservation via

$$(\nabla \cdot \mathbf{u}_h, q_h) = 0 \quad \forall q_h \in Q_h$$

implies strong (pointwise) mass conservation since we can choose the special test function $q_h = \nabla \cdot \mathbf{u}_h$

to get

$$\|\nabla \cdot \mathbf{u}_h\|^2 = 0\,.$$

In general, the same pressure test function cannot be used in the Taylor-Hood case, since $\nabla \cdot X_h \not\subset Q_h^{\mathrm{TH}}$. Hence the Taylor-Hood element only delivers discretely divergence-free approximations $\mathbf{u}_h$.

The temporal-spatial discretization we study, for either TH or SV, is the Crank-Nicolson Galerkin method, given in skew-symmetrized form by:
Find $(\mathbf{u}_h^n, p_h^n) \in X_h \times Q_h$ *with* $Q_h \in \{Q_h^{\mathrm{TH}}, Q_h^{\mathrm{SV}}\}$ *such that* $\forall (\mathbf{v}_h, q_h) \in X_h \times Q_h$ *for* $n = 1, 2, \ldots, M = T/\Delta t$,

$$\begin{aligned}
\frac{1}{\Delta t}(\mathbf{u}_h^{n+1} - \mathbf{u}_h^n, \mathbf{v}) - (p_h^{n+\frac{1}{2}}, \nabla \cdot \mathbf{v}_h) + \nu(\nabla \mathbf{u}_h^{n+\frac{1}{2}}, \nabla \mathbf{v}_h) \quad &+ \quad \gamma(\nabla \cdot \mathbf{u}_h^{n+\frac{1}{2}}, \nabla \cdot \mathbf{v}_h) \\
+(\mathbf{u}_h^{n+\frac{1}{2}} \cdot \nabla \mathbf{u}_h^{n+\frac{1}{2}}, \mathbf{v}_h) + \frac{1}{2}((\mathrm{div}\mathbf{u}_h^{n+\frac{1}{2}})\mathbf{u}_h^{n+\frac{1}{2}}, \mathbf{v}_h) \quad &= \quad (\mathbf{f}^{n+\frac{1}{2}}, \mathbf{v}_h) \qquad (4.8) \\
(\nabla \cdot \mathbf{u}_h^{n+1}, q_h) \quad &= \quad 0\,. \qquad (4.9)
\end{aligned}$$

For the discrete initial velocity, $\mathbf{u}_h^0$ we impose zero pointwise divergence for the initial condition for both SV or TH elements: $\forall (\mathbf{v}_h, q_h) \in (X_h, Q_h^{SV})$,

$$(\mathbf{u}_h^0, \mathbf{v}_h) + (\lambda_h, \nabla \cdot \mathbf{v}_h) + (\nabla \cdot \mathbf{u}_h^0, q_h) = (\mathbf{u}_0, \mathbf{v}_h)\,. \qquad (4.10)$$

This condition is necessary for TH elements due to the Crank-Nicolson temporal discretization and our enforcement of discrete mass conservation (4.9). For the backward Euler method, this would not be necessary. However, it is easy to implement.

Note that for SV elements, the term arising from skew-symmetrization vanishes, and is not necessary to use in computations.

4.3 A relation between the Taylor-Hood and the Scott-Vogelius element

Section 2 shows the Taylor-Hood and the Scott-Vogelius element are not unrelated to each other, as they only differ in their pressure space. But it turns out that much more can be said. For example, it is relatively easy to show that the H^1 projection of the TH solution to the Stokes problem into the space of divergence free functions is the SV solution of that Stokes problem (independent of grad-div stabilization). However, it is the results for the NSE are much more interesting.

We prove that as $\gamma \to \infty$, the TH solutions to (4.8)-(4.10) converge to the SV solution. Roughly speaking, this result can be understood in the following sense. Under the mesh restriction discussed above and with $k \geq d$, the grad-div stabilized solutions "lives between" the TH and SV solutions, which are both LBB stable and have optimal approximation properties. Thus, raising γ significantly larger than $O(1)$ in TH computations can provide excellent mass conservation without "destroying" the solution.

Theorem 4.3.1. *For Δt small enough, using a mesh constructed as a barycenter refinement of a regular mesh and $k \geq d$, any sequence $\{\mathbf{u}_h\}_{\gamma_i}$ of TH solutions to* (4.8)-(4.10) *converges to the SV solution as the grad-div parameter $\gamma_i \to \infty$.*

Remark 4. *The restriction that Δt be small enough arises from the discrete Gronwall inequality in exactly the same way as for convergence theories of finite element methods for the NSE.*

Proof. We begin by noting the a priori bound on the SV and TH solutions, which can be found by choosing the test function $\mathbf{v}_h = \mathbf{u}_h^{n+1/2}$ in (4.8): *For* $0 \leq j \leq M$

$$\left\|\mathbf{u}_h^j\right\|^2 + \Delta t \sum_{n=0}^{j-1} \left(\nu \left\|\nabla \mathbf{u}_h^{n+1/2}\right\|^2 + 2\gamma \left\|\nabla \cdot \mathbf{u}_h^{n+1/2}\right\|^2 \right) \leq \frac{\Delta t}{\nu} \sum_{n=0}^{j-1} \left\|f^{n+1/2}\right\|_{-1}^2 + \left\|u_h^0\right\|^2 \;=\; C(data)\,, \quad (4.11)$$

where $\|\cdot\|_*$ denotes the norm in X^*, the dual space of $X = H_0^1$ endowed with the norm $\|\mathbf{v}\|_X :=$

$\|\nabla \mathbf{v}\|$. (For the SV solution $\left\|\nabla \cdot \mathbf{u}_h^{n+1/2}\right\|^2 = 0$.) This bound is sufficient to show, using the Leray-Schauder fixed point theorem, that solutions to (4.8)-(4.10) exist for either element pair [30]. Since the timestep and mesh are fixed, uniqueness follows from the boundedness of solutions shown above.

In addition, by assumption of the existence of the SV solution (which is independent of γ) and LBB stability we have the SV pressure is bounded independent of γ. In particular we have that for $2 \leq j \leq M$

$$\Delta t \sum_{n=0}^{j-1} \left\| p_{SV}^{n+1/2} \right\|^2 \;\leq\; C(data)\,. \tag{4.12}$$

Note that from (4.11) it follows that as $\gamma \to \infty$, $\nabla \cdot \mathbf{u}_h^{n+1/2} \to 0$ for $n = 0, \ldots M-1$. Also, as $\nabla \cdot \mathbf{u}_h^0 = 0$, then $\nabla \cdot \mathbf{u}_h^{n+1} \to 0$ for $n = 0, \ldots M-1$. In addition, as $\left\|\mathbf{u}_h^j\right\|^2$ is uniformly bounded, then the terms $\left\|\nabla \mathbf{u}_h^j\right\|^2$ and $\left\|\nabla \cdot \mathbf{u}_h^j\right\|^2$ are also uniformly bounded. In these later cases the bound will depend upon the mesh parameter h. However, as we are discussing convergence on a fixed mesh, this dependence is not important.

Let $\mathbf{e} := \mathbf{u}_{SV} - \mathbf{u}_{TH} \in V_h^{TH}$, where $(\mathbf{u}_{SV}, p_{SV})$ and $(\mathbf{u}_{TH}, p_{TH})$ denote the SV and TH solutions respectively. (For convenience, in this proof we suppress the dependence on h.)

For $\mathbf{v} \in V_h^{TH}$, we have that $(p_{TH}^{n+\frac{1}{2}}, \nabla \cdot \mathbf{v}) = 0$ and thus that

$$\begin{aligned}
\frac{1}{\Delta t}(\mathbf{e}^{n+1} - \mathbf{e}^n, \mathbf{v}) - (p_{SV}^{n+\frac{1}{2}}, \nabla \cdot \mathbf{v}) + \nu(\nabla \mathbf{e}^{n+\frac{1}{2}}, \nabla \mathbf{v}) + \gamma(\nabla \cdot \mathbf{e}^{n+\frac{1}{2}}, \nabla \cdot \mathbf{v}) \\
+(\mathbf{u}_{SV}^{n+\frac{1}{2}} \cdot \nabla \mathbf{u}_{SV}^{n+\frac{1}{2}}, \mathbf{v}) - (\mathbf{u}_{TH}^{n+\frac{1}{2}} \cdot \nabla \mathbf{u}_{TH}^{n+\frac{1}{2}}, \mathbf{v}) + \frac{1}{2}((\mathrm{div}\mathbf{u}_{SV}^{n+\frac{1}{2}})\mathbf{u}_{SV}^{n+\frac{1}{2}}, \mathbf{v}) \\
-\frac{1}{2}((\mathrm{div}\mathbf{u}_{TH}^{n+\frac{1}{2}})\mathbf{u}_{TH}^{n+\frac{1}{2}}, \mathbf{v}) \;=\; \mathbf{0}\,,
\end{aligned} \tag{4.13}$$

which can be written as

$$\begin{aligned}
\frac{1}{\Delta t}(\mathbf{e}^{n+1} - \mathbf{e}^n, \mathbf{v}) \;+\; & \nu(\nabla \mathbf{e}^{n+\frac{1}{2}}, \nabla \mathbf{v}) + \gamma(\nabla \cdot \mathbf{e}^{n+\frac{1}{2}}, \nabla \cdot \mathbf{v}) \\
= -(\mathbf{e}^{n+1/2} \cdot \nabla \mathbf{u}_{SV}^{n+\frac{1}{2}}, \mathbf{v}) \;-\; & (\mathbf{u}_{TH}^{n+\frac{1}{2}} \cdot \nabla \mathbf{e}^{n+1/2}, \mathbf{v}) - \frac{1}{2}((\mathrm{div}\mathbf{e}^{n+1/2})\mathbf{u}_{SV}^{n+\frac{1}{2}}, \mathbf{v}) \\
& -\frac{1}{2}((\mathrm{div}\mathbf{u}_{TH}^{n+\frac{1}{2}})\mathbf{e}^{n+1/2}, \mathbf{v}) + (p_{SV}^{n+\frac{1}{2}}, \nabla \cdot \mathbf{v})\,.
\end{aligned} \tag{4.14}$$

With $\mathbf{v} = \mathbf{e}^{n+\frac{1}{2}}$, the identity

$$(\mathbf{u}_{TH}^{n+\frac{1}{2}} \cdot \nabla \mathbf{e}^{n+1/2}, \mathbf{e}^{n+\frac{1}{2}}) + \frac{1}{2}((\mathrm{div}\mathbf{u}_{TH}^{n+\frac{1}{2}})\mathbf{e}^{n+1/2}, \mathbf{e}^{n+\frac{1}{2}}) \;=\; 0\,,$$

and using Lemma 4.2.1, equation (4.14) becomes

$$\begin{aligned} & \frac{1}{2\Delta t}(\left\|\mathbf{e}^{n+1}\right\|^2 - \|\mathbf{e}^n\|^2) + \nu \left\|\nabla \mathbf{e}^{n+1/2}\right\|^2 + \gamma \left\|\nabla \cdot \mathbf{e}^{n+1/2}\right\|^2 \\ = \;& -\frac{1}{2}((\mathrm{div}\mathbf{e}^{n+\frac{1}{2}})\mathbf{u}_{SV}^{n+\frac{1}{2}}, \mathbf{e}^{n+1/2}) - (\mathbf{e}^{n+\frac{1}{2}} \cdot \nabla \mathbf{u}_{SV}^{n+\frac{1}{2}}, \mathbf{e}^{n+1/2}) + (p_{SV}^{n+\frac{1}{2}}, \nabla \cdot \mathbf{e}^{n+1/2}) \\ \leq \;& C \left\|\nabla \mathbf{e}^{n+1/2}\right\|^2 \left\|\nabla \mathbf{u}_{SV}^{n+1/2}\right\| + \left\|p_{SV}^{n+\frac{1}{2}}\right\| \left\|\nabla \cdot \mathbf{e}^{n+1/2}\right\|. \end{aligned} \tag{4.15}$$

Since the mesh is fixed, uniform boundedness, finite dimensionality of $\mathbf{u}_{SV}^{n+\frac{1}{2}}$, and Young's inequality imply

$$\begin{aligned} & \frac{1}{2\Delta t}(\left\|\mathbf{e}^{n+1}\right\|^2 - \|\mathbf{e}^n\|^2) + \nu \left\|\nabla \mathbf{e}^{n+1/2}\right\|^2 + \gamma \left\|\nabla \cdot \mathbf{e}^{n+1/2}\right\|^2 \\ \leq \;& C \left\|\mathbf{e}^{n+1/2}\right\|^2 + \frac{\gamma}{2} \left\|\nabla \cdot \mathbf{e}^{n+1/2}\right\|^2 + \frac{1}{2\gamma} \left\|p_{SV}^{n+1/2}\right\|^2. \end{aligned} \tag{4.16}$$

With $\left\|\mathbf{e}^0\right\| = 0$, subtracting $\frac{\gamma}{2} \left\|\nabla \cdot \mathbf{e}^{n+1/2}\right\|^2$ from both sides of (4.16), then summing from $n = 0$ to $j-1$, $2 \leq j \leq M$, we have

$$\begin{aligned} \left\|\mathbf{e}^j\right\|^2 + \Delta t \sum_{n=0}^{j-1} \left(2\nu \left\|\nabla \mathbf{e}^{n+1/2}\right\|^2 + \gamma \left\|\nabla \cdot \mathbf{e}^{n+1/2}\right\|^2\right) & \\ \leq C\Delta t \sum_{n=0}^{j} \|\mathbf{e}^n\|^2 + \frac{\Delta t}{\gamma} \sum_{n=0}^{j-1} \left\|p_{SV}^{n+1/2}\right\|^2. & \end{aligned} \tag{4.17}$$

The discrete Gronwall inequality [25] then implies that (for Δt sufficiently small)

$$\begin{aligned} \left\|\mathbf{e}^j\right\|^2 + \Delta t \sum_{n=0}^{j-1} \left(2\nu \left\|\nabla \mathbf{e}^{n+1/2}\right\|^2 + \gamma \left\|\nabla \cdot \mathbf{e}^{n+1/2}\right\|^2\right) &\leq C \frac{\Delta t}{\gamma} \sum_{n=0}^{j-1} \left\|p_{SV}^{n+1/2}\right\|^2 \\ &\leq C \frac{1}{\gamma}. \end{aligned}$$

Hence, as $\gamma \to \infty$, $\left\|\mathbf{e}^j\right\| \to 0$, $j = 1, 2, \ldots, M$, i.e. $\mathbf{u}_{TH} \to \mathbf{u}_{SV}$.

□

4.3.1 A connection for the steady NSE problem

An analogous result as proved above holds for the steady NSE. Consider the usual skew symmetrized finite element scheme for the NSE [30]: *Find* $(\mathbf{u}_h, p_h) \in (X_h, Q_h)$ *satisfying* $\forall (\mathbf{v}_h, q_h) \in (X_h, Q_h)$

$$\begin{aligned} \nu(\nabla \mathbf{u}_h, \nabla \mathbf{v}_h) - (p_h, \nabla \cdot \mathbf{v}_h) + \gamma(\nabla \cdot \mathbf{u}_h, \nabla \cdot \mathbf{v}_h) + (\mathbf{u}_h \cdot \nabla \mathbf{u}_h, \mathbf{v}_h) & \\ + \frac{1}{2}((\mathrm{div}\mathbf{u}_h)\mathbf{u}_h, \mathbf{v}_h) &= (\mathbf{f}, \mathbf{v}_h), \qquad (4.18) \\ (\nabla \cdot \mathbf{u}_h, q_h) &= 0, \qquad (4.19) \end{aligned}$$

where Q_h is either Q_h^{SV} or Q_h^{TH}. Note if $Q_h = Q_h^{SV}$, then trivially $\frac{1}{2}((\mathrm{div}\mathbf{u}_h)\mathbf{u}_h, \mathbf{v}_h) = \gamma(\nabla \cdot \mathbf{u}_h, \nabla \cdot \mathbf{v}_h) = 0$. It is not hard to show that solutions to (4.18) exist with the Leray-Schauder fixed point theorem, and under the small data condition $C^*\nu^{-2} \|\mathbf{f}\|_{-1} < 1$ (where $C^* = C^*(\Omega)$ is from Lemma 4.2.1), solutions are also unique [30].

Theorem 4.3.2. *Suppose the data in the problem* (4.18)-(4.19) *satifies* $\alpha := C^*\nu^{-2} \|f\|_{-1} < 1$. *Then for any sequence of grad-div stabilization parameters* $\gamma_i \to \infty$, *the corresponding TH solutions converge to the SV solution.*

Proof. Proceeding in an analogous manner as in the proof of Theorem 4.3.1, note that by choosing $\mathbf{v}_h = \mathbf{u}_h$

$$\nu \|\nabla \mathbf{u}_h\|^2 + 2\gamma \|\nabla \cdot \mathbf{u}_h\|^2 \leq \nu^{-1} \|\mathbf{f}\|_{-1}^2 \;=\; C(data). \qquad (4.20)$$

From (4.20) we have uniform boundedness of $\mathbf{u}_h$ (with respect to γ) by the Poincaré-Friedrichs inequality, and thus uniform boundedness of $\mathbf{e}_h$.

Following similar to the time dependent case, we have that $\mathbf{e}_h$ satisfies

$$\begin{aligned} \nu \|\nabla \mathbf{e}\|^2 + \gamma \|\nabla \cdot \mathbf{e}\|^2 &\leq C^* \|\nabla \mathbf{u}_{SV}\| \|\nabla \mathbf{e}\|^2 + \frac{\gamma}{2} \|\nabla \cdot \mathbf{e}\|^2 + \frac{1}{2\gamma} \|p_{SV}\|^2 \\ &\leq C^*\nu^{-1} \|\mathbf{f}\|_{-1} \|\nabla \mathbf{e}\|^2 + \frac{\gamma}{2} \|\nabla \cdot \mathbf{e}\|^2 + \frac{1}{2\gamma} \|p_{SV}\|^2, \qquad (4.21) \end{aligned}$$

and thus

$$(\nu - C^*\nu^{-1}\|\mathbf{f}\|_{-1})\|\nabla\mathbf{e}\|^2 + \frac{\gamma}{2}\|\nabla\cdot\mathbf{e}\|^2 \leq \frac{1}{2\gamma}\|p_{SV}\|^2. \tag{4.22}$$

Using the small data condition, this reduces to

$$\|\nabla\mathbf{e}\|^2 \leq \frac{C}{\gamma}\|p_{SV}\|^2, \tag{4.23}$$

which implies $\mathbf{e} \to \mathbf{0}$ as $\gamma \to \infty$.

□

4.4 2D Numerical Experiments

In this section we investigate the convergence theory of the previous section and the theory that NSE approximations using TH elements with large grad-div stabilization parameters will provide both good mass conservation and accurate solutions (when the SV solution is accurate), if $k \geq d$ and with the mesh restriction discussed in Section 2. Indeed we find this is the case.

4.4.1 Numerical Experiment 1: 2d channel flow around a cylinder on a barycenter refined mesh

The benchmark problem of 2D channel flow around a cylinder has been studied in numerous works, e.g. [50, 27, 29, 31], and is well documented in [50]. The domain is the rectangle $[0, 2.2] \times [0, 0.41]$ representing the channel with flow in the positive x direction, with a circle radius 0.05 centered at $(0.2, 0.2)$ representing the cylinder. No slip boundary conditions are prescribed on the top and bottom of the channel as well as on the cylinder, and the time dependent inflow and outflow velocity profiles are given by

$$\mathbf{u}(0, y, t) = \mathbf{u}(2.2, y, t) = \left[\frac{6}{0.41^2}\sin(\pi t/8)y(0.41 - y)\,,\, 0\right]^T, \quad 0 \leq y \leq 0.41.$$

The forcing function is set to zero, $\mathbf{f} = \mathbf{0}$, and the viscosity at $\nu = 0.001$, providing a time dependent Reynolds number, $0 \leq Re(t) \leq 100$. The initial condition is $\mathbf{u} = \mathbf{0}$, and we compute to end-time

$T = 8$ with time-step $\Delta t = 0.01$.

An accurate approximation of this flow's velocity field will show a vortex street forming behind the cylinder by $t = 4$, and a fully formed vortex street by $t = 7$. However, there is more than one way to measure accuracy. That is, even if the vortex street forms and the velocity vector field "appears" correct, if the velocity field does not conserve mass, then for many applications the solution may be unacceptable.

Solutions are computed for (P_2, P_1^{disc}) SV elements and for (P_2, P_1) TH elements with $\gamma = 0,\ 1,\ 100,\ 10,000$, all on the same barycenter refined mesh. This provides 6,578 velocity degrees of freedom and 4,797 pressure degrees of freedom for the SV pressure, and 845 pressure degrees of freedom for the TH simulation. Results of these simulations are shown in Table 4.1, and Figures 4.2 and 4.3.

γ	$\left\|\nabla \mathbf{u}_{TH}^{\gamma}(t=7) - \nabla \mathbf{u}_{SV}(t=7)\right\|$
0	5.7086
1	0.7616
100	7.9856e-3
10,000	8.5311e-5

Table 4.1: The table above shows convergence of the grad-div stabilized TH approximations to the SV approximation for numerical experiment 1.

Table 4.1 shows convergence of the TH approximations to the SV approximation as $\gamma \to \infty$. This agrees with the theory of Section 3. Figure 4.2 shows the plots of the velocity field, speed contours and pressure contours for SV and TH approximations with $\gamma = 0,\ 1,\ 100,\ 10,000$. The convergence as γ gets large of the TH approximations to the SV approximation is clear. We note the dramatic improvement for the TH approximation from changing $\gamma = 0$ to $\gamma = 1$, continuing to raise γ increases the accuracy further, until by $\gamma = 10,000$ when a very good approximation is found.

The benefit to mass conservation of increasing γ is shown in figure 4.3. Here we see with $\gamma = 10,000$, excellent mass conservation is achieved. Also we note that for the unstabilized TH approximation, $\|\nabla \cdot \mathbf{u}_h^n\| = O(1)$.

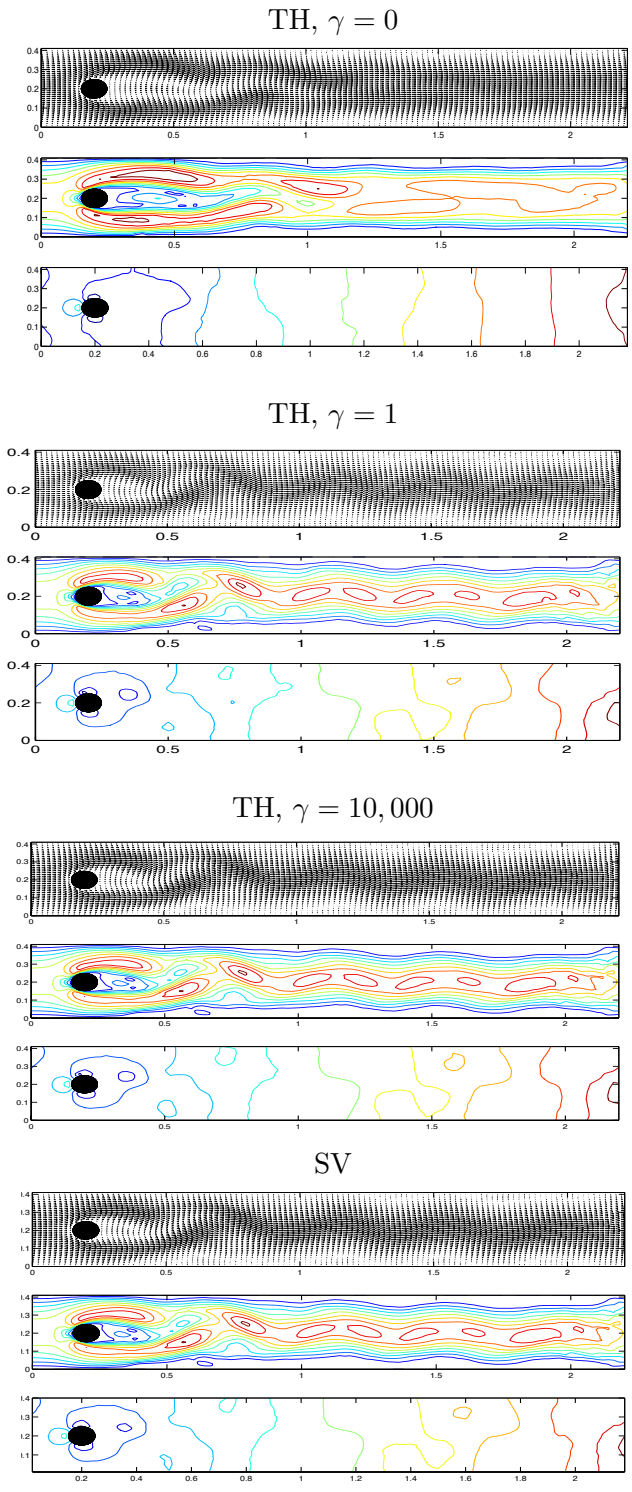

Figure 4.2: The t=7 velocity fields, speed contours, and pressure contour plots for approximations obtained using TH elements without grad-div stabilization (top), TH elements with $\gamma = 1$ (second from top), TH elements with $\gamma = 10,000$ (third from top), and the SV element approximation (bottom), on a barycentric mesh and $k = 2$. Convergence to the SV approximation as γ increases is clear. The SV and TH with $\gamma = 10,000$ approximations are nearly indistinguishable and agree well with known results [50, 27, 29]. Some slight differences with these and the plotted solution for TH elements with $\gamma = 1$ can be seen in the speed contours, and the $\gamma = 0$ solution is clearly underresolved.

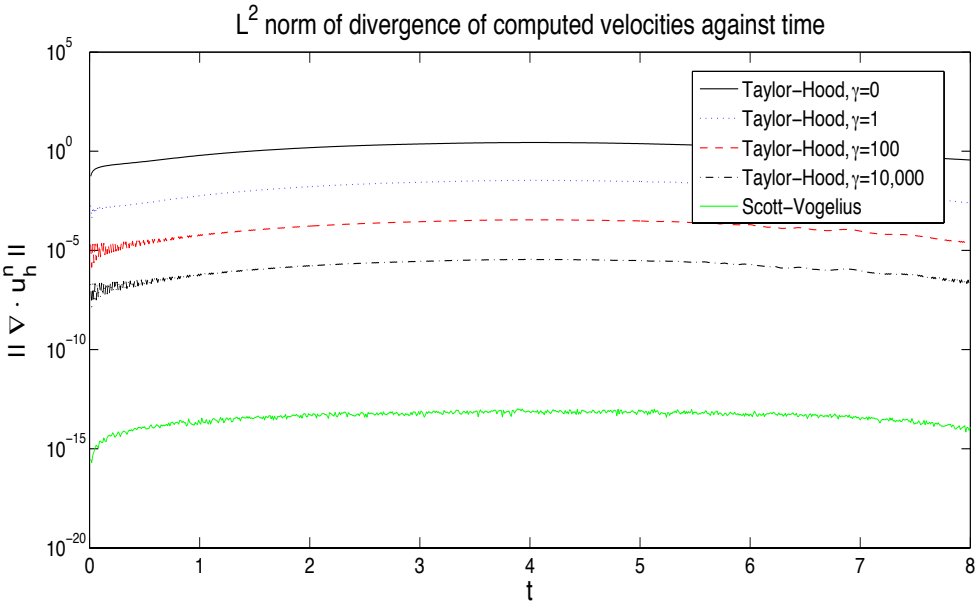

Figure 4.3: Shown above are the plots of $\|\nabla \cdot u_h^n\|$ vs. time for the SV and TH approximations for numerical experiment 1, with varying γ.

4.4.2 Numerical Experiment 2: The 3d driven cavity

In 3d, SV elements require $k \geq 3$. Here we compare the (P_3, P_2^{disc}) SV approximation with that obtained using by grad-div stabilized (P_3, P_2) TH elements.

We consider the benchmark problem of the 3D lid-driven cavity. This problem has been well-studied, [57, 44], and the description is as follows. The domain Ω is the $(-1, 1)^3$ cube, for boundary conditions the top of the box (lid) is prescribed the velocity $\mathbf{u} = [1, 0, 0]^T$ with the velocity on the the sides and bottom set to zero ($\mathbf{u} = \mathbf{0}$), and the viscosity $\nu = 1/50$, giving the Reynolds' number $Re = 2 \cdot 1 \cdot 50 = 100$. We compute with a barycenter refinement of a uniform tetrahedral mesh (as discussed in Section 2), consisting of 51,119 total dof for the TH elements (46,038 velocity and 5,081 pressure) and 76,038 total dof for SV elements (46,038 velocity and 30,000 pressure). The problem is solved directly for the steady state approximation with a Newton iteration, using as the initial guess $\mathbf{u}(\mathbf{x}) = \mathbf{0},\ \mathbf{x} \in \Omega$. Five iterations were required to converge to a tolerance of 10^{-10} for each of the tests. We compare the SV approximation and TH approximations with stabilization parameters $\gamma = 0,\ 1,\ 100,\ 10,000$. Plots of the approximations are presented in

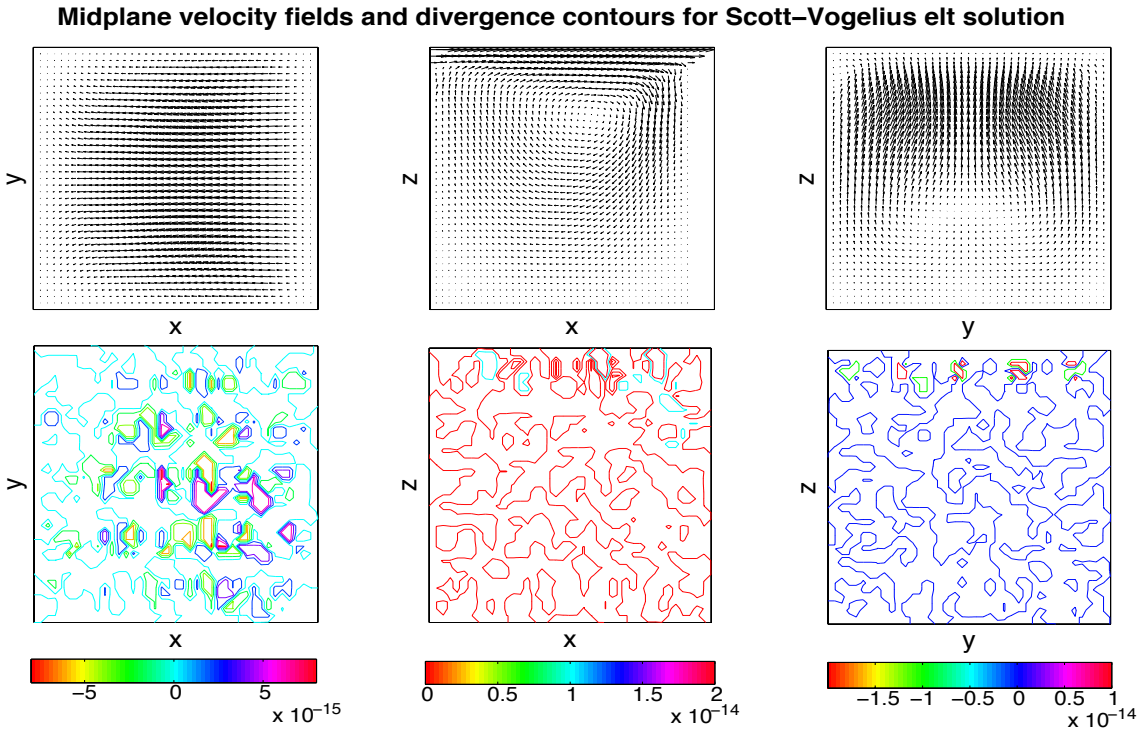

Figure 4.4: We see the expected velocity profiles for the lid-driven cavity problem with div $\mathbf{u}_h$ close to machine epsilon.

Figures 4.4-4.8.

Comparing the plots of the midplane velocity fields (Figures 4.4-4.8) with the documented solution [57, 44], the approximations "appear" correct. As noted in the the 2d experiments, the TH approximations with smaller γ exhibit poor mass conservation. In Figure 4.4, as expected, we see pointwise mass conservation for the SV element solution. In Figure 4.5 ($\gamma = 0$), we observe only $O(10^{-1})$ mass conservation. Figure 4.6 shows that $\gamma = 1$ improves the mass conservation to $O(10^{-2})$, and more grad-div stabilization (i.e. larger γ) further improves mass conservation as shown in Figures 4.7 and 4.8.

The convergence of the TH velocity approximations to the SV velocity approximation can be seen in Table 4.2, giving verification to the theory of Section 3.

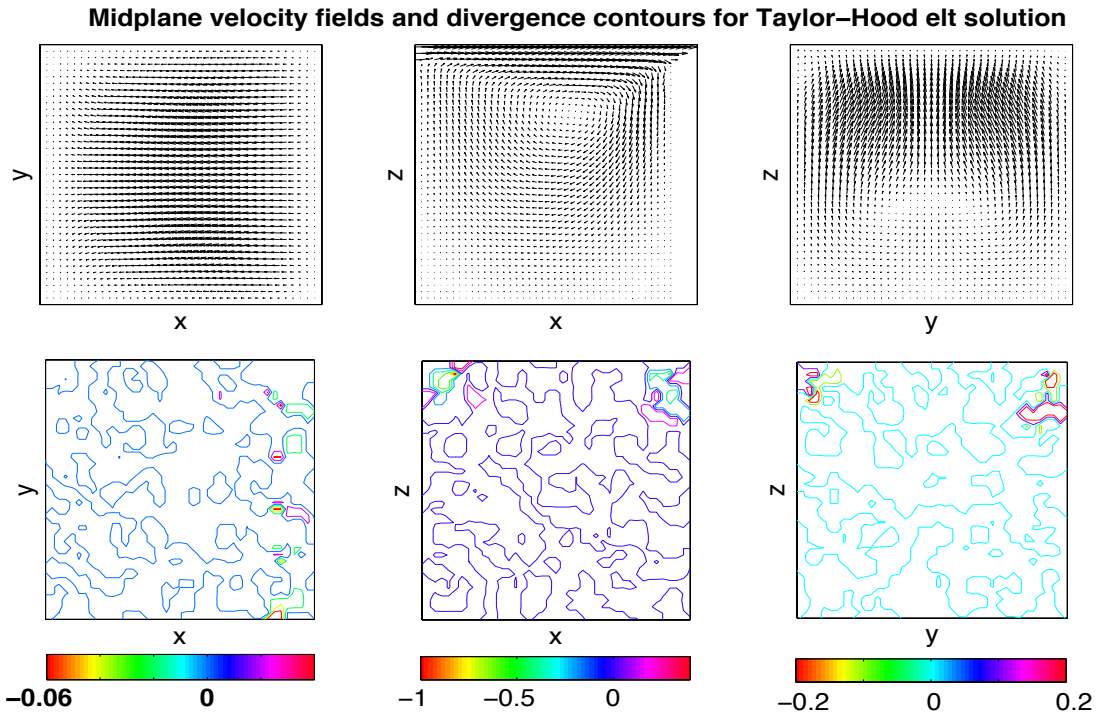

Figure 4.5: For TH with $\gamma = 0$, we see the expected velocity profiles for the lid-driven cavity problem, with non-negligible error for div $\mathbf{u}_h$.

γ	$\left\|\left\|\nabla \mathbf{u}_{TH}^{\gamma} - \nabla \mathbf{u}_{SV}\right\|\right\|$
0	1.0653
1	0.2093
100	0.0029
10,000	2.951e-5

Table 4.2: Convergence of the grad-div stabilized TH approximations toward the SV approximation as $\gamma \to \infty$ for the $Re = 100$ 3d driven cavity problem.

4.5 Conclusions and Future Directions

By proving (and then exploiting) a connection between Scott-Vogelius and grad-div stabilized Taylor Hood approximations of the NSE, we have shown that under a mild mesh restriction and by choosing the approximating polynomial degree $k \geq d$, grad-div stabilization can have a much greater positive effect on Taylor-Hood approximations than previously believed. In this situ-

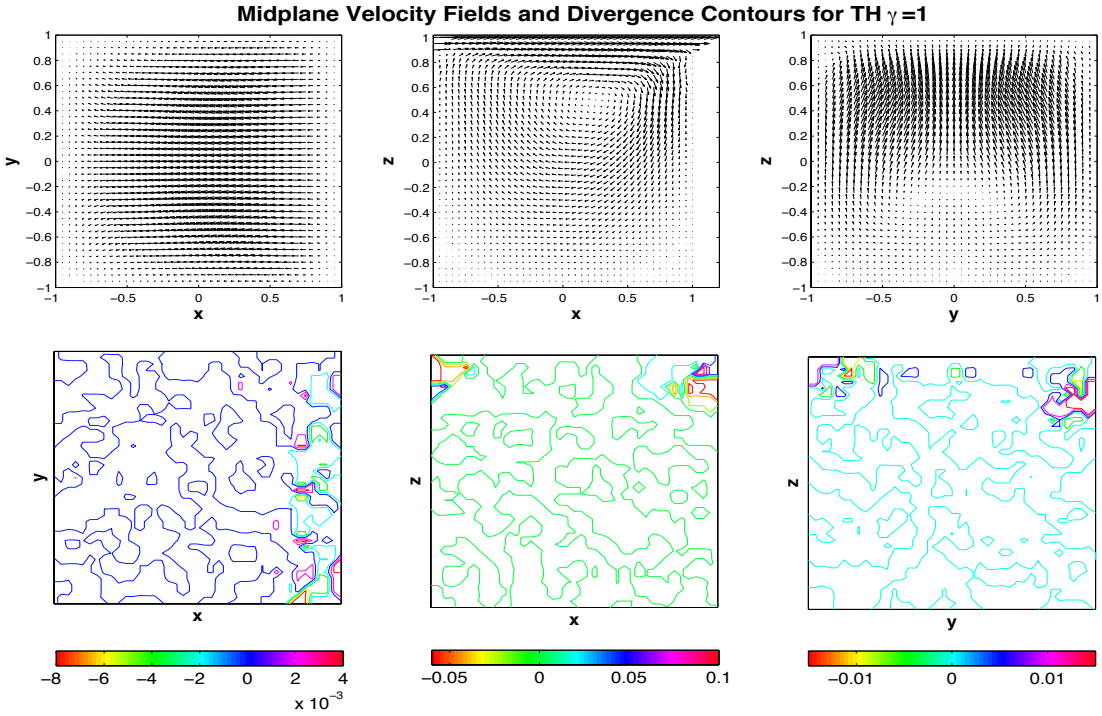

Figure 4.6: For TH with $\gamma = 1$, we see the expected velocity profiles for the lid-driven cavity problem with non-negligible error for div $\mathbf{u}_h$.

ation, we are able to raise the stabilization parameter larger than $O(1)$, thus achieving much better mass conservation.

We have also shown that Scott-Vogelius elements can be an excellent choice for approximating solutions to the NSE. To our knowledge, these are the first tests of this element pair on the time dependent Navier-Stokes equation.

Due to the similarity of Taylor-Hood elements and Scott-Vogelius elements, many existing codes using Taylor-Hood elements can be easily converted to use Scott-Vogelius elements (provided the mesh is as specified above). Hence we believe this element may be of great interest to engineers and fluid dynamicists interested in better mass conservation with reasonable development cost.

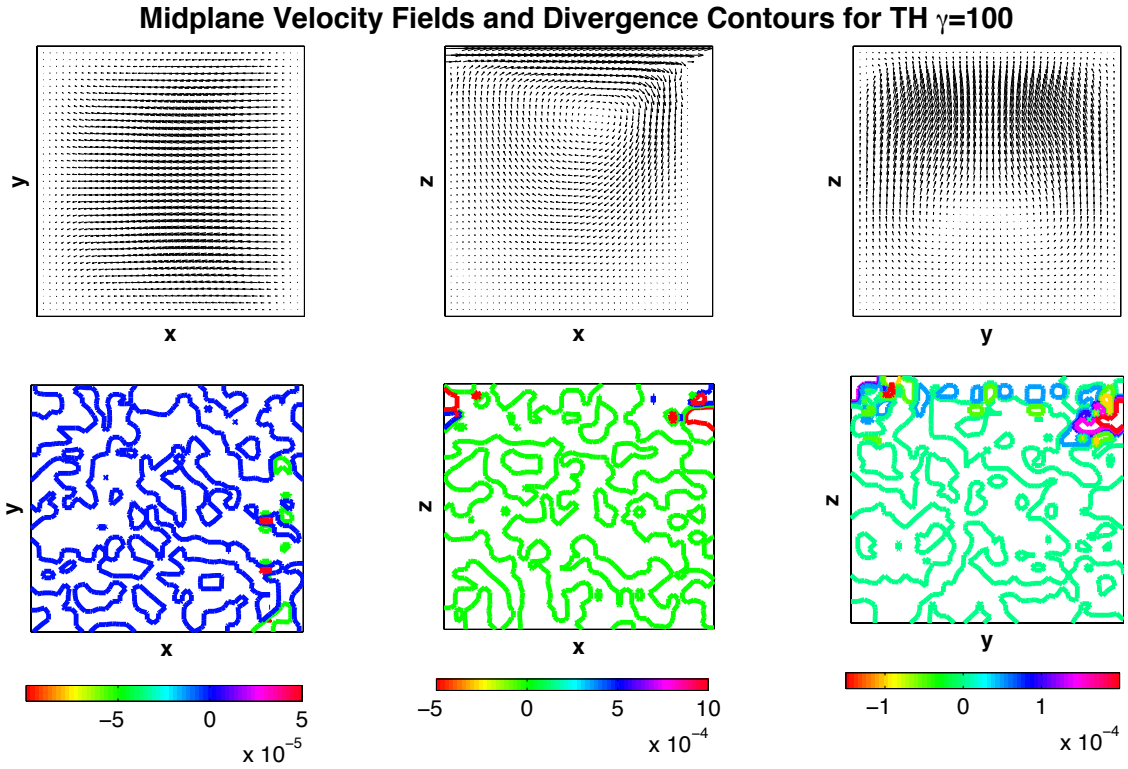

Figure 4.7: For TH with $\gamma = 100$, we see the expected velocity profiles for the lid-driven cavity problem with improved error for div $\mathbf{u}_h$.

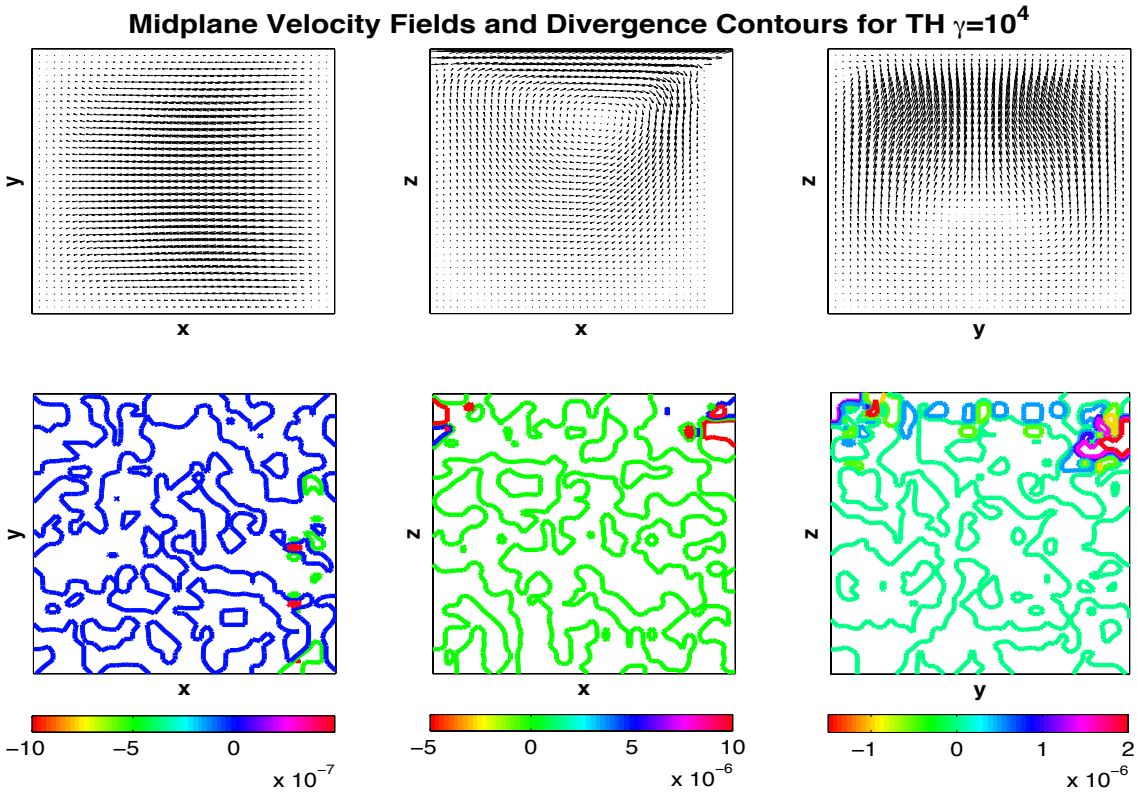

Figure 4.8: For TH with $\gamma = 10,000$, we see the expected velocity profiles for the lid-driven cavity problem with significantly improved error for div $\mathbf{u}_h$.

Chapter 5

An enhanced physics numerical scheme for MHD

5.1 Introduction

The study of magnetohydrodynamics (MHD) pertains to the interaction of fluid flow and magnetic fields. In order for the interaction of the fluid and magnetic field to be substantial, the fluids in question must be conductors and non-magnetic, which leads to the fields of study being salt water, liquid metals, plasmas and strong electrolytes. MHD is perhaps best known for its association with colossal failures in power generation, however in the last 30 years, it has been found to be pertinent to the flow of liquid sodium coolants in fast-breeder reactors, and the confinement of hot plasma thru magnetic forces during controlled thermonuclear fusion. Furthermore, magnetic fields are often used to heat, pump, stir and levitate liquid metals in the metallurgical industries [11].

The MHD conservation equations are given in magnetic field form by

$$\begin{aligned} u_t + \nabla \cdot (uu^T) - Re^{-1}\Delta u + \frac{S}{2}\nabla(B \cdot B) - S\nabla \cdot BB^T + \nabla p &= f, && (5.1)\\ \nabla \cdot u &= 0, && (5.2)\\ B_t + Re_m^{-1}\nabla \times (\nabla \times B) + \nabla \times (B \times u) &= \nabla \times g, && (5.3)\\ \nabla \cdot B &= 0, && (5.4) \end{aligned}$$

where u is velocity, p is pressure, f is body forces such as gravity, $\nabla \times g$ is a force on the magnetic field B, Re is the Reynolds number, Re_m is the magnetic Reynolds number, and S is the coupling number.

It is often the case that a careful treatment (or sometimes a clever trick) in the design of a numerical scheme to simulate physical phenomena can provide more physically relevant and accurate solutions. In particular, most schemes for fluid flow conserve energy, but there is often a second fundamental integral variant that is ignored. However, when this second quantity is accounted for in the design of the numerical scheme, the resulting scheme admits solutions with greater *physical accuracy*. The improved physical accuracy may not be evident over small time intervals but will ultimately manifest itself as time progresses. For example, Arakawas scheme for the 2D Navier-Stokes equations(NSE) that conserves energy and enstrophy[1], Arakawa and Lambs scheme for the shallow water equations that conserves enstrophy and potential enstrophy [2] and those of Navon [41, 42], J.G. Liu and W. Wangs schemes for 3D axi-symmetric NSE flow that conserves energy and helicity [36] and 3D axi-symmetric MHD flow that conserves energy and cross-helicity, and most recently a scheme for full 3D NSE that conserves energy and helicity [47], all exhibit better long time behavior than comparable schemes that conserve only energy.

This paper presents a study of a new Crank-Nicholson Galerkin finite element method (FEM) for incompressible MHD in general domains. It is the first to accurately treat both energy and cross-helicity, in the sense of global conservation, on general domains; as mentioned above, a scheme for axi-symmetric MHD flow was created in [36]. Moreover, with a carefully derived formulation and choice of finite elements, the scheme is also able to enforce pointwise mass conservation and pointwise enforcement of the magnetic field's incompressibility. Therefore, the proposed discrete scheme has the potential for excellent physical accuracy of its discrete solutions and therefore for long-time accuracy. We formally prove the conservation properties as well as stability and convergence for the scheme. Linearized extensions of the proposed scheme, which still preserve the same quantities, are also discussed.

This report is arranged as follows. Section 2 presents notation and preliminaries, section 3 derives the numerical scheme and proves conservation properties for it. Section 4 presents stability

and convergence analysis for the scheme, and section 5 discusses extensions of the scheme to a linearized form that still admits the conservation properties.

5.2 Notation and Preliminaries

We consider a polygonal or polyhedral domain Ω, with homogeneous Dirichlet boundary conditions for both velocity and the magnetic field. Extension to periodic boundaries is trivial, but requires the domain be a box, and extension to most other boundary conditions is done in the usual way.

We will denote the $L^2(\Omega)$ norma and inner product by $\|\cdot\|$ and $(\cdot,\cdot)$, respectively.

We will utilize the Poincare-Freidrich's inequality through our analysis: For $\phi \in H_0^1(\Omega)$,

$$\|\phi\| \leq C(\Omega)\,\|\nabla\phi\|\,.$$

The continuous function spaces natural for this problem are

$$\begin{aligned} X = H_0^1(\Omega) &= \{v \in H^1(\Omega) \;:\; v = 0 \text{ on } \partial\Omega\} \\ Q = L_0^2(\Omega) &= \{q \in L^2(\Omega) \;:\; \int_\Omega q = 0\} \end{aligned}$$

The following lemma for bounding the trilinear forms will be used heavily in our analysis.

Lemma 5.2.1. *For $u, v, w \in X$, there exists $C = C(\Omega)$ such that*

$$(u\cdot\nabla v, w) \leq C\,\|\nabla u\|\,\|\nabla v\|\,\|v\|^{1/2}\,\|\nabla v\|^{1/2} \tag{5.5}$$

$$(u\cdot\nabla v, w) \leq C\,\|\nabla u\|\,\|\nabla v\|\,\|\nabla v\| \tag{5.6}$$

Proof. These estimates follow from Holder's inequality, the Sobolev imbedding theorem and Poincare-Freidrich's inequality. □

The finite element spaces used throughout will be the Scott-Vogelius pair, $(X_h, Q_h) = (P_k, P_{k-1}^{disc})$, where it is required that $k \geq dim$ and the mesh be constructed as a barycenter re-

finement of a regular mesh. Under these conditions, it is known that this element pair is LBB stable [58]. This pair will be used to approximate the velocity-vorticity pair, and the magnetic field - lagrange multiplier pair. A fundamentally important property of this pair is that the usual Galerkin weak enforcement of incompressibility of an element $v_h \in X_h$ via

$$(\nabla \cdot v_h, q_h) = 0 \forall q_h \in Q_h,$$

implicitly enforces incompressibility pointwise since q_h can be chosen to be $\nabla \cdot v_h$, which provides

$$\|\nabla \cdot v_h\|^2 = 0 \implies \nabla \cdot v_h = 0$$

This is important in our proposed numerical scheme for three reasons. First, mass conservation can be enforced pointwise via the usual weak enforcement of incompressibility of velocity. Second, the incompressibility of the magnetic field can be enforced pointwise in the same manner; the magnetic field equation is derived from by taking the curl of the electric field, and since div of curl is zero, enforcing this incompressibility is of fundamental importance. Third, in all of our trilinear terms, skew-symmetry need not be enforced. This will lead to a cheaper assembly of linear systems.

Define the space of discretely divergence free function as

$$V_h := \{v_h \in X_h \ : \ (\nabla \cdot v_h, q_h) = 0 \ \forall q_h \in Q_h\}.$$

Note that functions in V_h, when using the Scott-Vogelius pair, are pointwise divergence free.

5.3 Derivation of energy and cross-helicity conserving scheme

We begin with the formulation (5.1)-(5.4), expand the curl operator in the (5.3) equation and use that $\nabla \cdot u = \nabla \cdot B = 0$ to get

$$\begin{aligned} u_t + u \cdot \nabla u - Re^{-1}\Delta u + \frac{S}{2}\nabla(B \cdot B) - SB \cdot \nabla B + \nabla p &= f && (5.7)\\ \nabla \cdot u &= 0 && (5.8)\\ B_t + Re_m^{-1}\nabla \times (\nabla \times B) + u \cdot \nabla B - B \cdot \nabla u &= \nabla \times g && (5.9)\\ \nabla \cdot B &= 0 && (5.10) \end{aligned}$$

So that (5.10) can be explicitly enforced, the addition of a Lagrange multiplier to (5.9) is done by adding the (zero) term $\nabla(\nabla \cdot B)$, then substituting $\lambda = \nabla \cdot B$ to get the new set of equations which has four unknowns and 4 equations,

$$\begin{aligned} u_t + u \cdot \nabla u - Re^{-1}\Delta u + \frac{S}{2}\nabla(B \cdot B) - SB \cdot \nabla B + \nabla p &= f && (5.11)\\ \nabla \cdot u &= 0 && (5.12)\\ B_t + Re_m^{-1}\nabla \times (\nabla \times B) + u \cdot \nabla B - B \cdot \nabla u + \nabla\lambda &= \nabla \times g && (5.13)\\ \nabla \cdot B &= 0 && (5.14) \end{aligned}$$

From here, we incorporate the homogeneous Dirichlet boundary condition into the function spaces, and discretize with the Galerkin finite element method and a four-leg Crank-Nicolson temporal discretization. We denote $u_h^{n+\frac{1}{2}} := \frac{1}{2}(u_h^n + u_h^{n+1})$, and require the initial u_h^0 and B_h^0 be in V_h. Then $\forall(v_h, \chi_h, q_h, r_h) \in (X_h, X_h, Q_h, Q_h)$ find $(u_h^{n+1}, B_h^{n+1}, p_h^{n+\frac{1}{2}}, \lambda_h^{n+\frac{1}{2}}) \in (X_h, X_h, Q_h, Q_h)$ for

$n = 0, 1, 2, ..., M = \frac{T}{\Delta t}$

$$\frac{1}{\Delta t}(u_h^{n+1} - u_h^n, v_h) + (u_h^{n+\frac{1}{2}} \cdot \nabla u_h^{n+\frac{1}{2}}, v_h) + Re^{-1}(\nabla \times u_h^{n+\frac{1}{2}}, \nabla \times v_h)$$
$$+\frac{s}{2}(B_h^{n+\frac{1}{2}} \cdot B_h^{n+\frac{1}{2}}, \nabla \cdot v_h) - s(B_h^{n+\frac{1}{2}} \cdot \nabla B_h^{n+\frac{1}{2}}, v_h) - (p_h^{n+\frac{1}{2}}, \nabla \cdot v_h) = (f(t^{n+\frac{1}{2}}), v_h) \tag{5.15}$$

$$(\nabla \cdot u_h^{n+1}, q_h) = 0 \tag{5.16}$$

$$\frac{1}{\Delta t}(B_h^{n+1} - B_h^n, \chi_h) + Re_m^{-1}(\nabla \times B_h^{n+\frac{1}{2}}, \nabla \times \chi_h) - (B_h^{n+\frac{1}{2}} \cdot \nabla u_h^{n+\frac{1}{2}}, \chi_h)$$
$$+(u_h^{n+\frac{1}{2}} \cdot \nabla B_h^{n+\frac{1}{2}}, \chi_h) + (\lambda_h^{n+\frac{1}{2}}, \nabla \cdot \chi_h) = (\nabla \times g(t^{n+\frac{1}{2}}), \chi_h) \tag{5.17}$$

$$(\nabla \cdot B_h^{n+1}, r_h) = 0 \tag{5.18}$$

Lemma 5.3.1. *Solutions to the scheme* (5.15)-(5.18) *admit the following conservation laws:*

- *Mass conservation*

$$\nabla \cdot u_h^n = 0 \text{ (pointwise)} \tag{5.19}$$

- *Incompressibility of the magnetic field*

$$\nabla \cdot B_h^n = 0 \text{ (pointwise)} \tag{5.20}$$

- *Global energy conservation*

$$\left(\left\|\frac{1}{2}u_h^M\right\|^2 + \frac{s}{2}\left\|B_h^M\right\|^2\right) + \Delta t \sum_{n=0}^{M-1}\left(Re^{-1}\left\|\nabla \times u_h^{n+\frac{1}{2}}\right\|^2 + sRe_m^{-1}\left\|\nabla \times B_h^{n+\frac{1}{2}}\right\|^2\right)$$
$$= \left(\frac{1}{2}\left\|u_h^0\right\|^2 + \frac{s}{2}\left\|B_h^0\right\|^2\right) + \Delta t \sum_{n=0}^{M-1}\left((f(t^{n+\frac{1}{2}}), u_h^{n+\frac{1}{2}}) + s(\nabla \times g(t^{n+\frac{1}{2}}), B_h^{n+\frac{1}{2}})\right) \tag{5.21}$$

- *Global cross-helicity conservation*

$$(u_h^M, B_h^M) + \Delta t \sum_{n=0}^{M-1}\left((Re^{-1} + Re_m^{-1})(\nabla \times u_h^{n+\frac{1}{2}}, \nabla \times B_h^{n+\frac{1}{2}})\right)$$
$$= (u_h^0, B_h^0) + \Delta t \sum_{n=0}^{M-1}\left((\nabla \times g(t^{n+\frac{1}{2}}), u_h^{n+\frac{1}{2}}) + (f(t^{n+\frac{1}{2}}), B_h^{n+\frac{1}{2}})\right) \tag{5.22}$$

Hence for $f = g = 0$ and $Re = Re_m = \infty$, we have exact conservation of both energy and cross-helicity.

Proof. First, we note that for Scott-Vogelius elements, we can choose $q_h = \nabla \cdot u_h^{n+1}$ and $r_h = \nabla \cdot B_h^{n+1}$. Hence we have that $\nabla \cdot u_h^{n+1} = \nabla \cdot B_h^{n+1} = 0$, and thus that $\nabla \cdot u_h^{n+1/2} = \nabla \cdot B_h^{n+1/2} = 0$. This proves the first two conservation laws, and moreover these results will be used in the proofs of the other laws.

To prove energy conservation choose $v_h = u_h^{n+\frac{1}{2}}$ and $\chi_h = B_h^{n+\frac{1}{2}}$ which vanishes the second, fourth, and sixth terms in (5.15) and the fourth and fifth terms in (5.17), leaving

$$\frac{1}{2\Delta t}\left(\left\|u_h^{n+1}\right\|^2 - \|u_h^n\|^2\right) + Re^{-1}\left\|\nabla \times u_h^{n+\frac{1}{2}}\right\|^2 - s(B_h^{n+\frac{1}{2}} \cdot \nabla B_h^{n+\frac{1}{2}}, u_h^{n+\frac{1}{2}}) = (f(t^{n+\frac{1}{2}}), u_h^{n+\frac{1}{2}}), \tag{5.23}$$

$$\frac{1}{2\Delta t}\left(\left\|B_h^{n+1}\right\|^2 - \|B_h^n\|^2\right) + Re_m^{-1}\left\|\nabla \times B_h^{n+\frac{1}{2}}\right\|^2 - (B_h^{n+\frac{1}{2}} \cdot \nabla u_h^{n+\frac{1}{2}}, B_h^{n+\frac{1}{2}}) = (\nabla \times g(t^{n+\frac{1}{2}}), B_h^{n+\frac{1}{2}}). \tag{5.24}$$

Multiplying (5.24) by s, rewriting the nonlinear term in (5.23) as $-s(B_h^{n+\frac{1}{2}} \cdot \nabla B_h^{n+\frac{1}{2}}, u_h^{n+\frac{1}{2}}) = s(B_h^{n+\frac{1}{2}} \cdot \nabla u_h^{n+\frac{1}{2}}, B_h^{n+\frac{1}{2}})$, and adding (5.23) and (5.24) gives

$$\frac{1}{2\Delta t}(\left\|u_h^{n+1}\right\|^2 - \|u_h^n\|) + \frac{s}{2\Delta t}(\left\|B_h^{n+1}\right\|^2 - \|B_h^n\|^2) + Re^{-1}\left\|\nabla \times u_h^{n+\frac{1}{2}}\right\|^2 + sRe_m^{-1}\left\|\nabla \times B_h^{n+\frac{1}{2}}\right\|^2 = (f(t^{n+\frac{1}{2}}), u_h^{n+\frac{1}{2}}) + s(\nabla \times g(t^{n+\frac{1}{2}}), B_h^{n+\frac{1}{2}}). \tag{5.25}$$

Multipling by Δt and summing over timesteps finishes the proof of (5.21).

To prove cross helicity is conserved we choose $v_h = B_h^{n+\frac{1}{2}}$ in (5.15) and $\chi_h = u_h^{n+\frac{1}{2}}$ in (5.17). This vanishes the fourth, fifth and sixth terms in (5.17) and the third and fifth terms in (5.15), leaving

$$\frac{1}{\Delta t}(u_h^{n+1}-u_h^n,B_h^{n+\frac{1}{2}})+(u_h^{n+\frac{1}{2}}\cdot\nabla u_h^{n+\frac{1}{2}},B_h^{n+\frac{1}{2}})+Re^{-1}(\nabla\times u_h^{n+\frac{1}{2}},\nabla\times B_h^{n+\frac{1}{2}})$$
$$=(f(t^{n+\frac{1}{2}}),B_h^{n+\frac{1}{2}}), \tag{5.26}$$
$$\frac{1}{\Delta t}(B_h^{n+1}-B_h^n,u_h^{n+\frac{1}{2}})+Re_m^{-1}(\nabla\times B_h^{n+\frac{1}{2}},\nabla\times u_h^{n+\frac{1}{2}})+(u_h^{n+\frac{1}{2}}\cdot\nabla B_h^{n+\frac{1}{2}},u_h^{n+\frac{1}{2}})$$
$$=(\nabla\times g(t^{n+\frac{1}{2}}),u_h^{n+\frac{1}{2}}). \tag{5.27}$$

Adding (5.26) and (5.27) and noting that:

$$\bullet\ (u_h^{n+\frac{1}{2}}\cdot\nabla u_h^{n+\frac{1}{2}},B_h^{n+\frac{1}{2}})=-(u_h^{n+\frac{1}{2}}\cdot\nabla B_h^{n+\frac{1}{2}},u_h^{n+\frac{1}{2}}) \tag{5.28}$$
$$\bullet\frac{1}{\Delta t}(u_h^{n+1}-u_h^n,B_h^{n+\frac{1}{2}})+\frac{1}{\Delta t}(B_h^{n+1}-B_h^n,u_h^{n+\frac{1}{2}}) \tag{5.29}$$
$$=\frac{1}{2\Delta t}\left((u_h^{n+1},B_h^{n+1})-(u_h^n,B_h^n)\right)+\frac{1}{2\Delta t}\left((u_h^{n+1},B_h^n)-(u_h^n,B_h^{n+1})\right) \tag{5.30}$$
$$+\frac{1}{2\Delta t}\left((B_h^{n+1},u_h^{n+1})-(B_h^n,u_h^n)\right)-\frac{1}{2\Delta t}\left((B_h^{n+1},u_h^n)-(B_h^n,u_h^{n+1})\right), \tag{5.31}$$

gives

$$\frac{1}{\Delta t}\left((u_h^{n+1},B_h^{n+1})-(u_h^n,B_h^n)\right)+(Re^{-1}+Re_m^{-1})(\nabla\times u_h^{n+\frac{1}{2}},\nabla\times B_h^{n+\frac{1}{2}})$$
$$=(\nabla\times g(t^{n+\frac{1}{2}}),u_h^{n+\frac{1}{2}})+(f(t^{n+\frac{1}{2}}),B_h^{n+\frac{1}{2}}) \tag{5.32}$$

Multiplying by Δt and summing over timesteps finishes the proof of (5.22).

□

5.4 Numerical analysis of the scheme

We prove that the scheme is both unconditionally stable and optimally convergent in this section.

Lemma 5.4.1. *Solutions to the scheme* (5.15)-(5.18) *are stable provided* $f\in L^2(0,T;H^{-1}(\Omega))$ *and*

$g \in L^2(0,T;L^2(\Omega))$, *and satisfy*

$$\left(\left\|u_h^M\right\|^2 + s\left\|B_h^M\right\|^2\right) + \Delta t \sum_{n=0}^{M-1}\left(Re^{-1}\left\|\nabla \times u_h^{n+\frac{1}{2}}\right\|^2 + sRe_m^{-1}\left\|\nabla \times B_h^{n+\frac{1}{2}}\right\|^2\right)$$
$$\leq \left(\left\|u_h^0\right\|^2 + s\left\|B_h^0\right\|^2\right) + \Delta t \sum_{n=0}^{M-1}\left(Re\left\|f(t^{n+\frac{1}{2}})\right\|_{-1}^2 + sRe_m\left\|g(t^{n+\frac{1}{2}})\right\|^2\right) = C(data). \quad (5.33)$$

Proof. We begin this proof with the energy conservation equality (5.21),

$$\left(\left\|\frac{1}{2}u_h^M\right\|^2 + \frac{s}{2}\left\|B_h^M\right\|^2\right) + \Delta t \sum_{n=0}^{M-1}\left(Re^{-1}\left\|\nabla \times u_h^{n+\frac{1}{2}}\right\|^2 + sRe_m^{-1}\left\|\nabla \times B_h^{n+\frac{1}{2}}\right\|^2\right)$$
$$= \left(\frac{1}{2}\left\|u_h^0\right\|^2 + \frac{s}{2}\left\|B_h^0\right\|^2\right) + \Delta t \sum_{n=0}^{M-1}\left((f(t^{n+\frac{1}{2}}), u_h^{n+\frac{1}{2}}) + s(\nabla \times g(t^{n+\frac{1}{2}}), B_h^{n+\frac{1}{2}})\right) \quad (5.34)$$

The forcing term can be majorized with Cauchy-Schwarz and Young's inequalities to get

$$(f(t^{n+\frac{1}{2}}), u_h^{n+\frac{1}{2}}) \leq \frac{Re}{2}\left\|f(t^{n+\frac{1}{2}})\right\|_{-1}^2 + \frac{Re^{-1}}{2}\left\|\nabla u_h^{n+1/2}\right\|^2, \quad (5.35)$$

and similarly for the magnetic forcing term,

$$s(\nabla \times g(t^{n+\frac{1}{2}}), B_h^{n+\frac{1}{2}}) \leq \frac{sRe_m}{2}\left\|g(t^{n+\frac{1}{2}})\right\|^2 + \frac{sRe_m^{-1}}{2}\left\|\nabla B_h^{n+\frac{1}{2}}\right\|^2. \quad (5.36)$$

Using (5.35) and (5.36) in (5.34) gives

$$\left(\left\|u_h^M\right\|^2 + s\left\|B_h^M\right\|^2\right) + \Delta t \sum_{n=0}^{M-1}\left(Re^{-1}\left\|\nabla \times u_h^{n+\frac{1}{2}}\right\|^2 + sRe_m^{-1}\left\|\nabla \times B_h^{n+\frac{1}{2}}\right\|^2\right)$$
$$\leq \left(\left\|u_h^0\right\|^2 + s\left\|B_h^0\right\|^2\right) + \Delta t \sum_{n=0}^{M-1}\left(Re\left\|f(t^{n+\frac{1}{2}})\right\|_{-1}^2 + sRe_m\left\|g(t^{n+\frac{1}{2}})\right\|^2\right), \quad (5.37)$$

which proves the lemma. □

We now prove convergence of the scheme.

Theorem 5.4.1. *Assuming the existence of a continuous solution,* (u,p,B) *to (3.5)-(3.8), then under the specified conditions*

1. *s is a positive constant,*

2. *Lemma 3.2 holds,*

3. *$(P_k, P_{k-1}^{disc.})$ elements (SV elements),*

4. *$B_t, u_t \in L^2(\Omega, [0,T])$,*

5. *$B_{tt}, u_{tt} \in L^2(\Omega, [0,T])$,*

6. *$B_{ttt}, u_{ttt} \in L^2(\Omega, [0,T])$,*

7. *$B, u \in L^\infty(0,T; H^m(\Omega))$, where $m = \max(3,k)$*

the solution to the discretized formulation, $(u_h, p_h, B_h, \lambda_h)$ converges to the continuous solution with optimal rate

$$\|u - u_h\|_{2,1} + \|B - B_h\|_{2,1} = O(\Delta t^2 + h^k).$$

Proof. Multiply the momentum and magnetic equations at $t^{n+1/2}$ by $v_h \in V_h$ and $\chi_h \in V_h$, respectively, and integrate over the domain. Denoting $e_u^k = u_h^k - u^k$, $e_B^k = B_h^k - B^k$, we get

$$\begin{aligned}(u_t(t^{n+\frac{1}{2}}), v_h) + (u(t^{n+\frac{1}{2}}) \cdot \nabla u(t^{n+\frac{1}{2}}), v_h) + Re^{-1}(\nabla u(t^{n+\frac{1}{2}}), \nabla v_h) \\ - s(B(t^{n+\frac{1}{2}}) \cdot \nabla B(t^{n+\frac{1}{2}}), \nabla \cdot v_h) - \frac{s}{2}(B(t^{n+\frac{1}{2}}) \cdot B(t^{n+\frac{1}{2}}), \nabla \cdot v_h) \\ = (f(t^{n+\frac{1}{2}}), v_h)\end{aligned} \tag{5.38}$$

$$\begin{aligned}(B_t(t^{n+\frac{1}{2}}), \chi_h) + Re_m^{-1}(B(t^{n+\frac{1}{2}}), \nabla \chi_h) - (B(t^{n+\frac{1}{2}}) \cdot \nabla u(t^{n+\frac{1}{2}}), \chi_h) \\ + (u^{n+\frac{1}{2}} \cdot \nabla B^{n+\frac{1}{2}}, \chi_h) = (\nabla \times g(t^{n+\frac{1}{2}}), \chi_h).\end{aligned} \tag{5.39}$$

As usual, we will look to subtract the continuous formulation of the variational problem from the discrete formulation. We start this process by introducing the following terms (5.40)-(5.44),

which replace the terms in the left-hand side of (5.38).

$$(u_t(t^{n+\frac{1}{2}}), v_h) \pm \frac{1}{\Delta t}(u(t^{n+1}) - u(t^n), v_h) = \frac{1}{\Delta t}(u(t^{n+1}) - u(t^n), v_h) + (u_t(t^{n+\frac{1}{2}}) - \{u(t^{n+1}) - u(t^n)\}\Delta t^{-1}, v_h). \tag{5.40}$$

$$(u(t^{n+\frac{1}{2}}) \cdot \nabla u(t^{n+\frac{1}{2}}), v_h) \pm (u^{n+\frac{1}{2}} \cdot \nabla u^{n+\frac{1}{2}}, v_h) = (u(t^{n+\frac{1}{2}}) \cdot \nabla (u(t^{n+\frac{1}{2}}) - u^{n+\frac{1}{2}}), v_h) + ((u(t^{n+\frac{1}{2}}) - u^{n+\frac{1}{2}}) \cdot \nabla u^{n+\frac{1}{2}}, v_h) + (u^{n+\frac{1}{2}} \cdot \nabla u^{n+\frac{1}{2}}, v_h). \tag{5.41}$$

$$Re^{-1}\left((\nabla u(t^{n+\frac{1}{2}}), \nabla v_h) \pm (\nabla u^{n+\frac{1}{2}}, \nabla v_h)\right) = Re^{-1}(\nabla (u(t^{n+\frac{1}{2}}) - u^{n+\frac{1}{2}}), \nabla v_h) + Re^{-1}(\nabla u^{n+\frac{1}{2}}, \nabla v_h) \tag{5.42}$$

$$-\frac{s}{2}(B(t^{n+\frac{1}{2}}) \cdot B(t^{n+\frac{1}{2}}), \nabla \cdot v_h) \pm \frac{s}{2}(B^{n+\frac{1}{2}} \cdot B^{n+\frac{1}{2}}, \nabla \cdot v_h) = \frac{s}{2}(B^{n+\frac{1}{2}} \cdot (B^{n+\frac{1}{2}} - B(t^{n+\frac{1}{2}})), \nabla \cdot v_h) + \frac{s}{2}((B^{n+\frac{1}{2}} - B(t^{n+\frac{1}{2}})) \cdot B_h^{n+\frac{1}{2}}, \nabla \cdot v_h) - \frac{s}{2}(B^{n+\frac{1}{2}} \cdot B^{n+\frac{1}{2}}, \nabla \cdot v_h) \tag{5.43}$$

$$-s(B(t^{n+\frac{1}{2}}) \cdot \nabla B(t^{n+\frac{1}{2}}), v_h) \pm s(B^{n+\frac{1}{2}} \cdot \nabla B^{n+\frac{1}{2}}, v_h) = s(B^{n+\frac{1}{2}} \cdot \nabla (B^{n+\frac{1}{2}} - B(t^{n+\frac{1}{2}})), v_h) + s((B^{n+\frac{1}{2}} - B(t^{n+\frac{1}{2}})) \cdot \nabla B(t^{n+\frac{1}{2}}), v_h) - s(B^{n+\frac{1}{2}} \cdot \nabla B^{n+\frac{1}{2}}, v_h). \tag{5.44}$$

Now we can directly subtract (5.38) from (5.15),

$$\begin{aligned}
&\frac{1}{\Delta t}(e_u^{n+1}-e_u^n,v_h)+Re^{-1}(\nabla e_u^{n+\frac{1}{2}},\nabla v_h)+(u_h^{n+\frac{1}{2}}\cdot\nabla e_u^{n+\frac{1}{2}},v_h)+(e_u^{n+\frac{1}{2}}\cdot\nabla u^{n+\frac{1}{2}},v_h)\\
&\qquad -s(B_h^{n+\frac{1}{2}}\cdot e_B^{n+\frac{1}{2}},v_h)-s(B_h^{n+\frac{1}{2}}]\cdot\nabla e_B^{n+\frac{1}{2}},v_h)-s(e_B^{n+\frac{1}{2}}\cdot\nabla B^{n+\frac{1}{2}},v_h)\\
&\qquad =(u_t(t^{n+\frac{1}{2}})-\{u(t^{n+1})-u(t^n)\}\Delta t^{-1},v_h)+Re^{-1}(\nabla(u(t^{n+\frac{1}{2}})-u^{n+\frac{1}{2}}),\nabla v_h)\\
&\qquad +(u(t^{n+\frac{1}{2}})\cdot\nabla(u(t^{n+\frac{1}{2}})-u^{n+\frac{1}{2}}),v_h)+((u(t^{n+\frac{1}{2}})-u^{n+\frac{1}{2}})\cdot\nabla u^{n+\frac{1}{2}},v_h)\\
&\qquad +\frac{s}{2}(B^{n+\frac{1}{2}}\cdot(B^{n+\frac{1}{2}}-B(t^{n+\frac{1}{2}})),\nabla\cdot v_h)+\frac{s}{2}((B^{n+\frac{1}{2}}-B(t^{n+\frac{1}{2}}))\cdot B(t^{n+\frac{1}{2}}),\nabla\cdot v_h)\\
&+s((B^{n+\frac{1}{2}}-B(t^{n+\frac{1}{2}}))\cdot\nabla B(t^{n+\frac{1}{2}}),v_h)+s(B^{n+\frac{1}{2}}\cdot\nabla(B^{n+\frac{1}{2}}-B(t^{n+\frac{1}{2}})),v_h)=:G_1(t,B,u,v_h)
\end{aligned}\tag{5.45}$$

Note that G_1 represents terms associated with interpolation error and are introduced to simplify the notation. Using the assumptions on the regularity of the solution, analysis similar to that in Chapter 3 will show

$$G_1(t,B,u,v_h)\le C\Delta t^2\|v_h\|. \tag{5.46}$$

Similar to the derivation of (5.45) we introduce terms (5.47)-(5.48) to the left hand side of (5.39) and then subtract from (5.17).

$$\begin{aligned}
-(B(t^{n+\frac{1}{2}})\cdot\nabla u(t^{n+\frac{1}{2}}),\chi_h)\pm(B^{n+\frac{1}{2}}\cdot\nabla u^{n+\frac{1}{2}},\chi_h)&=(B(t^{n+\frac{1}{2}})\cdot\nabla(u^{n+\frac{1}{2}}-u(t^{n+\frac{1}{2}})),\chi_h)\\
&\quad+((B^{n+\frac{1}{2}}-B(t^{n+\frac{1}{2}}))\cdot\nabla u^{n+\frac{1}{2}},\chi_h)\\
&\quad-(B^{n+\frac{1}{2}}\cdot\nabla u^{n+\frac{1}{2}},\chi_h).
\end{aligned}\tag{5.47}$$

$$\begin{aligned}
&(u(t^{n+\frac{1}{2}})\cdot\nabla(B(t^{n+\frac{1}{2}})-B^{n+\frac{1}{2}}),\chi_h)\pm(u^{n+\frac{1}{2}}\cdot\nabla B^{n+\frac{1}{2}},\chi_h)\\
&\qquad=(u(t^{n+\frac{1}{2}})\cdot\nabla(B(t^{n+\frac{1}{2}})-B^{n+\frac{1}{2}}),\chi_h)+((u(t^{n+\frac{1}{2}})-u^{n+\frac{1}{2}})\cdot\nabla B^{n+\frac{1}{2}},\chi_h)\\
&\qquad\quad+(u^{n+\frac{1}{2}}\cdot\nabla B^{n+\frac{1}{2}},\chi_h)
\end{aligned}\tag{5.48}$$

$$
\begin{aligned}
&\frac{1}{\Delta t}(e_B^{n+1} - e_B^n, \chi_h) + Re_m^{-1}(\nabla e_B^{n+\frac{1}{2}}, \nabla\chi_h) - (B_h^{n+\frac{1}{2}} \cdot \nabla e_u^{n+\frac{1}{2}}, \chi_h) \\
&\qquad - (e_B^{n+\frac{1}{2}} \cdot \nabla u^{n+\frac{1}{2}}, \chi_h) + (u^{n+\frac{1}{2}} \cdot \nabla e_B^{n+\frac{1}{2}}, \chi_h) + (e_u^{n+\frac{1}{2}} \cdot \nabla B^{n+\frac{1}{2}}, \chi_h) \\
&= (B_t(t^{n+\frac{1}{2}}) - \{B(t^{n+1}) - B(t^n)\}\Delta t^{-1}, \chi_h) \\
&\qquad + Re_m^{-1}(\nabla(B(t^{n+\frac{1}{2}}) - B^{n+\frac{1}{2}}), \nabla\chi_h) \\
&\qquad + (B(t^{n+\frac{1}{2}}) \cdot \nabla(u^{n+\frac{1}{2}} - u(t^{n+\frac{1}{2}})), \chi_h) + ((B^{n+\frac{1}{2}} - B(t^{n+\frac{1}{2}})) \cdot \nabla u^{n+\frac{1}{2}}, \chi_h) \\
&\qquad + (u(t^{n+\frac{1}{2}}) \cdot \nabla(B(t^{n+\frac{1}{2}}) - B^{n+\frac{1}{2}}), \chi_h) + ((u(t^{n+\frac{1}{2}}) - u^{n+\frac{1}{2}}) \cdot \nabla B^{n+\frac{1}{2}}, \chi_h) \\
&= G_2(t, B, u, \chi_h)
\end{aligned}
\tag{5.49}
$$

Similar to G_1, we bound G_2 by

$$
G_2(t, B, u, v_h) \leq C\Delta t^2 \|\chi_h\|. \tag{5.50}
$$

Define $\phi_h^n = (u_h^n - U^n)$ and $\eta^n = (u^n - U^n) \Rightarrow e_u^n = \phi_h^n - \eta_u^n$ and analogously $e_B^n = (B_h^n - \mathcal{B}^n) + (\mathcal{B}^n - B^n) = \psi_h^n - \eta_B^n$. Where $U^k \in V_h$ and $\mathcal{B}^k \in V_h$. Substituting into (5.45) and (5.49) results in:

$$
\begin{aligned}
&\frac{1}{\Delta t}(\phi_h^{n+1} - \phi_h^n, v_h) + Re^{-1}(\nabla\phi_h^{n+\frac{1}{2}}, \nabla v_h) + (u_h^{n+\frac{1}{2}} \cdot \nabla\phi_h^{n+\frac{1}{2}}, v_h) + (\phi_h^{n+\frac{1}{2}} \cdot \nabla u^{n+\frac{1}{2}}, v_h) \\
&\qquad - \frac{s}{2}(B_h^{n+\frac{1}{2}} \cdot \psi_h^{n+\frac{1}{2}}, \nabla \cdot v_h) - s(B_h^{n+\frac{1}{2}} \cdot \nabla\psi_h^{n+\frac{1}{2}}, v_h) \\
&\qquad - s(\psi_h^{n+\frac{1}{2}} \cdot \nabla B^{n+\frac{1}{2}}, v_h) - \frac{s}{2}(\psi_h^{n+\frac{1}{2}} \cdot B^{n+\frac{1}{2}}, \nabla \cdot v_h) \\
&= \frac{1}{\Delta t}(\eta_u^{n+1} - \eta_u^n, v_h) + Re^{-1}(\nabla\eta_u^{n+\frac{1}{2}}, \nabla v_h) + (u_h^{n+\frac{1}{2}} \cdot \nabla\eta_u^{n+\frac{1}{2}}, v_h) \\
&\qquad + (\eta_u^{n+\frac{1}{2}} \cdot \nabla u^{n+\frac{1}{2}}, v_h) - s(B_h^{n+\frac{1}{2}} \cdot \eta_B^{n+\frac{1}{2}}, v_h) - s(B_h^{n+\frac{1}{2}} \cdot \nabla\eta_B^{n+\frac{1}{2}}, v_h) \\
&\qquad - s(\eta_B^{n+\frac{1}{2}} \cdot \nabla B^{n+\frac{1}{2}}, v_h) - \frac{s}{2}(\eta_B^{n+\frac{1}{2}} \cdot B^{n+\frac{1}{2}}, \nabla \cdot v_h) + G_1(t, u, B, v_h)
\end{aligned}
\tag{5.51}
$$

$$\begin{aligned}\frac{1}{\Delta t}(\psi_h^{n+1}-\psi_h^n,\chi_h)+Re_m^{-1}(\nabla\psi_h^{n+1},\nabla\chi_h)-(B_h^{n+\frac{1}{2}}\cdot\nabla\phi_h^{n+\frac{1}{2}},\chi_h)-(\psi_h^{n+\frac{1}{2}}\cdot\nabla u^{n+\frac{1}{2}},\chi_h)\\ +(u^{n+\frac{1}{2}}\cdot\nabla\psi_h^{n+\frac{1}{2}},\chi_h)+(\phi_h^{n+\frac{1}{2}}\cdot\nabla B^{n+\frac{1}{2}},\chi_h)\\ =\frac{1}{\Delta t}(\eta_B^{n+1}-\eta_B^n,\chi_h)+Re_m^{-1}(\nabla\eta_B^{n+\frac{1}{2}},\nabla\chi_h)-(B_h^{n+\frac{1}{2}}\cdot\nabla\eta_u^{n+\frac{1}{2}},\chi_h)\\ -(\eta_B^{n+\frac{1}{2}}\cdot\nabla u^{n+\frac{1}{2}},\chi_h)+(u^{n+\frac{1}{2}}\cdot\nabla\eta_B^{n+\frac{1}{2}},\chi_h)+(\eta_u^{n+\frac{1}{2}}\cdot\nabla B^{n+\frac{1}{2}},\chi_h)\\ +G_2(t,u,B,\chi_h)\end{aligned}\tag{5.52}$$

A second substitution of $\chi_h=\psi_h^{n+\frac{1}{2}}$ and $v_h=\phi_h^{n+\frac{1}{2}}$ into (5.51) and (5.52) while also noting $(u\cdot\nabla w,w)=0$ and $\phi_h^{n+\frac{1}{2}}$ is divergence free, yields the following pair of inequalities:

$$\begin{aligned}\frac{1}{2\Delta t}(\left\|\phi_h^{n+1}\right\|^2-\|\phi_h^n\|^2)+Re^{-1}\left\|\nabla\phi_h^{n+\frac{1}{2}}\right\|^2+(\phi_h^{n+\frac{1}{2}}\cdot\nabla u^{n+\frac{1}{2}},\phi_h^{n+\frac{1}{2}})\\ -s(B_h^{n+\frac{1}{2}}\cdot\nabla\psi_h^{n+\frac{1}{2}},\phi_h^{n+\frac{1}{2}})-s(\psi_h^{n+\frac{1}{2}}\cdot\nabla B^{n+\frac{1}{2}},\phi_h^{n+\frac{1}{2}})\\ =\frac{1}{\Delta t}(\eta_u^{n+1}-\eta_u^n,\phi_h^{n+\frac{1}{2}})+Re^{-1}(\nabla\eta_u^{n+\frac{1}{2}},\nabla\phi_h^{n+\frac{1}{2}})+(u_h^{n+\frac{1}{2}}\cdot\nabla\eta_u^{n+\frac{1}{2}},\phi_h^{n+\frac{1}{2}})\\ +(\eta_u^{n+\frac{1}{2}}\cdot\nabla u^{n+\frac{1}{2}},\phi_h^{n+\frac{1}{2}})-s(B_h^{n+\frac{1}{2}}\cdot\nabla\eta_B^{n+\frac{1}{2}},\phi_h^{n+\frac{1}{2}})\\ -s(\eta_B^{n+\frac{1}{2}}\cdot\nabla B^{n+\frac{1}{2}},\phi_h^{n+\frac{1}{2}})+G_1(t,u,B,\phi_h^{n+\frac{1}{2}})\end{aligned}\tag{5.53}$$

$$\begin{aligned}\frac{1}{2\Delta t}(\left\|\psi_h^{n+\frac{1}{2}}\right\|^2-\left\|\psi_h^{n+\frac{1}{2}}\right\|^2)+Re_m^{-1}\left\|\nabla\psi_h^{n+\frac{1}{2}}\right\|^2-(B_h^{n+\frac{1}{2}}\cdot\nabla\phi_h^{n+\frac{1}{2}},\psi_h^{n+\frac{1}{2}})-(\psi_h^{n+\frac{1}{2}}\cdot\nabla u^{n+\frac{1}{2}},\psi_h^{n+\frac{1}{2}})\\ +(\phi_h^{n+\frac{1}{2}}\cdot\nabla B^{n+\frac{1}{2}},\psi_h^{n+\frac{1}{2}})=\frac{1}{\Delta t}(\eta_B^{n+1}-\eta_B^n,\psi_h^{n+\frac{1}{2}})+Re_m^{-1}(\nabla\eta_B^{n+\frac{1}{2}},\nabla\psi_h^{n+\frac{1}{2}})\\ -(B_h^{n+\frac{1}{2}}\cdot\nabla\eta_u^{n+\frac{1}{2}},\psi_h^{n+\frac{1}{2}})-(\eta_B^{n+\frac{1}{2}}\cdot\nabla u^{n+\frac{1}{2}},\psi_h^{n+\frac{1}{2}})+(u^{n+\frac{1}{2}}\cdot\nabla\eta_B^{n+\frac{1}{2}},\psi_h^{n+\frac{1}{2}})\\ +(\eta_u^{n+\frac{1}{2}}\cdot\nabla B^{n+\frac{1}{2}},\psi_h^{n+\frac{1}{2}})+G_2(t,u,B,\psi_h^{n+\frac{1}{2}})\end{aligned}\tag{5.54}$$

Using the inequality,

$$\frac{1}{\Delta t}(\eta^{n+1}-\eta_u^n,\phi_h^{n+\frac{1}{2}})\le\frac{1}{2\Delta t}\int_{t^n}^{t^{n+1}}\|\partial(\eta_u)\|^2\,dt+\frac{1}{2}\left\|\phi_h^{n+\frac{1}{2}}\right\|^2,\tag{5.55}$$

along with Hölder's Inequality and (5.46),

$$\begin{aligned}
&\frac{1}{2\Delta t}(\left\|\phi_h^{n+1}\right\|^2 - \|\phi_h^n\|^2) + \frac{Re^{-1}}{2}\left\|\nabla\phi_h^{n+\frac{1}{2}}\right\|^2 \\
&\qquad\leq \frac{1}{2\Delta t}\int_{t^n}^{t^{n+1}} \|\partial_t(\eta_u)\|^2\ dt + \frac{1}{2}\left\|\phi_h^{n+\frac{1}{2}}\right\|^2 + \left(\frac{Re^{-1}}{2}\right)\left\|\eta_u^{n+\frac{1}{2}}\right\|^2 \\
&\quad + \left\|\nabla u^{n+\frac{1}{2}}\right\|_\infty \left\|\phi_h^{n+\frac{1}{2}}\right\|^2 + s(B_h^{n+\frac{1}{2}}\cdot\nabla\psi_h^{n+\frac{1}{2}}, \phi_h^{n+\frac{1}{2}}) + s\left\|\nabla B^{n+\frac{1}{2}}\right\|_\infty \left\|\psi_h^{n+\frac{1}{2}}\right\| \left\|\phi_h^{n+\frac{1}{2}}\right\| \\
&+C\left\|\nabla u_h^{n+\frac{1}{2}}\right\| \left\|\nabla\eta_u^{n+\frac{1}{2}}\right\| \left\|\nabla\phi_h^{n+\frac{1}{2}}\right\| + \left\|\nabla u^{n+\frac{1}{2}}\right\|_\infty \left\|\eta_u^{n+\frac{1}{2}}\right\| \left\|\phi_h^{n+\frac{1}{2}}\right\| + Cs\left\|\nabla B_h^{n+\frac{1}{2}}\right\| \left\|\nabla\eta_B^{n+\frac{1}{2}}\right\| \left\|\nabla\phi_h^{n+\frac{1}{2}}\right\| \\
&\qquad + s\left\|\nabla B^{n+\frac{1}{2}}\right\|_\infty \left\|\eta_B^{n+\frac{1}{2}}\right\| \left\|\phi_h^{n+\frac{1}{2}}\right\| + C\Delta t^2\left\|\phi_h^{n+\frac{1}{2}}\right\| \quad (5.56)
\end{aligned}$$

This reduces, with Cauchy-Schwarz and Young's inequalities and the assumption of the regularity of the solution, to

$$\begin{aligned}
&\frac{1}{2\Delta t}(\left\|\phi_h^{n+1}\right\|^2 - \|\phi_h^n\|^2) + \frac{Re^{-1}}{4}\left\|\nabla\phi_h^{n+\frac{1}{2}}\right\|^2 \leq \frac{1}{2\Delta t}\int_{t^n}^{t^{n+1}} \|\partial_t(\eta_u)\|^2\ dt + \left(\frac{Re^{-1}}{2}\right)\left\|\eta_u^{n+\frac{1}{2}}\right\|^2 \\
&+ C(\left\|\phi_h^{n+\frac{1}{2}}\right\|^2 + \left\|\psi_h^{n+\frac{1}{2}}\right\|^2 + \Delta t^4 + \left\|\eta_u^{n+\frac{1}{2}}\right\|^2 + \left\|\nabla u_h^{n+\frac{1}{2}}\right\|^2 \left\|\nabla\eta_u^{n+\frac{1}{2}}\right\|^2 + s^2\left\|\nabla B_h^{n+\frac{1}{2}}\right\|^2 \left\|\nabla\eta_B^{n+\frac{1}{2}}\right\|^2 \\
&\qquad + s^2\left\|\eta_B^{n+\frac{1}{2}}\right\|^2) + s(B_h^{n+\frac{1}{2}}\cdot\nabla\psi_h^{n+\frac{1}{2}}, \phi_h^{n+\frac{1}{2}}) \quad (5.57)
\end{aligned}$$

We now step back from (5.57) and return to (5.54), which implies

$$\begin{aligned}
&\frac{1}{2\Delta t}(\left\|\psi_h^{n+1}\right\|^2 - \|\psi_h^n\|^2) + \frac{Re_m^{-1}}{2}\left\|\nabla\psi_h^{n+1/2}\right\|^2 \leq \frac{1}{2\Delta t}\int_{t^n}^{t^{n+1}} \|\partial_t(\eta_B)\|^2\ dt \\
&\quad + \frac{1}{2}\left\|\psi_h^{n+\frac{1}{2}}\right\|^2 + Re_m^{-1}\left\|\nabla\eta_B^{n+\frac{1}{2}}\right\|^2 + (B_h^{n+\frac{1}{2}}\cdot\nabla\phi_h^{n+\frac{1}{2}}, \psi_h^{n+\frac{1}{2}}) + \left\|\nabla B^{n+\frac{1}{2}}\right\|_\infty \left\|\phi_h^{n+\frac{1}{2}}\right\| \left\|\psi_h^{n+\frac{1}{2}}\right\| \\
&+ \left\|\nabla u^{n+\frac{1}{2}}\right\|_\infty \left\|\psi_h^{n+\frac{1}{2}}\right\|^2 + C\left\|\nabla B_h^{n+\frac{1}{2}}\right\| \left\|\nabla\eta_u^{n+\frac{1}{2}}\right\| \left\|\nabla\psi_h^{n+\frac{1}{2}}\right\| + C\left\|\nabla u^{n+\frac{1}{2}}\right\|_\infty \left\|\nabla\eta_B^{n+\frac{1}{2}}\right\| \left\|\psi_h^{n+\frac{1}{2}}\right\| \\
&\qquad + \left\|\nabla B^{n+\frac{1}{2}}\right\|_\infty \left\|\eta_u^{n+\frac{1}{2}}\right\| \left\|\psi_h^{n+\frac{1}{2}}\right\| + C\Delta t^2\left\|\psi_h^{n+\frac{1}{2}}\right\|. \quad (5.58)
\end{aligned}$$

Under the regularity assumptions, Cauchy-Schwarz and Young's inequalities, this can be

reduced to

$$\frac{1}{2\Delta t}(\left\|\psi_h^{n+1}\right\|^2 - \|\psi_h^n\|^2) + \frac{Re_m^{-1}}{4}\left\|\nabla\psi_h^{n+1}\right\|^2 \leq \frac{1}{2\Delta t}\int_{t^n}^{t^{n+1}} \|\partial_t(\eta_B)\|^2\, dt$$
$$+ Re_m^{-1}\left\|\nabla\eta_B^{n+\frac{1}{2}}\right\|^2 + C(\left\|\psi_h^{n+\frac{1}{2}}\right\|^2 + \Delta t^4 + \left\|\phi_h^{n+\frac{1}{2}}\right\|^2 + \left\|\nabla\eta_B^{n+\frac{1}{2}}\right\|^2 + \left\|\eta_u^{n+\frac{1}{2}}\right\|^2$$
$$+ Re\left\|\nabla B_h^{n+\frac{1}{2}}\right\|^2\left\|\nabla\eta_u^{n+\frac{1}{2}}\right\|^2) + (B_h^{n+\frac{1}{2}}\cdot\nabla\phi_h^{n+\frac{1}{2}}, \psi_h^{n+\frac{1}{2}}). \quad (5.59)$$

Multiplying (5.59) by s and adding it to (5.57), and using that

$$(B_h^{n+\frac{1}{2}}\cdot\nabla\phi_h^{n+\frac{1}{2}}, \psi_h^{n+\frac{1}{2}}) = -(B_h^{n+\frac{1}{2}}\cdot\nabla\psi_h^{n+\frac{1}{2}}, \phi_h^{n+\frac{1}{2}}),$$

along with the Poincare inequality and reducing, we get

$$\frac{1}{2\Delta t}(\left\|\phi_h^{n+1}\right\|^2 - \|\phi_h^n\|^2) + \frac{s}{2\Delta t}(\left\|\psi_h^{n+1}\right\|^2 - \|\psi_h^n\|^2) + \frac{Re^{-1}}{4}\left\|\nabla\phi_h^{n+\frac{1}{2}}\right\|^2 + \frac{sRe_m^{-1}}{4}\left\|\nabla\psi_h^{n+1/2}\right\|^2$$
$$\leq \frac{1}{2\Delta t}\int_{t^n}^{t^{n+1}} \|\partial_t(\eta_u)\|^2\, dt + \frac{s}{2\Delta t}\int_{t^n}^{t^{n+1}} \|\partial_t(\eta_B)\|^2\, dt + \left(\frac{Re^{-1}}{2}\right)\left\|\eta_u^{n+\frac{1}{2}}\right\|^2 + sRe_m^{-1}\left\|\nabla\eta_B^{n+\frac{1}{2}}\right\|^2$$
$$+ C(s)(\left\|\phi_h^{n+\frac{1}{2}}\right\|^2 + \left\|\psi_h^{n+\frac{1}{2}}\right\|^2 + \Delta t^4 + \left\|\eta_u^{n+\frac{1}{2}}\right\|^2 + \left\|\nabla u_h^{n+\frac{1}{2}}\right\|^2\left\|\nabla\eta_u^{n+\frac{1}{2}}\right\|^2 + \left\|\nabla B_h^{n+\frac{1}{2}}\right\|^2\left\|\nabla\eta_B^{n+\frac{1}{2}}\right\|^2$$
$$+ \left\|\nabla\eta_B^{n+\frac{1}{2}}\right\|^2 + Re\left\|\nabla B_h^{n+\frac{1}{2}}\right\|^2\left\|\nabla\eta_u^{n+\frac{1}{2}}\right\|^2) \quad (5.60)$$

Multiplying by $2\Delta t$ and summing over timesteps now gives

$$\left\|\phi_h^M\right\|^2 + s\left\|\psi_h^M\right\|^2 + \sum_{n=0}^{M-1}\left(Re^{-1}\left\|\nabla\phi_h^{n+\frac{1}{2}}\right\|^2 + sRe_m^{-1}\left\|\nabla\psi_h^{n+\frac{1}{2}}\right\|^2\right)$$
$$\leq \int_0^T \left(\|\partial_t(\eta_u)\|^2 + s\|\partial_t(\eta_B)\|^2\right) dt + CT\Delta t^4 + C\Delta t\sum_{n=0}^{M-1}(\left\|\nabla\eta_u^{n+\frac{1}{2}}\right\|^2 + \left\|\nabla\eta_B^{n+\frac{1}{2}}\right\|^2$$
$$+ \left\|\nabla u_h^{n+\frac{1}{2}}\right\|^2\left\|\nabla\eta_u^{n+\frac{1}{2}}\right\|^2 + \left\|\nabla B_h^{n+\frac{1}{2}}\right\|^2\left\|\nabla\eta_B^{n+\frac{1}{2}}\right\|^2 + \left\|\nabla B_h^{n+\frac{1}{2}}\right\|^2\left\|\nabla\eta_u^{n+\frac{1}{2}}\right\|^2)$$
$$+ C\sum_{n=1}^{M}(\left\|\phi_h^{n+1}\right\|^2 + \left\|\psi_h^{n+1}\right\|^2) \quad (5.61)$$

Next we use approximation properties of the spaces and the stability estimate, which reduces

(5.61) to

$$\left\|\phi_h^M\right\|^2 + s\left\|\psi_h^M\right\|^2 + \sum_{n=0}^{M-1}\left(Re^{-1}\left\|\nabla\phi_h^{n+\frac{1}{2}}\right\|^2 + sRe_m^{-1}\left\|\nabla\psi_h^{n+\frac{1}{2}}\right\|^2\right)$$
$$\leq C(\Delta t^4 + h^{2k}) + C\sum_{n=1}^{M}(\left\|\phi_h^{n+1}\right\|^2 + \left\|\psi_h^{n+1}\right\|^2) \quad (5.62)$$

Applying the Gronwall inequality followed by the triangle inequality completes the proof.

□

Bibliography

[1] A. Arakawa. Computational design for long-term numerical integration of the equations of fluid motion: Two dimensional incompressible flow, Part I. *J. Comput. Phys.*, 1:119–143, 1966.

[2] A. Arakawa and V. Lamb. A potential enstrophy and energy conserving scheme for the shallow water equations. *Monthly Weather Review*, 109:18–36, 1981.

[3] M. Benzi and M. Olshanksii. An augmented lagrangian-based approach to the Oseen problem. *SIAM Journal of Scientific Computing*, 28(6):2095–2113, 2005.

[4] M. Benzi, M. Olshanskii, and Z. Wang. Augmented lagrangian preconditioners for the incompressible Navier-Stokes equations. Technical report, Emory University, 2009.

[5] F. Brezzi and M. Fortin. *Mixed and hybrid finite element methods.* Springer-Verlag, 1991.

[6] E. Burman and A. Linke. Stabilized finite element schemes for incompressible flow using scott-vogelius elements. *Applied Numerical Mathematics*, 58(11):1704–1719, 2008.

[7] Q. Chen, S. Chen, and G. Eyink. The joint cascade of energy and helicity in three dimensional turbulence. *Physics of Fluids*, 15(2):361–374, 2003.

[8] B. Cockburn, G. Kanschat, and D. Schötzau. A locally conservative LDG method for the incompressible Navier-Stokes equations. *Mathematics of Computation*, 74:1067–1095, 2005.

[9] B. Cockburn, G. Kanschat, and D. Schötzau. A note on discontinuous Galerkin divergence-free solutions to the Navier-Stokes equations. *Journal of Scientific Computing*, 31:61–73, 2007.

[10] J. Conners. Convergence analysis and computational testing of the finite element discretization of the Navier-Stokes-alpha model. *Submitted*, 2009.

[11] P. Davidson. *An Introduction to Magnetohydrodynamics.* Cambridge, 2001.

[12] P. Ditlevson and P. Guiliani. Cascades in helical turbulence. *Physical Review E*, 63, 2001.

[13] H. Elman and D. Silvester. Fast nonsymmetric iterations and preconditioning for Navier-Stokes equations. *SIAM journal of scientific computing*, 17(1):33–46, 1996.

[14] H. Elman, D. Silvester, and A. Wathen. *Finite Elements and Fast Iterative Solvers with applications in incompressible fluid dynamics.* Oxford Science, 1996.

[15] H.C. Elman, D.J. Silvester, and A.J. Wathen. Performance and analysis of saddle point preconditioners for the discrete steady-state Navier-Stokes equations. *Numerische Mathematik*, 90:665–688, 2002.

[16] V.J. Ervin and N. Heuer. Approximation of time-dependent, viscoelastic fluid flow: Crank-Nicolson, finite element approximation. *Numer. Methods Partial Differential Eq.*, 20:248–283, 2003.

[17] C. Ethier and D. Steinman. Exact fully 3d Navier-Stokes solutions for benchmarking. *International Journal for Numerical Methods in Fluids*, 19(5):369–375, 1994.

[18] S. Ganesan and V. John. Pressure separation — a technique for improving the velocity error in finite element discretisations of the Navier-Stokes equations. *Appl. Math. Comp.*, 165(2):275–290, 2005.

[19] M. Gavrilov and Z. Janji. Computed rotational energy spectra of two energy and enstrophy conserving schemes on semi-staggered grids. *Meteorology and Atmospheric Physics*, 41(1):1–4, 1989.

[20] T. Gelhard, G. Lube, M.A. Olshanskii, and J.-H. Starcke. Stabilized finite element schemes with LBB-stable elements for incompressible flows. *J. Comput. Appl. Math.*, 177:243–267, 2005.

[21] V. Girault and P.-A. Raviart. *Finite element methods for Navier-Stokes equations : Theory and algorithms*. Springer-Verlag, 1986.

[22] P. Gresho and R. Sani. *Incompressible Flow and the Finite Element Method*, volume 2. Wiley, 1998.

[23] M. Gunzburger. *Finite Element Methods for Viscous Incompressible Flow: A Guide to Theory, Practice, and Algorithms*. Academic Press, Boston, 1989.

[24] J. Heywood and R. Rannacher. Finite element approximation of the nonstationary Navier-Stokes problem. I. Regularity of solutions and second-order error estimates for spatial discretization. *SIAM Journal on Numerical Analysis*, 19(2):275–311, 1982.

[25] J. Heywood and R. Rannacher. Finite element approximation of the nonstationary Navier-Stokes problem. Part IV: Error analysis for the second order time discretization. *SIAM J. Numer. Anal.*, 2:353–384, 1990.

[26] V. John. *Large Eddy Simulation of Turbulent Incompressible Flows. Analytical and Numerical Results for a Class of LES Models"*, volume 34 of *Lecture Notes in Computational Science and Engineering*. Springer-Verlag Berlin, Heidelberg, New York, 2004.

[27] V. John. Reference values for drag and lift of a two dimensional time-dependent flow around a cylinder. *International Journal for Numerical Methods in Fluids*, 44:777–788, 2004.

[28] V. John and W. J. Layton. Analysis of numerical errors in Large Eddy Simulation. *SIAM J. Numer. Anal.*, 40(3):995–1020, 2002.

[29] A. Labovsky, W. Layton, C. Manica, M. Neda, and L. Rebholz. The stabilized extrapolated trapezoidal finite element method for the Navier-Stokes equations. *Comput. Methods Appl. Mech. Engrg.*, 198:958–974, 2009.

[30] W. Layton. *An introduction to the numerical analysis of viscous incompressible flows.* SIAM, 2008.

[31] W. Layton, C. Manica, M. Neda, M.A. Olshanskii, and L. Rebholz. On the accuracy of the rotation form in simulations of the Navier-Stokes equations. *J. Comput. Phys.*, 228(5):3433–3447, 2009.

[32] W. Layton, C. Manica, M. Neda, and L. Rebholz. Numerical analysis and computational testing of a high-accuracy Leray-deconvolution model of turbulence. *Numerical Methods for Partial Differential Equations*, 24(2):555–582, 2008.

[33] W. Layton, C. Manica, M. Neda, and L. Rebholz. Numerical analysis and computational comparisons of the NS-omega and NS-alpha regularizations. *Comput. Methods Appl. Mech. Engrg.*, to appear, 2009.

[34] A. Linke. *Divergence-free mixed finite elements for the incompressible Navier-Stokes Equation.* PhD thesis, University of Erlangen, 2007.

[35] A. Linke. Collision in a cross-shaped domain — A steady 2d Navier-Stokes example demonstrating the importance of mass conservation in CFD. *Comp. Meth. Appl. Mech. Eng.*, 198(41–44):3278–3286, 2009.

[36] J. Liu and W. Wang. Energy and helicity preserving schemes for hydro and magnetohydrodynamics flows with symmetry. *J. Comput. Phys.*, 200:8–33, 2004.

[37] C. Manica, M. Neda, M. Olshanskii, and L. Rebholz. Enabling accuracy of Navier-Stokes-alpha through deconvolution and enhanced stability. *Submitted*, 2009.

[38] G. Matthies and L. Tobiska. Mass conservation of finite element methods for coupled flow-transport problems. In G. Lube and G. Rapin, editors, *Proceedings of the International Conference on Boundary and Interior Layers.* BAIL, 2006.

[39] M.Benzi and J. Liu. An efficient solver for the Navier-Stokes equations in rotational form. *SIAM Journal on Scientific Computing*, 29:1959–1981, 2007.

[40] H. Moffatt and A. Tsoniber. Helicity in laminar and turbulent flow. *Annual Review of Fluid Mechanics*, 24:281–312, 1992.

[41] I.M Navon. Implementation of a posteriori methods for enforcing conservation of potential enstrophy and mass in discretized shallow water equation models. *Monthly Weather Review*, 109:946–958, 1981.

[42] I.M. Navon. A Numerov-Galerkin technique applied to a finite element shallow water equations model with enforced conservation of integral invariants and selective lumping. *J. Comput. Phys.*, 52:313–339, 1983.

[43] M. Olshanskii, G. Lube, T. Heister, and J. Löwe. Grad-div stabilization and subgrid pressure models for the incompressible Navier-Stokes equations. *Comp. Meth. Appl. Mech. Eng.*, 2009, to appear.

[44] M. Olshanskii and L. Rebholz. Velocity-vorticity-helicity formulation and a solver for the Navier-Stokes equations. submitted, 2009.

[45] M.A. Olshanskii. A low order Galerkin finite element method for the Navier-Stokes equations of steady incompressible flow: A stabilization issue and iterative methods. *Comp. Meth. Appl. Mech. Eng.*, 191:5515–5536, 2002.

[46] M.A. Olshanskii and A. Reusken. Grad-Div stabilization for the Stokes equations. *Math. Comp.*, 73:1699–1718, 2004.

[47] L. Rebholz. An energy and helicity conserving finite element scheme for the Navier-Stokes equations. *SIAM Journal on Numerical Analysis*, 45(4):1622–1638, 2007.

[48] B. Riviere. *Discontinuous Galerkin Methods for Solving Elliptic and Parabolic Equations: Theory and Implementation.* SIAM, 2008.

[49] H.-G Roos, M. Stynes, and L. Tobiska. *Robust Numerical Methods for singularly perturbed differential equations*, volume 24. Springer, Berlin, 2nd edition, 2008.

[50] M. Schäfer and S. Turek. The benchmark problem 'flow around a cylinder' flow simulation with high performance computers ii. *in E.H. Hirschel (Ed.), Notes on Numerical Fluid Mechanics*, 52, Braunschweig, Vieweg:547–566, 1996.

[51] L.R. Scott and M. Vogelius. Conforming finite element methods for incompressible and nearly incompressible continua. In *Large-scale computations in fluid mechanics, Part 2*, volume 22-2 of *Lectures in Applied Mathematics*, pages 221–244. Amer. Math. Soc., 1985.

[52] L.R. Scott and M. Vogelius. Norm estimates for a maximal right inverse of the divergence operator in spaces of piecewise polynomials. *Mathematical Modelling and Numerical Analysis*, 19(1):111–143, 1985.

[53] H. Sohr. *The Navier-Stokes Equations, An Elementary Functional Analytic Approach.* Birhäuser Advanced Texts. Birkhäuser Verlag Basel, Boston, Berlin, 2001.

[54] R. Temam. *Navier-Stokes equations : theory and numerical analysis.* Elsevier North-Holland, 1979.

[55] M. Vogelius. An analysis of the p-version of the finite element method for nearly incompressible materials. uniformly valid, optimal error estimates. *Numer. Math.*, 41:39–53, 1983.

[56] M. Vogelius. A right-inverse for the divergence operator in spaces of piecewise polynomials. Application to the p-version of the finite element method. *Numer. Math.*, 41:19–37, 1983.

[57] K.L. Wong and A.J. Baker. A 3d incompressible Navier-Stokes velocity-vorticity weak form finite element algorithm. *International Journal For numerical methods in fluids*, 38:99–123, 2002.

[58] S. Zhang. A new family of stable mixed finite elements for the 3d stokes equations. *Mathematics of Computation*, 74:543–554, 2005.

[59] S. Zhang. On the P1 Powell-Sabin divergence-free finite element for the Stokes equations. *J. Comput. Math.*, 26(3):456–470, 2008.

[60] S. Zhang. A family of $Q_{k+1,k} \times Q_{k,k+1}$ divergence-free finite elements on rectangular grids. *SIAM J. Numer. Anal.*, 47(3):2090–2107, 2009.